

# Bulletin of Volcanology

## Origin and ascent history of unusually crystal-rich alkaline basaltic magmas from the western Pannonian Basin --Manuscript Draft--

<b>Manuscript Number:</b>	BUVO-D-12-00136R2
<b>Full Title:</b>	Origin and ascent history of unusually crystal-rich alkaline basaltic magmas from the western Pannonian Basin
<b>Article Type:</b>	Collection: Monogenetic volcanism
<b>Corresponding Author:</b>	M. Éva Jankovics HUNGARY
<b>Corresponding Author Secondary Information:</b>	
<b>Order of Authors:</b>	M. Éva Jankovics Gábor Dobosi Antal Embey-Isztin Balázs Kiss Tamás Sági Szabolcs Harangi Theodoros Ntaflou
<b>Abstract:</b>	<p>The last eruptions of the monogenetic Bakony-Balaton Highland Volcanic Field (western Pannonian Basin, Hungary) produced unusually crystal- and xenolith-rich alkaline basalts which are unique among the alkaline basalts of the Carpathian-Pannonian Region. Similar alkaline basalts are only rarely known in other volcanic fields of the world. These special basaltic magmas fed the eruptions of two closely located volcanic centres: the Bondoró-hegy and the Fűzes-tó scoria cone. Their uncommon enrichment in diverse crystals produced unique rock textures and modified original magma compositions (13.1-14.2 wt.% MgO, 459-657 ppm Cr, 455-564 ppm Ni contents).</p> <p>Detailed mineral-scale textural and chemical analyses revealed that the Bondoró-hegy and Fűzes-tó alkaline basaltic magmas have a complex ascent history, and that most of their minerals (~30 vol.% of the rocks) represent foreign crystals derived from different levels of the underlying lithosphere. The most abundant xenocrysts, olivine, orthopyroxene, clinopyroxene and spinel, were incorporated from different regions and rock types of the subcontinental lithospheric mantle. Megacrysts of clinopyroxene and spinel could have originated from pegmatitic veins / sills which probably represent magmas crystallized near the crust-mantle boundary. Green clinopyroxene xenocrysts could have been derived from lower crustal mafic granulites. Minerals that crystallized in situ from the alkaline basaltic melts (olivine with Cr-spinel inclusions, clinopyroxene, plagioclase, Fe-Ti oxides) are only represented by microphenocrysts and overgrowths on the foreign crystals. The vast amount of peridotitic (most common) and mafic granulitic materials indicates a highly effective interaction between the ascending magmas and wall rocks at lithospheric mantle and lower crustal levels. However, fragments from the middle and upper crust are absent from the studied basalts, suggesting a change in the style (and possibly rate) of magma ascent in the crust. These xenocryst- and xenolith-rich basalts yield diverse tools for estimating magma ascent rate that is important for hazard forecasting in monogenetic volcanic fields. According to the estimated ascent rates, the Bondoró-hegy and Fűzes-tó alkaline basaltic magmas could have reached the surface within hours to few days, similarly to the estimates for other eruptive centres in the Pannonian Basin which were fed by "normal" (crystal- and xenolith-poor) alkaline basalts.</p>
<b>Response to Reviewers:</b>	Dear Professor I.E.M. Smith,

thank you very much for your corrections, we have approved all of your changes.

Yours sincerely,  
M. Éva Jankovics  
on behalf of the authors

**Eötvös Loránd University**  
**Department of Petrology and Geochemistry**

H-1117 Budapest, Pázmány Péter sétány 1/C  
Hungary  
Tel: (36-1) 3722500  
Fax: (36-1) 3812108

---



J. D. L. White  
Department of Geology  
University of Otago  
Dunedin 9054  
New Zealand

27 October 2012

Dear J. D. L. White,

please find enclosed a manuscript what we intend to publish in the Bulletin of Volcanology Thematic Issue: *Monogenetic volcanism and its relevance to the evolution of volcanic fields*:

M. Éva Jankovics, Gábor Dobosi, Antal Embey-Isztin, Balázs Kiss, Tamás Sági, Szabolcs Harangi, Theodoros Ntaflos:

***Origin and ascent history of unusually crystal-rich alkaline basaltic magmas from the western Pannonian Basin***

It is about the detailed mineral-scale textural and chemical analyses, revealed ascent history and estimated magma ascent rates of the unusually crystal- and xenolith-rich alkaline basalts which are the youngest volcanic products in the Bakony-Balaton Highland Volcanic Field, western Pannonian Basin (Hungary).

We suggest three appropriate reviewers:

- 1) Ronald V. Fodor - rfodor@ncsu.edu, Department of Marine, Earth, and Atmospheric Sciences, North Carolina State University
- 2) Hilary Downes - h.downes@ucl.ac.uk, Department of Earth and Planetary Sciences, Birkbeck University of London
- 3) Hannes B. Mattsson - hannes.mattsson@erdw.ethz.ch, Institute of Geochemistry and Petrology, Swiss Federal Institute of Technology (ETH Zürich)

Yours sincerely,

M. Éva Jankovics  
e-mail: jeva182@gmail.com

**Eötvös Loránd University**  
**Department of Petrology and Geochemistry**

H-1117 Budapest, Pázmány Péter sétány 1/C  
Hungary  
Tel: (36-1) 3722500  
Fax: (36-1) 3812108

---



J. D. L. White  
Department of Geology  
University of Otago  
Dunedin 9054  
New Zealand

27 October 2012

Dear J. D. L. White,

we would like to submit our manuscript in the **Thematic Issue: *Monogenetic volcanism and its relevance to the evolution of volcanic fields***. It is about the detailed analyses, revealed ascent history and estimated magma ascent rates of the unusually crystal- and xenolith-rich alkaline basalts which are the youngest volcanic products in the Bakony-Balaton Highland Volcanic Field, western Pannonian Basin (Hungary). Our manuscript is longer than what is given for Research Articles (7000 words). This is because we applied a number of different methods to estimate magma ascent times and rates which, in our opinion, requires a detailed description about the background and applicability in the case of every method. We tried to shorten the extent of the manuscript but we were not able to, and now we think that the descriptions and interpretations compose a whole in the present form. However, if the editors and reviewers find it groundlessly long, we are of course open to cut down where needed.

Yours sincerely,

M. Éva Jankovics

Figure1  
[Click here to download high resolution image](#)

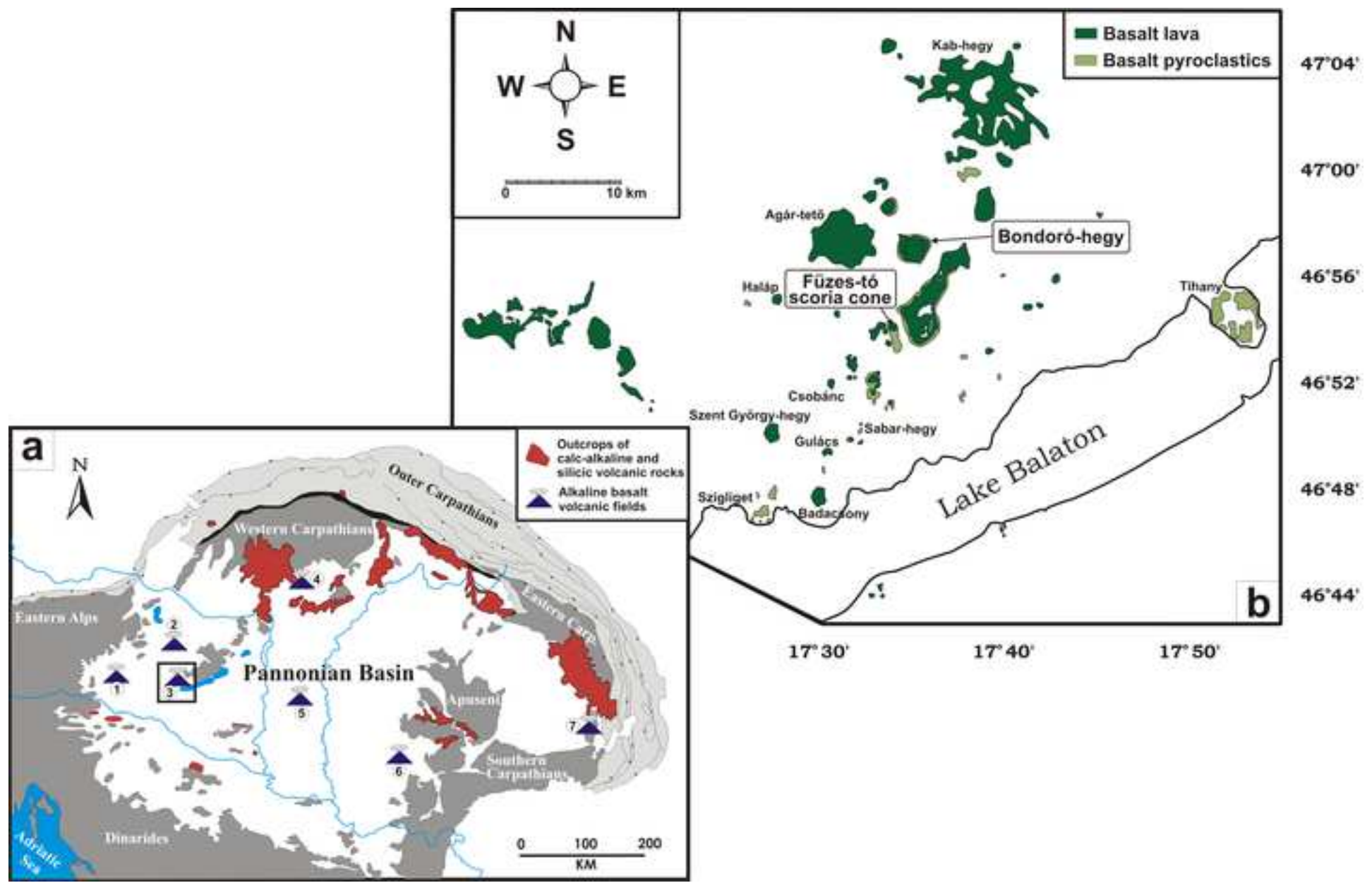




Figure3  
[Click here to download high resolution image](#)

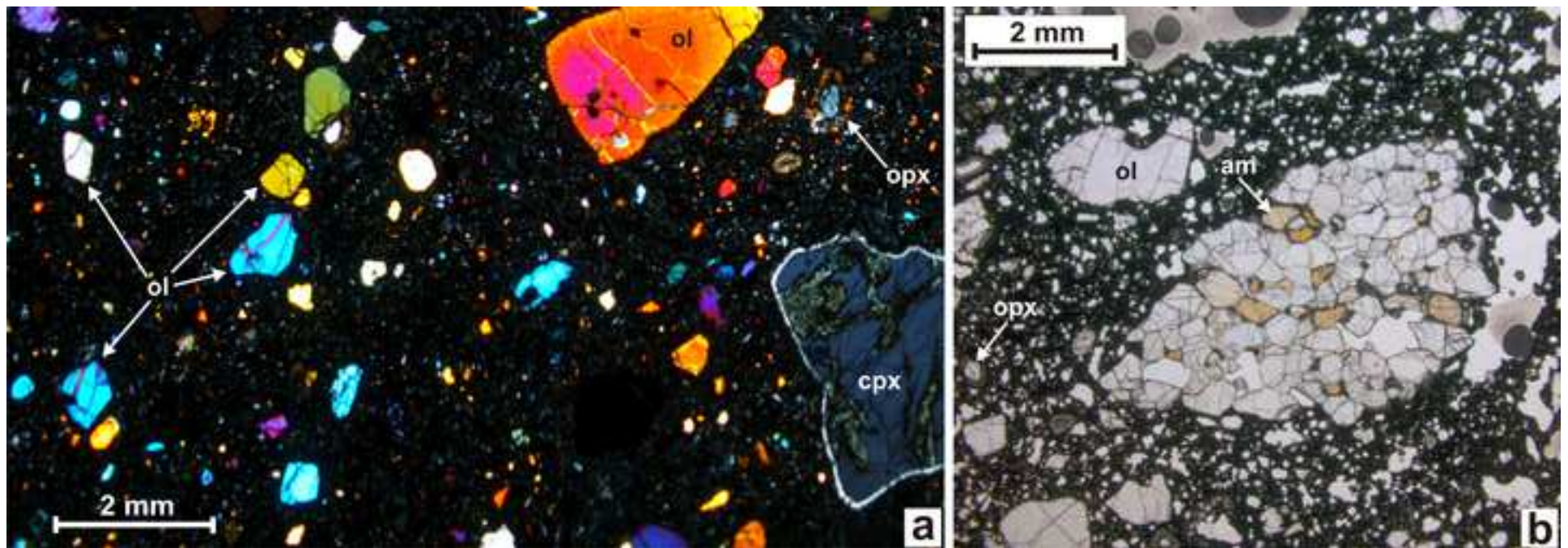


Figure 4  
[Click here to download high resolution image](#)

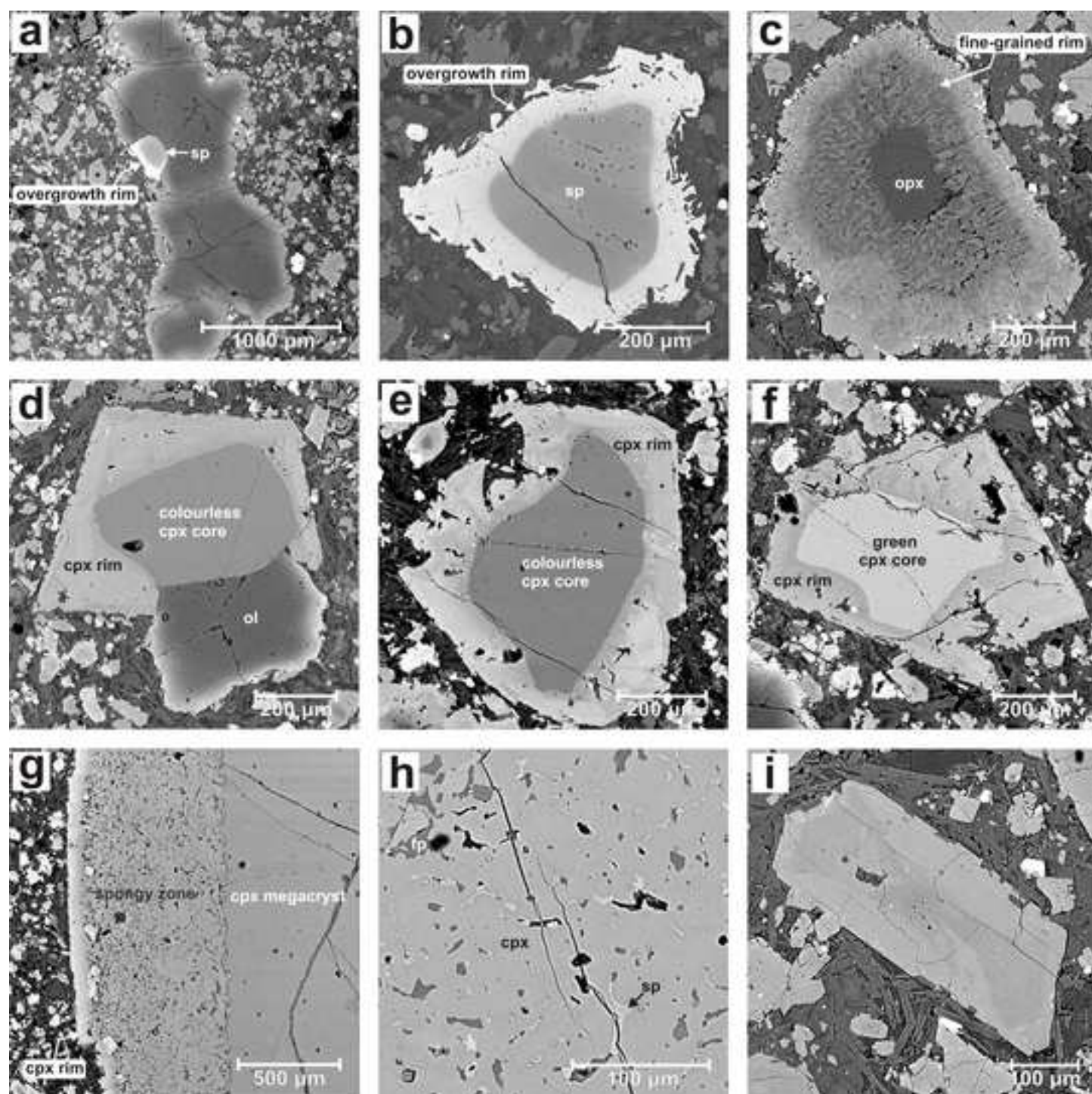


Figure5  
[Click here to download high resolution image](#)

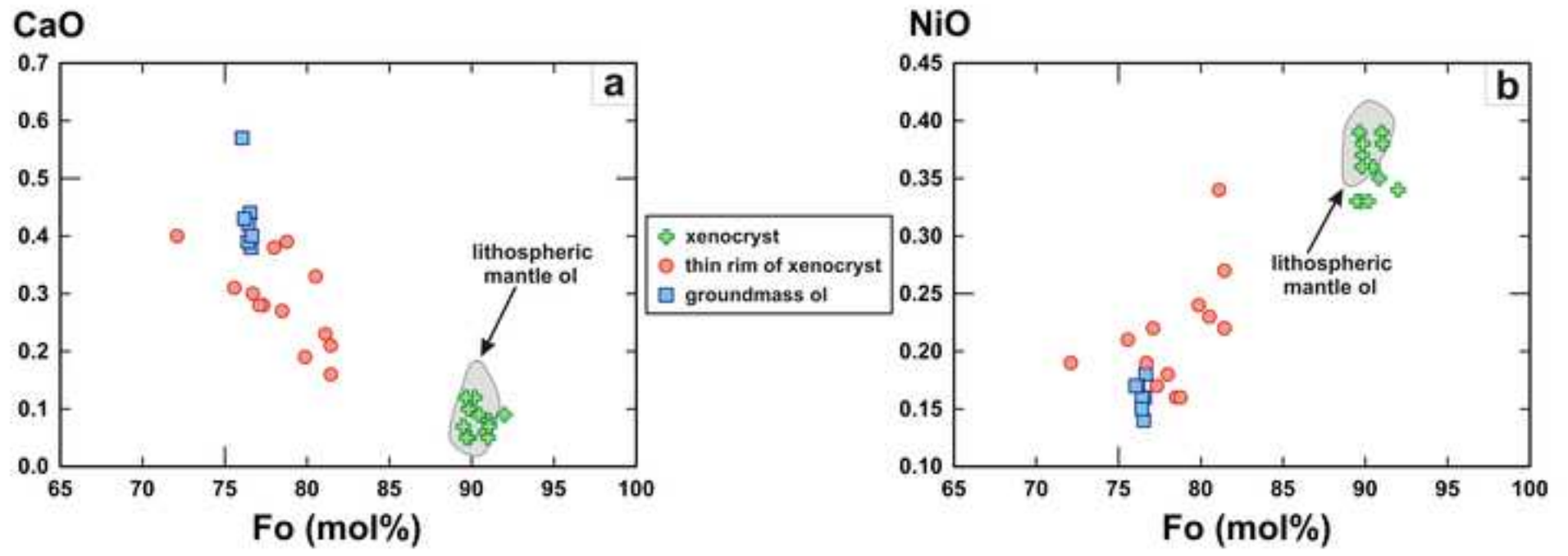




Figure6  
[Click here to download high resolution image](#)

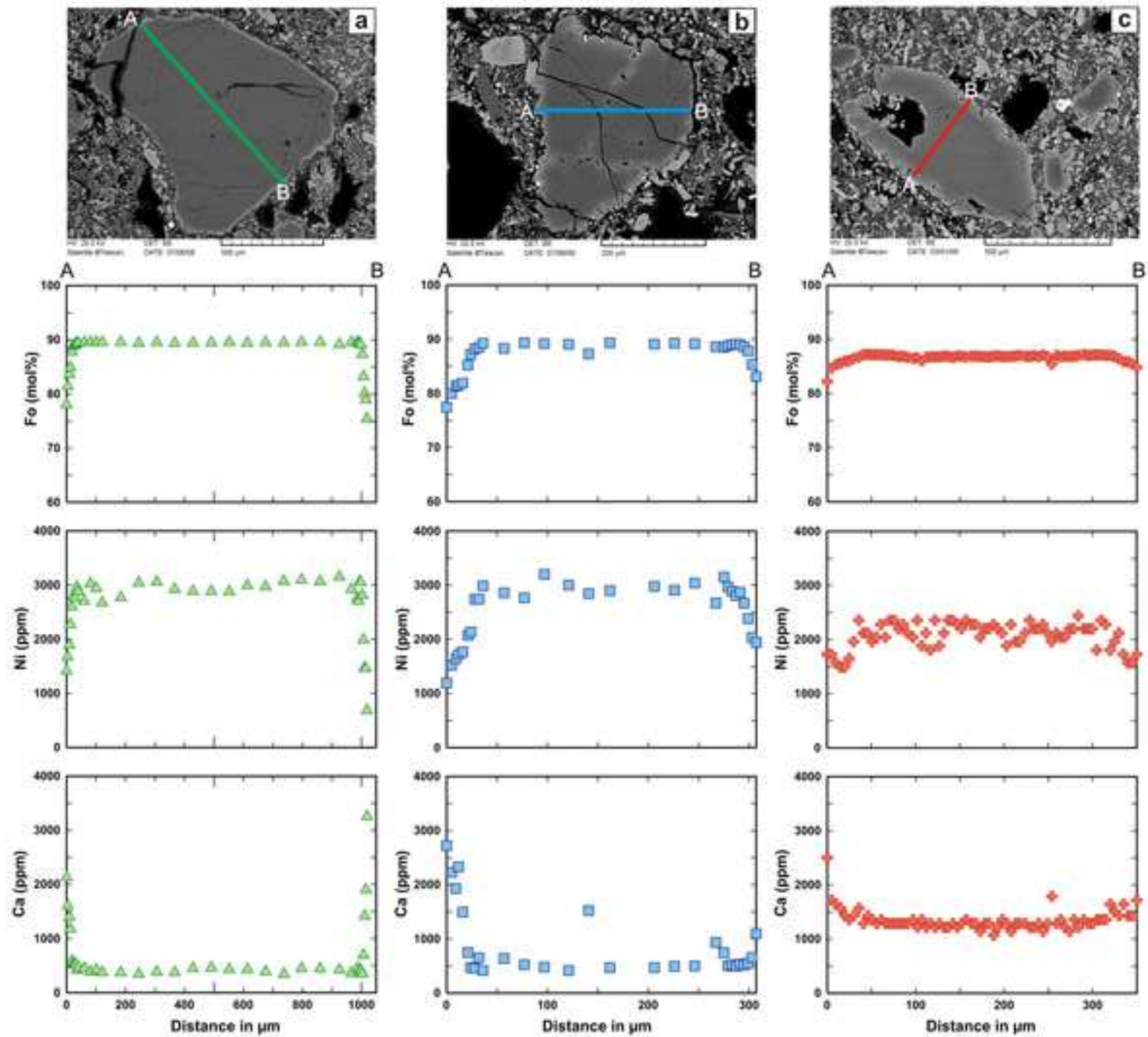


Figure 7  
[Click here to download high resolution image](#)

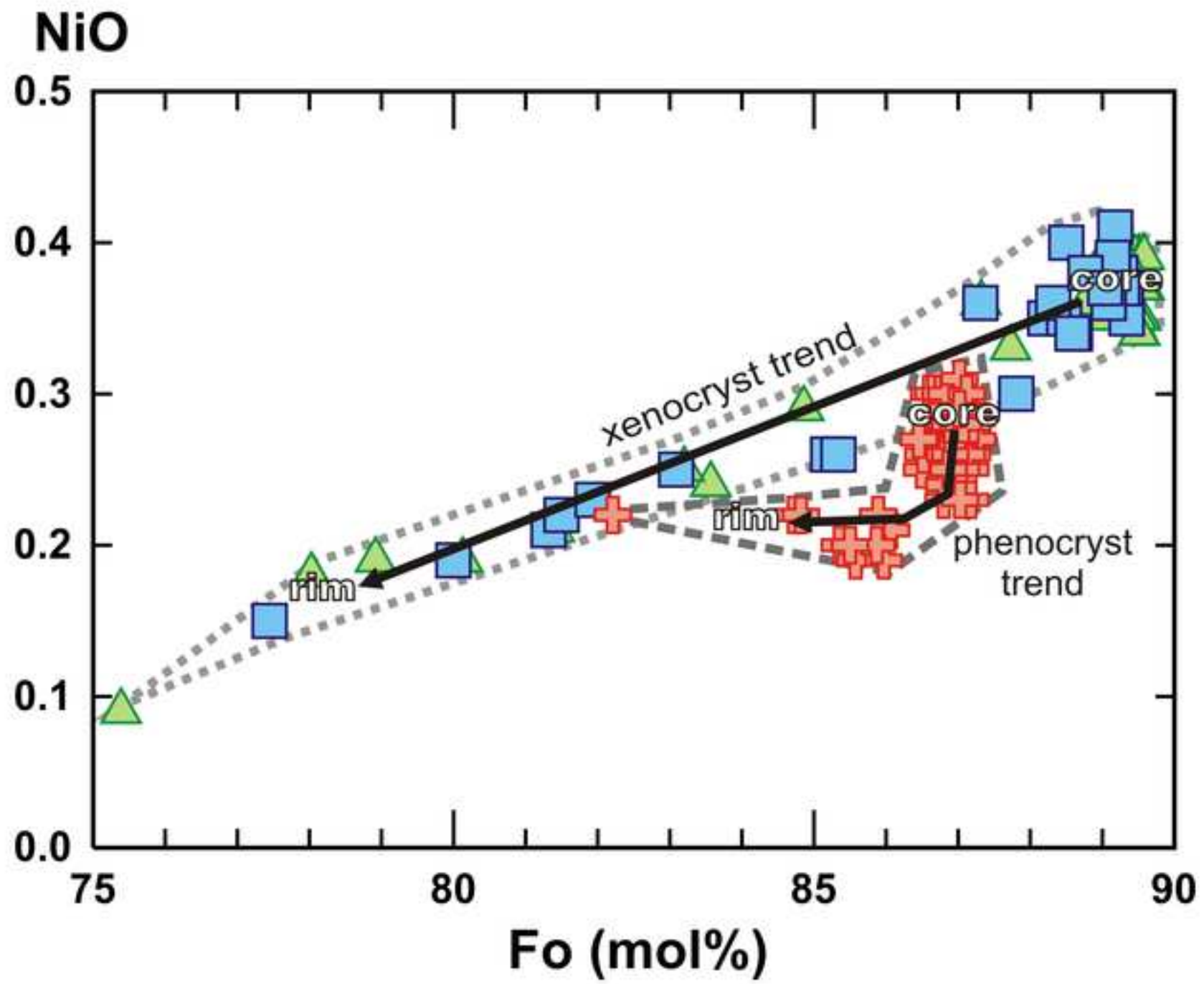
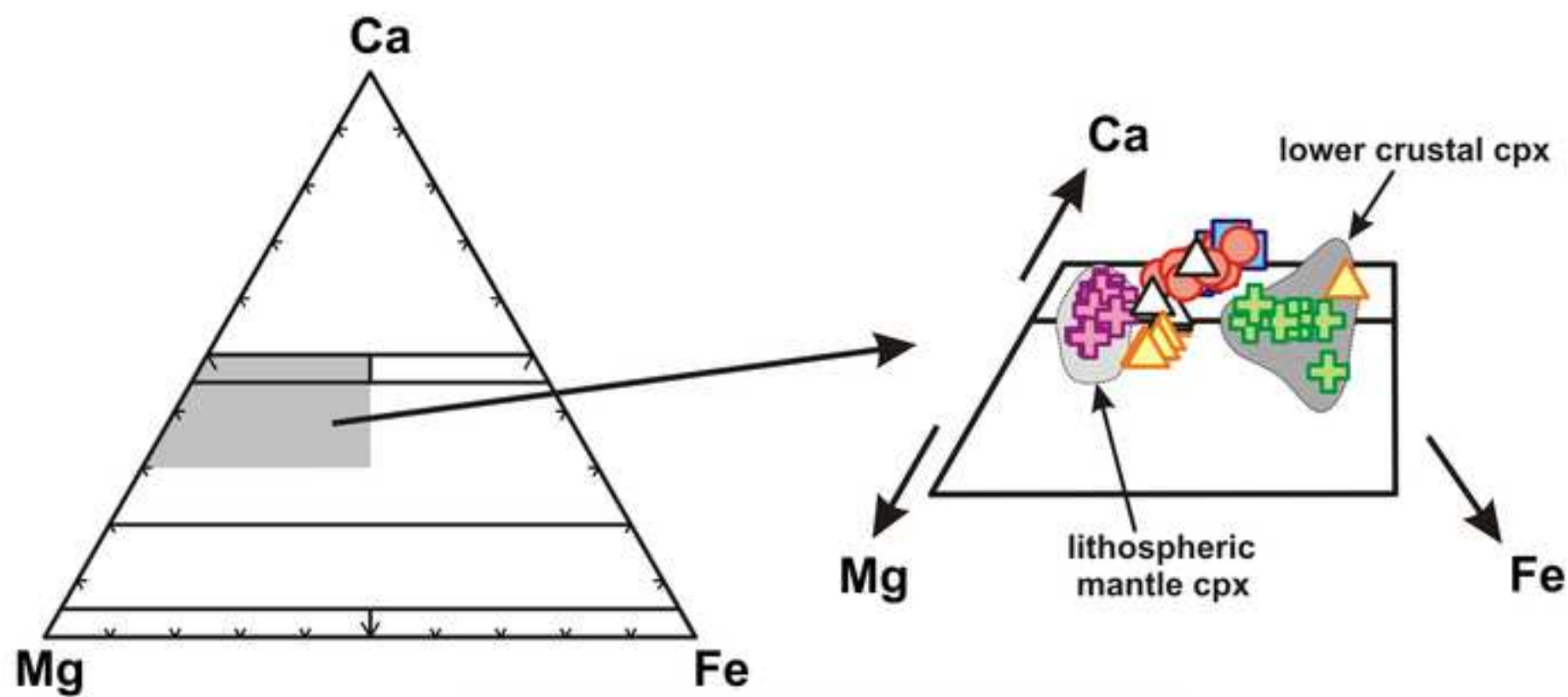


Figure8  
[Click here to download high resolution image](#)









-  megacryst
-  spongy part of megacryst
-  colourless xenocryst
-  green xenocryst
-  overgrowth on mega- and xenocryst
-  groundmass cpx

Figure9

[Click here to download high resolution image](#)

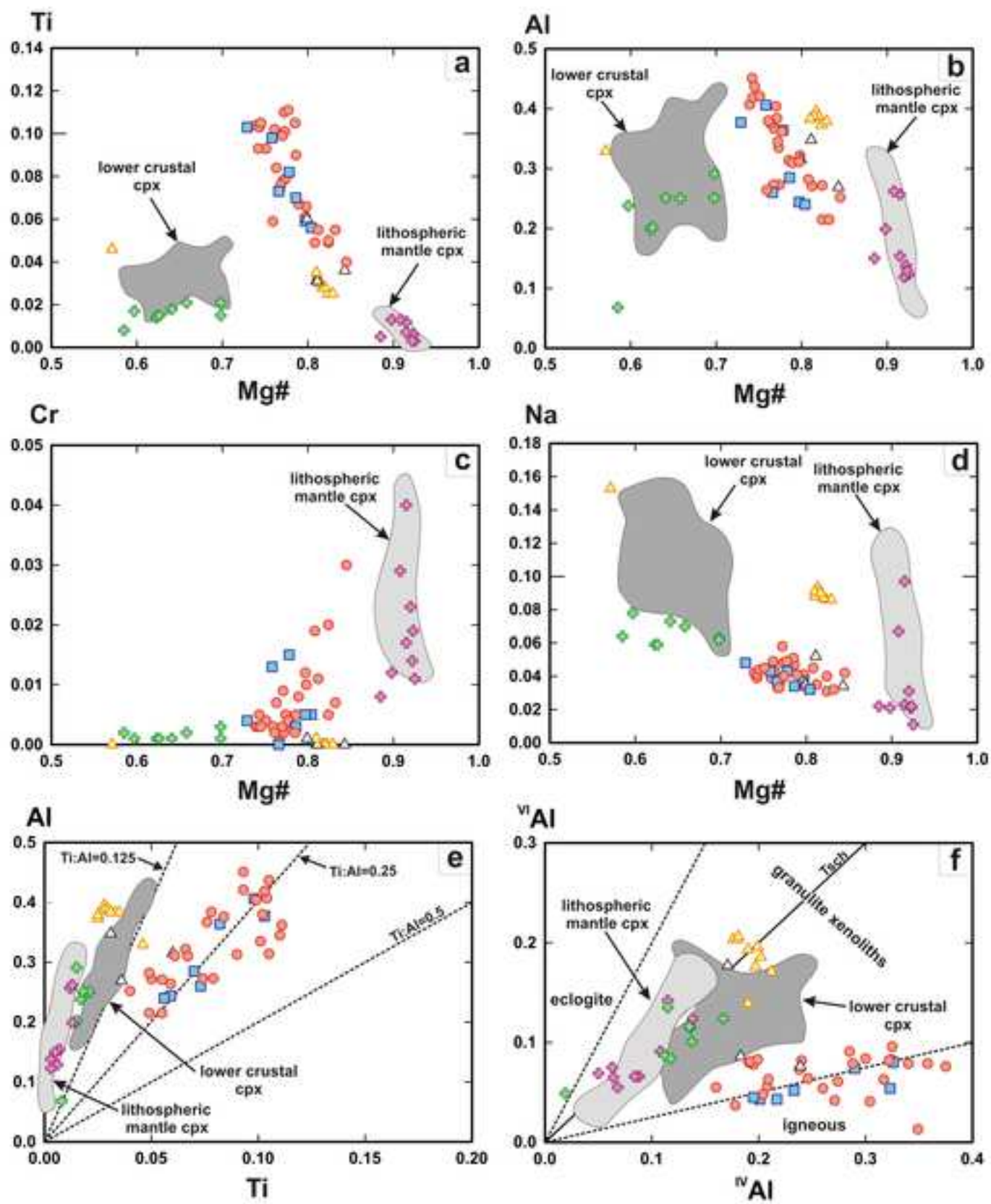




Figure10  
[Click here to download high resolution image](#)

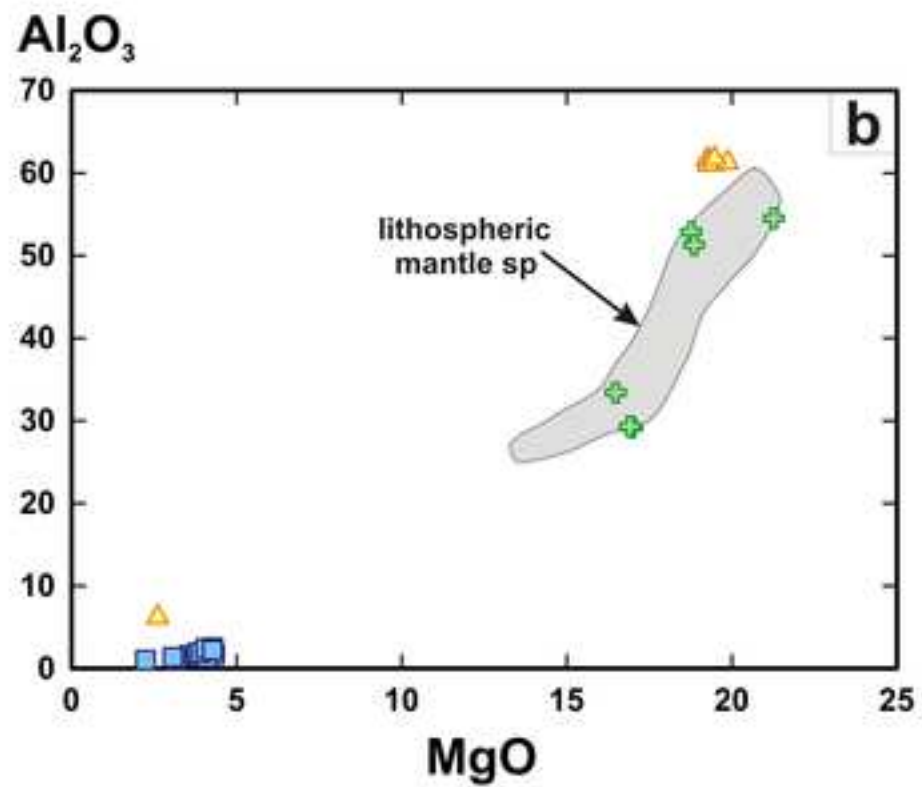
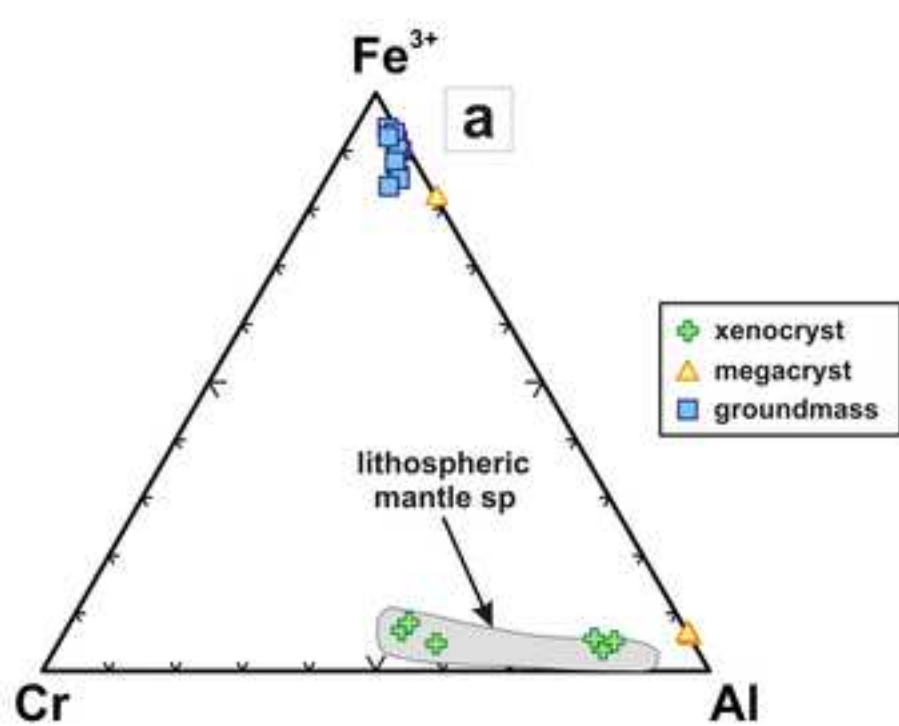


Table 1

Major and trace element analyses of the BON683 sample from Bondoró-hegy (Embey-lsztin et al., 1993)

Major elements (wt%)		Trace elements (ppm)	
SiO <sub>2</sub>	45.58	Ni	455
TiO <sub>2</sub>	1.74	Cr	459
Al <sub>2</sub> O <sub>3</sub>	13.64	V	144
Fe <sub>2</sub> O <sub>3</sub> *	10.09	Sr	790
MnO	0.16	Rb	56
MgO	13.94	Zr	260
CaO	8.13	Nb	72
Na <sub>2</sub> O	3.88	Ba	772
K <sub>2</sub> O	1.97	Y	25
P <sub>2</sub> O <sub>5</sub>	0.75	La	47.4
Sum	99.88	Ce	91.02
LOI	0.23	Sm	6.74
SI	-16.73	Eu	2.11
ne	12.4	Yb	1.93
Mg#	76.3	Lu	0.3

total Fe is in the form of Fe<sub>2</sub>O<sub>3</sub>\*

$$\text{Mg\#} = 100 \cdot \text{Mg} / (\text{Mg} + \text{Fe}^{2+})$$

3a)

Table 2  
Representative compositions of the studied olivines

	1	2	3	4	5
	Xenocryst (Fig. 2a)		Xenocryst		Groundmass
	core	rim	core	rim	ol
SiO <sub>2</sub>	40.52	39.42	41.01	39.57	38.74
FeO <sup>tot</sup>	10.08	18.03	8.78	21.09	21.24
NiO	0.39	0.23	0.38	0.19	0.16
MnO	0.19	0.50	0.12	0.49	0.49
MgO	48.96	41.82	50.03	38.94	39.01
CaO	0.12	0.33	0.08	0.30	0.38
Sum	100.26	100.33	100.39	100.58	100.02

Cations based on 4 oxygens

Si	0.994	1.001	0.998	1.016	1.003
Fe	0.207	0.383	0.179	0.453	0.460
Ni	0.008	0.005	0.007	0.004	0.003
Mn	0.004	0.011	0.002	0.011	0.011
Mg	1.790	1.583	1.814	1.490	1.505
Ca	0.003	0.009	0.002	0.008	0.011
Fo (m%)	89.64	80.52	91.04	76.69	76.60

ol=olivine



Table 3  
Representative analyses of the studied orthopyroxenes and clinopyroxenes

	1	2	3	4	5	6	7
	Opx xeno- cryst (Fig. 2b) homogeneous core	Zoned cpx phenocryst (Fig. 2c) colourless core	rim	Zoned cpx phenocryst colourless core	rim	Zoned cpx phenocryst (Fig. 2e) light green core	rim
SiO <sub>2</sub>	56.07	52.47	42.92	53.25	45.43	49.95	44.61
TiO <sub>2</sub>	0.02	0.26	3.25	0.22	2.79	0.75	3.50
Al <sub>2</sub> O <sub>3</sub>	2.99	3.57	10.09	3.00	8.71	5.63	9.12
Cr <sub>2</sub> O <sub>3</sub>	0.59	0.58	0.11	0.65	0.30	0.06	0.10
FeO <sup>tot</sup>	5.67	2.79	7.05	2.55	6.42	10.54	6.33
MnO	0.13	0.10	0.14	0.07	0.12	0.14	0.13
MgO	33.70	16.89	11.38	17.05	12.13	11.39	11.87
CaO	0.78	22.58	22.66	22.72	22.67	19.66	22.57
Na <sub>2</sub> O	0.03	0.33	0.53	0.32	0.54	0.95	0.51
Sum	99.98	99.56	98.13	99.80	99.11	99.04	98.74

Formulae for 4 cations and 6 oxygens

Si	1.933	1.913	1.626	1.937	1.700	1.886	1.678
Al <sup>IV</sup>	0.067	0.087	0.374	0.063	0.300	0.114	0.322
Al <sup>VI</sup>	0.055	0.066	0.076	0.065	0.084	0.136	0.083
Ti	0.001	0.007	0.093	0.006	0.078	0.021	0.099
Cr	0.016	0.017	0.003	0.019	0.009	0.002	0.003
Fe <sup>3+</sup>	0.000	0.014	0.148	0.000	0.089	0.004	0.075
Fe <sup>2+</sup>	0.163	0.071	0.074	0.077	0.111	0.328	0.124
Mn	0.004	0.003	0.004	0.002	0.004	0.004	0.004
Mg	1.731	0.917	0.642	0.924	0.676	0.640	0.665
Ca	0.029	0.882	0.920	0.885	0.909	0.795	0.910
Na	0.002	0.023	0.039	0.022	0.039	0.069	0.037
Mg#	0.91	0.92	0.74	0.92	0.77	0.66	0.77

opx=orthopyroxene; cpx=clinopyroxene; Mg# = Mg/(Mg+Fe<sup>tot</sup>)

8		9		10		11		12		13		14		15	
Zoned cpx phenocryst		Cpx megacryst (Fig. 2f)						Cpx megacryst							
light green		colourless						colourless							
core		rim		homogeneous		spongy		overgrowth		homogeneous		spongy		overgrowth	
				core		zone		rim		core		zone		rim	
49.01	47.29			49.21	49.47			44.51			49.63	49.38			44.47
0.53	2.41			1.08	1.29			3.66			1.11	1.11			3.29
6.62	7.07			9.03	6.22			9.17			8.85	7.96			9.49
0.03	0.28			0.01	0.00			0.10			0.00	0.00			0.14
9.26	6.26			5.87	5.02			7.08			5.86	5.74			6.79
0.22	0.16			0.15	0.14			0.14			0.13	0.13			0.13
12.01	13.15			14.39	15.10			11.27			13.98	13.82			11.52
20.76	22.48			18.49	21.83			22.54			18.59	20.02			22.21
0.87	0.57			1.31	0.48			0.57			1.24	0.73			0.62
99.29	99.67			99.54	99.55			99.04			99.39	98.89			98.66
1.833	1.755			1.798	1.817			1.676			1.820	1.830			1.675
0.167	0.245			0.202	0.183			0.324			0.180	0.170			0.325
0.125	0.064			0.187	0.087			0.083			0.203	0.178			0.097
0.015	0.067			0.030	0.036			0.104			0.031	0.031			0.093
0.001	0.008			0.000	0.000			0.003			0.000	0.000			0.004
0.075	0.079			0.049	0.059			0.072			0.003	0.000			0.082
0.214	0.114			0.130	0.095			0.151			0.176	0.177			0.131
0.007	0.005			0.005	0.004			0.004			0.004	0.004			0.004
0.669	0.727			0.783	0.826			0.632			0.764	0.763			0.647
0.832	0.894			0.724	0.859			0.909			0.731	0.795			0.896
0.063	0.041			0.093	0.034			0.042			0.088	0.052			0.045
0.70	0.79			0.81	0.84			0.74			0.81	0.81			0.75

16	17
Cpx megacryst green homogeneous core	Groundmass cpx
48.33	47.37
1.63	2.48
7.46	6.49
0.00	0.10
11.73	6.40
0.21	0.12
8.78	13.20
19.87	22.62
2.11	0.47
100.13	99.25
1.811	1.767
0.189	0.233
0.140	0.053
0.046	0.070
0.000	0.003
0.110	0.072
0.257	0.127
0.007	0.004
0.490	0.734
0.798	0.904
0.153	0.034
0.57	0.79

Table 4  
Representative compositions of the studied spinels

	1	2	3	5	6
	Spinel megacryst	Ti-magnetite megacryst	Spinel in ol xenocryst (Fig. 2a)	Spinel in ol xenocryst	Groundmass Ti-magnetite
TiO <sub>2</sub>	0.47	10.40	0.16	0.37	20.46
Al <sub>2</sub> O <sub>3</sub>	61.67	6.19	52.86	29.20	1.70
Cr <sub>2</sub> O <sub>3</sub>	0.00	0.01	13.46	35.07	0.51
FeO <sup>tot</sup>	18.47	76.61	15.38	17.52	68.76
MnO	0.14	0.43	0.21	0.22	0.76
MgO	19.26	2.61	18.77	16.98	4.33
Sum	100.00	96.24	100.84	99.35	96.52

Formulae for 3 cations and 4 oxygens

Ti	0.009	0.281	0.003	0.008	0.560
Al	1.859	0.262	1.638	1.007	0.073
Cr	0.000	0.000	0.280	0.811	0.015
Fe <sup>3+</sup>	0.123	1.175	0.075	0.166	0.792
Fe <sup>2+</sup>	0.272	1.128	0.263	0.263	1.302
Mn	0.003	0.013	0.005	0.005	0.023
Mg	0.734	0.140	0.736	0.740	0.235
Mg#	0.65	0.06	0.68	0.63	0.10
Cr#	0.00	0.07	14.59	44.62	16.75

ol=olivine; Mg# = Mg/(Mg+Fe<sup>tot</sup>); Cr# = 100\*Cr/(Cr+Al)



Figure2

[Click here to download high resolution image](#)





Figure 11  
[Click here to download high resolution image](#)

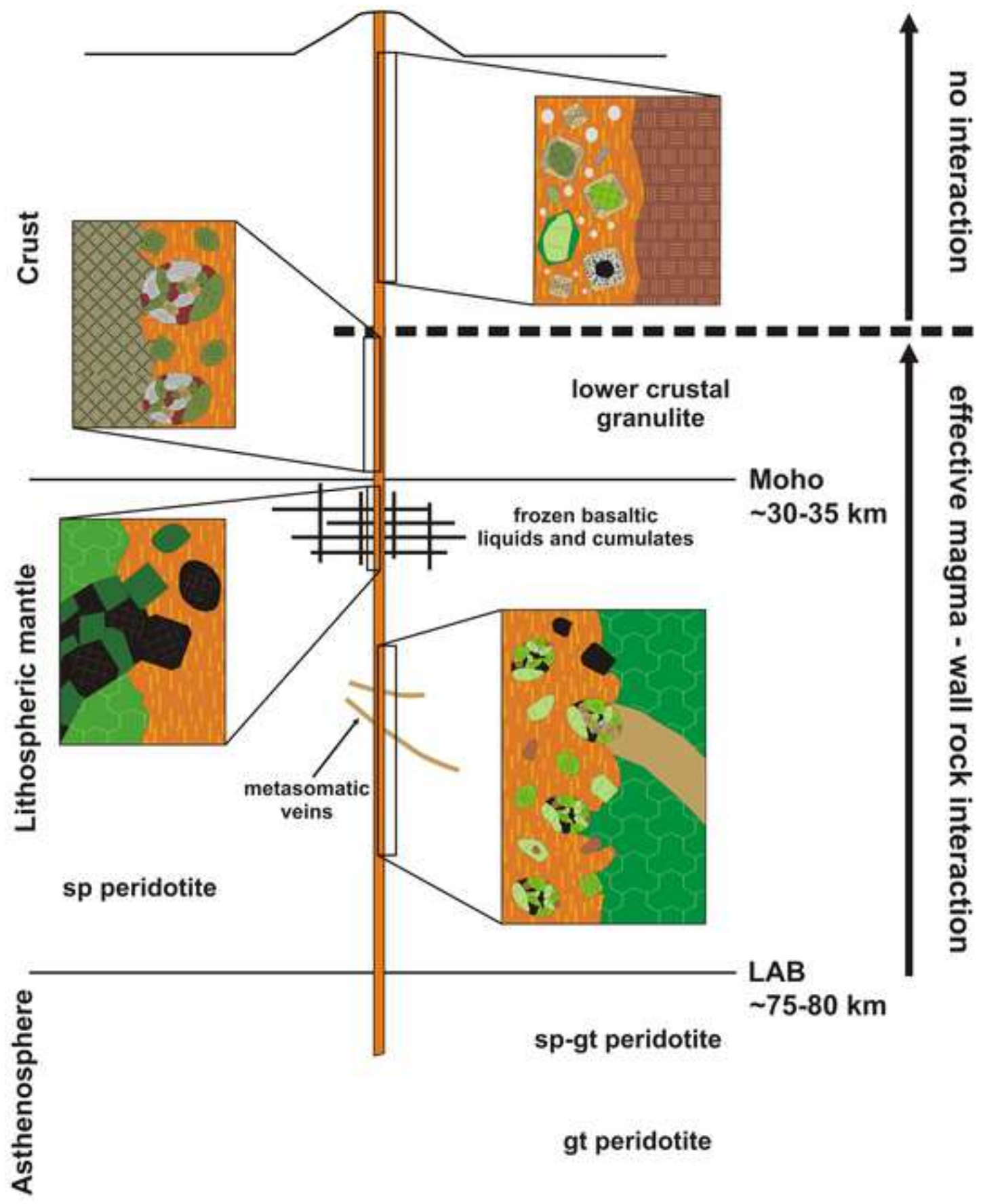


Table 5  
Details of the different methods and results of the estimated magma ascent rates and times

Volcanic field	Eruptive centre	Method	details	parameters	ascent time t (h)
	alkaline basaltic magma in general	fluid filled crack propagation velocity	Eq. (8) in Sparks et al. (2006)	$\Delta\rho=100 \text{ kg/m}^3$ ; $2w=0.5 \text{ m}$ ; $\eta=5.5 \text{ Pa s}$ $\Delta\rho=300 \text{ kg/m}^3$ ; $2w=1.5 \text{ m}$ ; $\eta=5.5 \text{ Pa s}$	<i>1.8*</i> <i>0.4*</i>
BBHVF	Bondoró-hegy	fluid filled crack propagation velocity	Eq. (8) in Sparks et al. (2006)	$\Delta\rho=100 \text{ kg/m}^3$ ; $2w=0.625-0.055 \text{ m}$ ; $\eta=5.5 \text{ Pa s}$ $\Delta\rho=300 \text{ kg/m}^3$ ; $2w=0.625+0.055 \text{ m}$ ; $\eta=5.5 \text{ Pa s}$	<i>1.6*</i> <i>0.8*</i>
BBHVF	Bondoró-hegy + Füzés-tó	xenolith settling rate	Eq. (1) in Spera (1984)	$R_n=0.1 \text{ m}$ ; $\Delta\rho=400 \text{ kg/m}^3$ ; $\eta=35 \text{ Pa s}$ $R_n=0.1 \text{ m}$ ; $\Delta\rho=600 \text{ kg/m}^3$ ; $\eta=5.5 \text{ Pa s}$	<i>166**</i> <i>40**</i>
BBHVF	Füzés-tó	Ca profile of olivine xenocryst	$T_{1/2}=(X_{1/2})^2/2D$ in Lasaga (1998)	in Table 6	<b>86.4</b>
BBHVF	Bondoró-hegy + Füzés-tó	dissolution of orthopyroxene xenocryst	$y=ax^b$ in Shaw (1999)	max. rim width=0.48 mm; $p=2 \text{ GPa}$ max. rim width=0.48 mm; $p=1 \text{ GPa}$ max. rim width=0.48 mm, $p=0.4 \text{ GPa}$	<b>1.4</b> <b>2.2</b> <b>7.1</b>
BBHVF	Szigliget + Sabar-hegy	Chemical profile of Fe-Ti oxides in granulite xenoliths	Eq. in Dégi et al. (2009)		<b>9</b> <b>20</b>
NGVF		thickness of chemical zoning bands in spinel	$t=x^2/D$		<b>18</b>
NGVF		transport and physical properties of the magmas			<b>37.5</b>
PVF	Racoş Bârc	Ca profile of olivine xenocryst	$T_{1/2}=(X_{1/2})^2/2D$ in Lasaga (1998)		<b>86.4</b> <b>115.2</b>

Numbers in bold: results of the calculations. Numbers in italics: ascent rates and times computed from the given results assuming 25 km (numbers with \*) and 60 km  
BBHVF=Bakony-Balaton Highland Volcanic Field, NGVF=Nógrád-Gömör Volcanic field, PVF=Perşani Volcanic Field  
For the details see the Electronic Appendix.

<b>ascent rate v (m/s)</b>	<b>result of calculation</b>	<b>reference</b>
<b>3.9</b>	v (m/s) ascent rate	this work
<b>15.9</b>		
<b>4.4</b>	v (m/s) ascent rate	this work
<b>9.2</b>		
<b>0.10</b>	v (m/s) settling rate	this work
<b>0.41</b>		
<i>0.19**</i>	t (h) interaction time	this work
<i>11.9**</i>	t (h) interaction time	this work
<i>7.5**</i>		
<i>2.3**</i>		
<i>0.77*</i>	t (h) interaction time	Dégi et al. (2009)
<i>0.35*</i>		
<i>0.93**</i>	t (h) interaction time	Szabó and Bodnar (1996)
	t (h) residence time	Szabó and Bodnar (1996)
<i>0.19**</i>	t (h) interaction time	Harangi et al. (in press)
<i>0.14**</i>		

(numbers with \*\*) long ascent path in the lithosphere.



Table 6  
 Calculated residence times of the studied olivine xenocrysts

Crystal	Rim A		Rim B		inner plateau	
	$X_{1/2}$ A ( $\mu\text{m}$ )	$T_{1/2}$ A (days)	$X_{1/2}$ B ( $\mu\text{m}$ )	$T_{1/2}$ B (days)	$X_{1/2}$ I P ( $\mu\text{m}$ )	$T_{1/2}$ I P (days)
<b>xen 1 (Fig. 6a)</b>	10	3.5	9	2.9	108	425
<b>xen 2</b>	12	5.2				
<b>xen 3</b>	8	2.3	12	5.2		
<b>xen 4</b>	10	3.6				
<b>xen 5_p1</b>	12	5.2	8	2.3		
<b>xen 5_p2</b>	8	2.3				
<b>Average</b>	<b>10</b>	<b>3.7</b>	<b>9.7</b>	<b>3.5</b>	<b>108</b>	<b>425</b>

$T_{1/2} = (X_{1/2})^2 / 2D$ , where  $T_{1/2}$  is the time necessary to reach the half of the equilibration concentration of Ca in olivine;  $X_{1/2}$  is the distance from crystal rim to this point; D=diffusion coefficient for Ca in olivine.

Appendix

[Click here to download Supplementary Material: Appendix.doc](#)

Figure A1

[Click here to download Supplementary Material: FigA1.tif](#)

Figure A2

[Click here to download Supplementary Material: FigA2.tif](#)

Dear Professor I.E.M. Smith and Professor R.V. Fodor,

we are thankful for your valuable suggestions and comments which were very helpful in the revision.

Please find below our answers / comments (text with blue colour) to your suggestions.

Yours sincerely,

M. Éva Jankovics

on behalf of the authors

**Comments of Professor I.E.M. Smith:**

This manuscript has been reviewed and the recommendation is that you be given the opportunity to revise. My additional comment is that in your revision you should try to shorten the manuscript. I have no specific suggestions as to how best to do this but if you can shorten to a length more typical of Bulletin of Volcanology - approximately 7000 words you will have achieved a more focussed manuscript on this very interesting topic.

We extensively shortened the former version of the manuscript. On one hand, we deleted a lot of unnecessary sentences and repetitions with the help of Professor R.V. Fodor's suggestions. On the other hand, we took out the detailed descriptions and hypothetical background of the magma ascent rate estimations from the main article text, and took them into an appendix (after numerous corrections, changes and shortening as well). In the main body text, we made a separate heading (before the Discussion heading) for the magma ascent rate estimates and wrote there only shortly our results given by the different methods. We tried to focus the discussion as far as possible.

**Comments of Professor R.V. Fodor:**

1) My comments and edits are in the attached **Word document**. Please note that I converted the PDF into Word for easier and clearer editing, especially for line-editing – namely, correcting and improving the written English by cross-outs and insertions. Also important to

note is that the PDF to Word conversion put the line numbers into the text, and it distorted or omitted some symbols. Even though there are these distortions in the Word doc, the editing process, while long for me, was much faster compared to creating edit 'flags' in a PDF.

I put my corrected English in **red font**, and where I questioned or commented on something, I wrote in *red italics*. The authors will see that I removed many unnecessary words to help shorten the text, and to make the reading more clear and concise.

Also note this: there are many places where a comma is needed in the sentence. To call attention to those places, I purposely left an extra space before the comma (and I did not make the comma red). So, this will require carefully looking at each line in the Word doc

Thank you for all of the English corrections and questions / comments. We corrected the text carefully and based on your comments / questions we made a lot of changes.

2) My general comments are that this manuscript is certainly appropriate for Bulletin of Volcanology. It is a detailed, well thought-out presentation of the characteristics and dynamics of some basalts and their eruptions that will make a contribution in its many ways for which ascent rates are evaluated. One concern I have, however (and it's mentioned in the edited Word doc), is that the descriptions for these various calculations (for ascent) are too long. My editing includes some suggestions for shortening, but the authors can better address this concern about shortening such a lengthy section within the Discussion. I think that there is a chance the authors will lose the reader if they don't make the ascent rate presentation more concise.

You are right concerning the length of these descriptions. We took them out from the main article text, and moved them into an appendix (after numerous corrections, shortening and changes as well). In the main body text, we made a separate heading (before the Discussion heading) for the magma ascent rate estimates and wrote there only shortly our results given by the different methods.

Maybe more important to address here is the presentation on style of eruption (in the Discussion). It adds little to the paper. This is because there are too many unknowns (and the authors acknowledge this in some words) (e.g., channelway diameters; availability of crustal rocks to ascending magma, .....is the crustal rock easily fragmented; wider channelways may

lessen the chances of entraining, and more....). I don't think that you can make judgments about a style because something is missing from the magma (such as crustal fragments). Most alkalic basalt do not have xenoliths of any type. The main contribution of the paper seems to be ascent rate calculations, and placing weight on whether or not certain kinds of xenoliths are present or absent distracts from the calculations by making speculations about 'style'.

We think that because of the length and inadequate construction of the former version of the manuscript, it was difficult to understand what the main points are. We tried to change the construction a lot and to focus on the essentials. We omitted the highly uncertain parts from the text (concerning mainly the ascent style) and tried to write clearly the suggested ascent history of these basaltic magmas.

We think that based on the absence of something, some suggestions can be made (it is a similar case as when somebody write in a paper that "based on the absence of garnets in the peridotite xenoliths, they can derive from shallower depths, i.e., from the spinel peridotite region"). Here, we just would like to draw attention to the fact, that the magmas incorporated a huge amount of fragments and crystals from the lithosphere at mantle depths as well as a number of fragments from the lower crust, but at shallower depths (middle-upper crust) no additional wall rock fragments were entrained. We tried to think about what could be the reason for this, but because there are many unknown parameters, we did not go into the details in the revised version how to interpret this fact. We only made the suggestion that the absence of any middle-upper crustal materials in the magmas, together with the fact that from greater depths the magmas incorporated a vast amount of fragments, can suggest some changes in the ascent style (an effective magma-wall rock interaction can be reasonable at greater depths, but no interaction can be inferred between magma and wall rock at shallower depths).

3) Some other suggestions:

a) when reporting the wt.% in the text, use on 00.0 and not 00.00. The detail of the hundredths decimal place is for the Tables....and it only burdens readers of the text with largely insignificant numbers. You only have to present the general composition in the text (e.g. 50.2 wt.%, and not 50.17), as leaving only tenths place makes for a cleaner text. One exception is for numbers <1.0%. Using two decimal places is justified there (e.g., 0.78 wt.%).

Thank you, we corrected every numbers in the text, as suggested.



b) about the word 'alkaline' when used with basalt. The US Geological Survey guidelines for authors reports that 'alkalic' is the proper adjective for basalts, and not 'alkaline'. I have scanned and included below the USGS recommendations for such geologic adjectives.

I know that this is a European authorship, but I think that alkalic is used world-wide. I understand, too, that the authors may have a history of using 'alkaline' and will want to keep it that way – but I wanted to give my opinion and the recommendations for US government publications (and also, the Hawaiian terminology has long used 'alkalic').

We accept the comment on the usage of the alkalic versus alkaline adjective for basalts. So far, we have used consistently the alkaline adjective as we could read and hear it in many publications and conferences. We do not know whether there is a difference in the American and British English usage for this term. If both adjectives are acceptable we would like to keep the alkaline term.

c) line 166: 'Petrography and whole-rock compositions' may be a better heading. It's not really presenting petrochemistry as the headline presently read.

All right, we corrected.

line 288: Remove heading 'olivine profiles' -- what following line 288 can be part of the olivine presentation before line 288. (also, as noted in my edits: much of that profile information is for Figure caption that goes with the profiles).

All right, we changed.

line 422 'Crystal diversity' doesn't say much. I thing 'Mineral Sources', or 'Sources for the diverse mineral assemblage' is more what this section presents.

All right, we corrected for 'Sources for the diverse mineral assemblage'.

1 | M. Éva Jankovics<sup>1,2,\*</sup>, Gábor Dobosi<sup>2,3</sup>, Antal Embey-Isztin<sup>4</sup>, Balázs Kiss<sup>1,2</sup>, Tamás Sági<sup>2,1</sup>,  
2 | Szabolcs Harangi<sup>1,2</sup>, Theodoros Ntaflos<sup>5</sup>

3 |  
4 | Origin and ascent history of unusually crystal-rich alkaline basaltic magmas from the western  
5 | Pannonian Basin

6 |  
7 | <sup>1</sup>[Department of Petrology and Geochemistry, Eötvös Loránd University, Pázmány Péter](#)  
8 | [sétány 1/C, H-1117 Budapest, Hungary](#)

9 | <sup>2</sup>MTA-ELTE Volcanology Research Group, Pázmány Péter sétány 1/C, H-1117 Budapest,  
10 | Hungary

11 | <sup>2</sup>[Department of Petrology and Geochemistry, Eötvös Loránd University, Pázmány Péter](#)  
12 | [sétány 1/C, H-1117 Budapest, Hungary](#)

13 | <sup>3</sup>Institute for Geological and Geochemical Research, Research Centre for Astronomy and  
14 | Earth Sciences, Hungarian Academy of Sciences, Budaörsi út 45., H-1112 Budapest, Hungary

15 | <sup>4</sup>Department of Mineralogy and Petrology, Hungarian Natural History Museum, Ludovika tér  
16 | 2., H-1083 Budapest, Hungary

17 | <sup>5</sup>Department of Lithospheric Research, University of Vienna, Althanstrasse 14, A-1090  
18 | Vienna, Austria

19 |  
20 | \*Corresponding author. E-mail address: jeva182@gmail.com

21 | Telephone number: +36-1/372 25 00/8359; +36-30/547 33 71

22 | Fax number: +36-1/381 21 08

23 |

24 | **Abstract**

25 |

26 The last eruptions of the monogenetic Bakony-Balaton Highland Volcanic Field (western  
27 Pannonian Basin, Hungary) produced unusually crystal- and xenolith-rich alkaline basalts  
28 which are unique among the alkaline basalts of the Carpathian-Pannonian Region. Similar  
29 alkaline basalts are only rarely known in other volcanic fields of the world. These special  
30 basaltic magmas fed the eruptions of two closely located volcanic centres: the Bondoró-hegy  
31 and the Fűzes-tó scoria cone. Their uncommon enrichment in diverse crystals produced  
32 unique rock textures and modified original magma compositions (13.1-14.2 wt.% MgO, 459-  
33 657 ppm Cr, 455-564 ppm Ni contents).

34 Detailed mineral-scale textural and chemical analyses revealed that the Bondoró-hegy and  
35 Fűzes-tó alkaline basaltic magmas have a complex ascent history, and that most of their  
36 minerals (~30 vol.% of the rocks) represent foreign crystals derived from different levels of  
37 the underlying lithosphere. The most abundant xenocrysts, olivine, orthopyroxene,  
38 clinopyroxene and spinel, were incorporated from different regions and rock types of the  
39 subcontinental lithospheric mantle. Megacrysts of clinopyroxene and spinel could have  
40 originated from pegmatitic veins / sills which probably represent magmas crystallized near the  
41 crust-mantle boundary. Green clinopyroxene xenocrysts could have been derived from lower  
42 crustal mafic granulites. Minerals that crystallized in situ from the alkaline basaltic melts  
43 (olivine with Cr-spinel inclusions, clinopyroxene, plagioclase, Fe-Ti oxides) are only  
44 represented by microphenocrysts and overgrowths on the foreign crystals. The vast amount of  
45 peridotitic (most common) and mafic granulitic materials indicates a highly effective  
46 interaction between the ascending magmas and wall rocks at lithospheric mantle and lower  
47 crustal levels. However, fragments from the middle and upper crust are absent from the  
48 studied basalts, suggesting a change in the style (and possibly rate) of magma ascent in the  
49 crust. These xenocryst- and xenolith-rich basalts yield diverse tools for estimating magma  
50 ascent rate that is important for hazard forecasting in monogenetic volcanic fields. According

51 to the estimated ascent rates, the Bondoró-hegy and Füzes-tó alkaline basaltic magmas could  
52 have reached the surface within hours to few days, similarly to the estimates for other eruptive  
53 centres in the Pannonian Basin which were fed by "normal" (crystal- and xenolith-poor)  
54 alkaline basalts.

55

56 **Keywords**

57 alkaline basalt, ascent history, crystal-rich, magma ascent rate, monogenetic volcanism,

58 xenocryst, xenolith

59

## 60 Introduction

61

62 Monogenetic basaltic volcanic fields consist of small individual eruptive centres  
63 characterized by a single brief eruption (Walker, 1993) and low magma supply (e.g.,  
64 Hasenaka and Carmichael, 1985; Takada, 1994). These monogenetic eruptions of basalt are  
65 generally assumed to be simple in terms of volcanology and petrology. That is, they produce  
66 small volcanic edifices during continuous activity within a relatively short time span, and are  
67 fed by a single, compositionally discrete batch of magma (e.g., Connor and Conway 2000).  
68 However, several authors suggested that individual eruptive centres can be characterized by  
69 multiple eruptions involving different magma batches with hiatuses during their activity (e.g.,  
70 Reiners 2002; Martin and Németh 2005; Brenna et al. 2010, 2011; Needham et al. 2011,  
71 Shane et al. 2013) implying a complex evolution history of the magmatic system. These  
72 studies focused mainly on the compositional variations of the feeding magma batches and  
73 suggest differences in their source regions and / or degrees of partial melting. However,  
74 processes acting during the ascent of the magma batches are also important ~~to determine~~  
75 (Brenna et al. 2010). This is essential information because the evolution of the magma in the  
76 feeding system can have a significant effect on the rate and style of magma ascent, and  
77 therefore on the nature of eruptions (e.g., Ruprecht and Bachmann 2010; McGee et al. 2012;  
78 Russell et al. 2012). Detailed textural and chemical analyses of phenocrysts in basalts can  
79 provide insights into the details of their magma evolution (e.g., Dobosi 1989; Dobosi et al.  
80 1991; Roeder et al. 2001, 2003, 2006; Smith and Leeman 2005; Jankovics et al. 2009, 2012).

81 The monogenetic Bakony-Balaton Highland Volcanic Field, located in the western part of  
82 the Carpathian-Pannonian Region, was active for approximately 6 My. Its last active phase  
83 was closed by two eruptive centres: the Bondoró-hegy (2.3 Ma; Balogh and Pécskay 2001)  
84 and the Füzés-tó scoria cone (2.6 Ma; Wijbrans et al. 2007) each fed by alkaline basaltic

85 | magmas with special compositions and petrological appearances (Jankovics et al. 2009,  
86 | 2012). These alkaline basalts are characterized by extremely high Mg, Ni and Cr contents and  
87 | are unusually rich in diverse crystals and xenoliths (peridotite, mafic granulite). Similar  
88 | magmas did not erupt in the above mentioned volcanic field and even in the other six volcanic  
89 | fields in the whole Carpathian-Pannonian Region (CPR). Nevertheless, basalts of numerous  
90 | eruptive centres in the region contain diverse xenoliths. In other volcanic fields of the world,  
91 | magmas with characteristics similar to those of the Bondoró-hegy and Füzes-tó scoria cone  
92 | are known (e.g., Ancochea et al. 1987; Mattsson 2012; Kozákov Hill in Ulrych et al. in press)  
93 | but they are rare. Due to their crystal-rich feature these rocks provide unique insights into the  
94 | ascent history of basaltic magmas. Following the detailed investigations and descriptions of  
95 | the Füzes-tó basalt (Jankovics et al. 2009, 2012), in this study we analysed the highly-similar  
96 | (both in age and petrology) basalt of Bondoró-hegy ~~(both in age and petrology)~~ and revealed  
97 | its ascent history. It is generally assumed that such xenolith-rich magmas can reach the  
98 | surface very rapidly. We estimated the ascent rates of these xenocryst- and xenolith-rich  
99 | alkaline basalts, and compared the results with xenolith-poor basalts. Understanding the  
100 | ascent history and estimating the magma ascent velocity is important in monogenetic volcanic  
101 | fields for their volcanic hazard assessments. This study demonstrates the importance of the  
102 | especially crystal-rich basaltic magmas of monogenetic volcanic fields for enabling  
103 | estimating the magma ascent rate by several different methods.

104

## 105 **Geological setting**

106

107 | The Pannonian Basin is a Miocene extensional back-arc basin surrounded by the Alpine,  
108 | Carpathian and Dinarides orogenic belts (Fig.1a). It is characterized by thin lithosphere (50-  
109 | 80 km) and crust (22-30 km) coupled with high heat flow ( $>80 \text{ mW/m}^2$ ; Csontos et al. 1992;

110 Fodor et al. 1999; Tari et al. 1999; Bada and Horváth 2001; Lenkey et al. 2002). These  
111 features are due to the initial syn-rift phase (17–12 Ma; Horváth 1995) of the Pannonian Basin  
112 that was characterized by subduction roll-back, related back-arc extension and lithospheric  
113 thinning (Csontos et al. 1992; Horváth 1993; Tari et al. 1999). This was followed by the Late  
114 Miocene–Pliocene post-rift phase (e.g., Horváth 1995) which was accompanied by thermal  
115 subsidence, thickening of the lithosphere and sedimentation in the basin areas. Tectonic  
116 inversion has characterized the Pannonian Basin since the late Pliocene due to the push of the  
117 Adriatic plate from the southwest and blocking by the East European platform in the east  
118 (Horváth and Cloetingh 1996).

119 Post-extensional alkaline basaltic volcanism occurred from 11 to 0.13 Ma in the region,  
120 mainly on its marginal parts, which formed monogenetic volcanic fields. The tectonic  
121 background of the alkaline basaltic magmatism is still under debate. Several researchers  
122 suggested that localised mantle plume fingers (deriving from a common mantle reservoir  
123 named “European Asthenospheric Reservoir”; Hoernle et al. 1995) could be responsible for  
124 the alkaline basaltic volcanism in Western and Central Europe, accordingly in the Pannonian  
125 Basin as well (Granet et al. 1995; Seghedi et al. 2004). However, Harangi and Lenkey (2007)  
126 and Harangi (2009) argued against the plume-related magmatism. They suggested that the  
127 significantly stretched Pannonian Basin provided suction in the sublithospheric mantle and  
128 generated an asthenospheric mantle flow from below the thick Alpine regime which could  
129 lead to the partial melting of the heterogeneous upper mantle.

130 The Bakony-Balaton Highland Volcanic Field (Fig. 1b) comprises approximately 150-200  
131 eruptive centres (Németh and Martin 1999a, 1999b) that are erosional remnants of maars, tuff  
132 rings, scoria cones and shield volcanoes (e.g., Jugovics 1968; Németh and Martin 1999a,  
133 1999b; Martin et al. 2003). Several of these alkaline basalt occurrences contain ultramafic and  
134 mafic xenoliths, as well as discrete megacrysts which were extensively studied in the past

135 decades (e.g., Embey-Isztin 1976; Embey-Isztin et al. 1989, 1990, 2001a, 2001b, 2003;  
136 Downes et al. 1992; Downes and Vaselli 1995; Dobosi et al. 2003; Dégi et al. 2009). These  
137 studies together with those for whole-rock geochemistry of the basalts (e.g., Embey-Isztin et  
138 al. 1993a, 1993b; Embey-Isztin and Dobosi 1995; Seghedi et al. 2004) have yielded important  
139 information on the nature of the upper mantle beneath the area and the partial melting  
140 processes. Based on several studies (e.g., Embey-Isztin et al. 1989, 1990, 2001a; Szabó et al.  
141 2004; Hidas et al. 2007; Dégi et al. 2009) we have an extensive knowledge about the structure  
142 of the whole lithosphere as well.

143

#### 144 **Volcanological background**

145

146 In this paper, we describe the volcanological background for the Bondoró-hegy eruptive  
147 centre. The features of the Füzes-tó scoria cone were reported in a previous paper (Jankovics  
148 et al. 2009). Bondoró-hegy volcano is one of the most complex eruption centres of this  
149 volcanic field ~~which and~~ consists of several discrete different eruptive units: basal tuff ring  
150 pyroclastics with a lava lake, reworked basaltic debris beds, lava flow units (1<sup>st</sup> and 2<sup>nd</sup> lava  
151 flow) and capping scoria cone associated with the 3<sup>rd</sup> lava flow (Kereszturi et al. 2010). The  
152 capping scoriaceous basalt (e.g., spindle and scoriaceous bombs) and the 3<sup>rd</sup> lava flow unit  
153 (representing the youngest eruptive phase) are rich in xenoliths of upper mantle and lower  
154 crustal origins (peridotite, wehrlite, clinopyroxenite, mafic granulite) and in clinopyroxene  
155 and spinel megacrysts.

156 In an outcrop of the capping scoria unit (in the breached side of the scoria cone remnant),  
157 Kereszturi et al (2010) described a dyke that crosscuts the scoriaceous breccia. Based on our  
158 field observations (Fig. 2), this massive dyke has an average width of  $0.625 \pm 0.055$  m and can  
159 be interpreted as a feeder dyke of the scoria cone.



160 Several K-Ar ages are available: the basalt of the lava lake is estimated at about  
161  $\leq 3.86 \pm 0.20$  Ma and the 2<sup>nd</sup> lava unit at about  $2.90 \pm 0.62$  Ma (Balogh et al. 1986). A sample  
162 from the 3<sup>rd</sup> lava flow unit gave an age of  $2.29 \pm 0.22$  Ma (Balogh and Pécskay 2001).  
163 According to Kereszturi et al. (2010), these ages represent the best fit with the geological and  
164 stratigraphical observations. Unfortunately, Bondoró-hegy was not included in the  $^{40}\text{Ar}/^{39}\text{Ar}$   
165 dating of the Balaton Highland basaltic rocks (Wijbrans et al. 2007). Based on the preferred  
166 K-Ar ages (that indicate prolonged volcanic activity) and the discordance between the  
167 phreatomagmatic unit and the subsequent lava flows (implying a significant time gap),  
168 Bondoró-hegy can be regarded as a polycyclic monogenetic volcano (Kereszturi et al. 2010).

169

## 170 **Petrography and whole-rock compositions**

171

172 Samples of the Bondoró-hegy were collected from the 3<sup>rd</sup> lava flow unit. Samples of the  
173 Fűzes-tó scoria cone were collected in the inner slope around the central depression (various  
174 basaltic bombs). In this paper, we describe only the features of the Bondoró-hegy basalt, the  
175 descriptions of the Fűzes-tó basalt are in Jankovics et al. (2009, 2012). Figure 3a shows the  
176 typical petrographic appearance of the studied crystal-rich alkaline basalts.

177 | ~~In this heading, the~~ The term ‘phenocryst’ is here used in a general sense, i.e., for larger, up  
178 | to 5 mm, crystals in fine-grained groundmasses, regardless of their origins (i.e., phenocryst  
179 | *sensu lato*). ~~After that, in the next headings following,~~ the term ‘phenocryst’ ~~is already has~~  
180 | been used in a genetic sense, i.e., for crystals that have grown in situ in the magma in which  
181 | they are found now (i.e., phenocryst *sensu stricto*).

182 The studied lava samples have porphyritic texture characterized by non- to low-  
183 vesicularity and ~30 vol.% anhedral to euhedral phenocrysts (on a vesicle-free basis). The  
184 phenocryst assemblage consists of olivine, clinopyroxene, orthopyroxene and spinel

185 | characterized by variable forms and sizes, and ~~they crystals~~ often occur together as crystal  
186 | clots (Fig. 4d). Microphenocrysts (<150 µm) are clinopyroxene, olivine, plagioclase and Fe-  
187 | Ti-oxides. The fine-grained groundmass is composed of microlitic feldspars (plagioclase and  
188 | alkali feldspar), clinopyroxene, olivine, Fe-Ti-oxides, apatite and some glass.

189 | Most of the olivine phenocrysts (up to 5 mm) are characterized by rounded and embayed  
190 | margins. These crystals ~~often~~commonly show undulose extinction, and have bright rims (with  
191 | diffuse boundaries toward the crystal interiors) in the backscattered electron (BSE) images  
192 | (e.g., Fig. 4a). They frequently contain subhedral-anhedral (often rounded), light green to  
193 | brown spinel inclusions which range in size from ~50 to 300 µm. The smaller (150-900 µm)  
194 | olivine grains are euhedral to subhedral and often skeletal and their outermost margin is  
195 | frequently iddingsitised. They often contain black, euhedral-subhedral chromian spinel  
196 | inclusions (~3-10 µm).

197 | Orthopyroxene crystals (up to 2.4 mm) are always surrounded by fine-grained rims of  
198 | various thicknesses (Fig. 4c) consisting of olivine, clinopyroxene, glass and rarely spinel. The  
199 | outermost part of this corona often contains numerous Fe-Ti-oxides as well. This fine-grained  
200 | rim is frequently overgrown by a pale brown, twinned and sector zoned clinopyroxene.

201 | Clinopyroxene phenocrysts (up to 3 mm) are euhedral to subhedral in shape and usually  
202 | have an anhedral, rounded core (with a sharp boundary) and a pale brown, twinned, sector  
203 | zoned rim characterized by various thicknesses (rarely some sector zoned clinopyroxenes  
204 | without a rounded crystal core are also found; Fig. 4i). Two types of the anhedral, variously  
205 | resorbed cores can be distinguished. The first and more frequent type is colourless under the  
206 | optical microscope, and darker grey than the rim in the BSE images (Fig. 4d, e). The other  
207 | type is light green under the optical microscope, and lighter grey than the surrounding rim in  
208 | the BSE images (Fig. 4f) which indicates reverse zoning. The green cores often have spongy  
209 | or sieved texture.

210 Spinel crystals (up to 0.5 mm) occur as individual crystals in the matrix (Fig. 4b) and as  
211 inclusions in olivine phenocrysts (Fig. 4a). They usually have ragged, anhedral margins, are  
212 characterized by variable colours (light green to brown), and often have a bright (Ti-  
213 magnetite) overgrowth rim (with a relatively sharp boundary toward the crystal interior) in the  
214 BSE images where it is in contact with the groundmass (Fig. 4a, b).

215 All these disequilibrium textures (ragged, rounded, resorbed, embayed, spongy features)  
216 suggest a xenocrystic origin for the anhedral olivines, colourless and green cores of  
217 clinopyroxene phenocrysts, orthopyroxenes and spinels.

218 In addition to the abundant xenocrysts, the studied samples include numerous peridotite  
219 xenoliths. These are spinel peridotites which occasionally contain amphiboles (Fig. 3b).  
220 Along the contact between the peridotite and basalt the peridotitic orthopyroxene grains have  
221 the same fine-grained rims as the orthopyroxene xenocrysts in the basaltic groundmass.  
222 Therefore, these rims are interpreted as mineral-melt reaction products. Similarly to most of  
223 the olivine xenocrysts, the olivine grains in the peridotite xenoliths often have undulose  
224 extinction which implies deformation.

225 Additionally, clinopyroxene and spinel megacrysts are also common. Most of the  
226 clinopyroxene megacrysts (up to 6 cm, elongated) are colourless, they have homogeneous  
227 interiors crosscutting with ~~former~~ cracks filled with secondary fluid inclusions, and are  
228 overgrown by a pale brown, zoned clinopyroxene rim similar to that of the clinopyroxene  
229 xenocrysts. Spongy zones are present between this rim and the homogeneous part of the  
230 megacrysts (Fig. 4g). In the spongy zones, small inclusions of feldspars (plagioclase and  
231 alkali feldspar) and skeletal spinels are present (Fig. 4h). Besides the colourless megacrysts,  
232 one piece of a green clinopyroxene megacryst has also been found. The spinel megacrysts are  
233 ~1-2 cm in size, mostly dark green, but one was black, under the optical microscope.

234 The whole rock composition of the Bondoró-hegy basalt has been described by [Jugovics](#)  
235 [\(1976\)](#) and [Embey-Isztin et al. \(1993a, 1993b\)](#). The compositional data identify the lavas of  
236 Bondoró-hegy as undersaturated basanite ([Table 1](#)), similar to the compositions of the other  
237 basalts in the region, however, the basaltic rocks from Bondoró-hegy are extremely rich in  
238 MgO (13.1-13.9 wt.%). Similar MgO enrichment has been reported only at the Fűzes-tó  
239 scoria cone from the Pannonian Basin (see [Fig. 1b](#)), which has 13.4-14.2 wt.% MgO content  
240 ([Jankovics et al. 2009](#)). This is ~~correlated~~ consistent with the abundance of xenocrystic olivine  
241 and orthopyroxene. The high MgO content is accompanied by extreme enrichment in Ni and  
242 Cr contents (455-474 and 459-489 ppm, respectively; [Embey-Isztin et al. 1993a, 1993b](#)), also  
243 caused by the presence of abundant peridotitic xenocrysts. The incompatible trace element  
244 content of the Bondoró-hegy basalt is approximately the same as that of the other basalts of  
245 the region, though some incompatible trace element and radiogenic isotope ratios are  
246 different. While the lavas of the Bakony-Balaton Highland Volcanic Field tend to show  
247 higher K/Nb, Rb/Nb and lower Ce/Pb, as well as higher  $^{207}\text{Pb}/^{204}\text{Pb}$  and  $^{87}\text{Sr}/^{86}\text{Sr}$ , the opposite  
248 is true for the Bondoró-hegy basalt. This is explained by the involvement of an enriched  
249 lithospheric component in the lavas, which is missing from the Bondoró-hegy basaltic magma  
250 ([Embey-Isztin et al. 1993b](#)).

251

## 252 Mineral chemistry

253

254 Analyses of minerals in the Bondoró-hegy basalt were obtained on a JEOL Superprobe  
255 733 using wavelength-dispersive spectrometers at the Institute for Geological and  
256 Geochemical Research in Budapest, Hungary. Analytical conditions were 20 kV accelerating  
257 voltage, 35 nA beam current, and all analyses were made against mineral standards. Raw data  
258 were corrected by the ZAF correction program of JEOL. Olivine profiles of the Fűzes-tó

259 basalt were determined using a CAMECA SX100 electron microprobe equipped with four  
260 WDS and one EDS at the University of Vienna, Department of Lithospheric Research  
261 (Austria). The operating conditions were as follows: 15 kV accelerating voltage, 20 nA beam  
262 current, 20 s counting time on peak position, focused beam diameter and PAP correction  
263 procedure for data reduction. The following standards were applied: albite (for Si, Al);  
264 almandine (for Fe); olivine (for Mg); wollastonite (for Ca); spessartine (for Mn) and Ni-oxide  
265 (for Ni). The mineral compositions of the Füzés-tó basalt are discussed in [Jankovics et al.](#)  
266 [\(2009, 2012\)](#).

267

### 268 *Olivine*

269

270 Olivine crystals display a wide range of Fo ([Table 2](#)). The xenocrysts are chemically  
271 homogeneous and typically have Fo from 89.5 to 92 mol% ( $Fo=100*Mg/(Mg+Fe)$ , all Fe is  
272 assumed to be divalent). They have thin rims with lower Fo (72.1-81.4 mol%), which overlap  
273 that of the groundmass olivines (76.1-76.7 mol%).

274 Olivine xenocrysts have low CaO and high NiO contents (0.05-0.12 wt.% and 0.33-0.39  
275 wt.%, respectively), while their rims are enriched in CaO (0.16-0.40 wt.%) and depleted in  
276 NiO (0.16-0.34 wt.%) ([Fig. 5](#)). CaO shows a weak negative, whereas NiO shows a weak  
277 positive correlation with Fo content ([Fig. 5](#)). The highest Ca and lowest Ni contents are in  
278 groundmass olivines (0.38-0.57 wt.% CaO and 0.14-0.18 wt.% NiO). The compositions of  
279 the studied xenocrysts resemble those of the olivines of the peridotite xenoliths in the Balaton  
280 Highland ([Fig. 5](#)).

281 All olivine Fo profiles are symmetric to the centre of the grain, but their shapes differ  
282 ([Fig. 6](#)). Olivine xenocrysts have well-defined inner plateaus bounded by large compositional  
283 gradients toward the rims ([Fig. 6a, b](#)). Their inner part contains less than 500 ppm Ca, ~3000

284 ppm Ni and ~90 mol% Fo. In the rims, Ca sharply increases to >3000 ppm, while Ni and Fo  
285 sharply decrease to <1000 ppm and to 75 mol%, respectively. In several xenocrysts, the inner  
286 plateaus show some compositional variations (maybe related to healed cracks or tiny  
287 inclusions) (Fig. 6b). The profiles of olivine phenocrysts have a shield-like shape indicating a  
288 gradual compositional variation toward the rims (Fig. 6c). The Ca and Ni profiles are less  
289 smooth than those in xenocrysts, which may be the result of skeletal growth of the  
290 phenocrysts. Compared to the xenocrysts, the Ca content of their inner part is significantly  
291 higher (~1250 ppm), while the Ni and Fo contents are lower (between ~2000-2500 ppm and  
292 ~87 mol%, respectively). Phenocrysts and xenocrysts can be distinguished in the Fo-NiO  
293 diagram (Fig. 7), which shows that olivine xenocrysts show linear trends towards the rims  
294 indicating that the formation of core-to-rim zoning ~~was~~ were mainly driven by diffusion.  
295 However, phenocrystic olivine has a curved trend towards the rims that can be interpreted as  
296 mainly growth-related core-to-rim zoning considering the implications of Costa et al. (2008).

297 The compositions of the xenocryst rims (Fig. 5, 6a) are similar to those of the olivine  
298 xenocryst rims and olivine phenocryst rims in the Füzestó basalt (Jankovics et al. 2009,  
299 2012). The formation of these Fe-rich, ~~bright~~ rims ~~of olivine xenocrysts~~ can be explained by  
300 diffusion during re-equilibration of the xenocryst with the host basaltic magma (note the  
301 diffuse boundary toward the crystal interior; Fig. 4a, d) as well as some subsequent  
302 crystallization of phenocrystic olivine on the xenocrysts.

303

#### 304 *Orthopyroxene*

305

306 Orthopyroxenes occur only as xenocrysts in the studied basalt. They are enstatites  
307 (Morimoto et al., 1988) with high Mg#s (0.91-0.92;  $Mg/(Mg+Fe^{tot})$ ) and contain 2.9-3 wt.%

308 Al<sub>2</sub>O<sub>3</sub> (Table 3). These compositions are characteristic for mantle orthopyroxenes similar to  
309 those of the peridotite xenoliths in the Balaton Highland (Embey-Isztin et al. 2001a).

310

311 *Clinopyroxene*

312

313 The clinopyroxene compositions are highly variable (Table 3, Figs. 8, 9) but basically four  
314 different types can be distinguished. They are: 1) colourless xenocrystic cores, 2) light green  
315 xenocrystic cores, 3) megacrysts, 4) phenocrysts, microphenocrysts and groundmass  
316 clinopyroxenes.

317

318 Colourless cores

319

320 Colourless cores (Table 3, analyses No. 2 and 4) are homogeneous but have variable  
321 compositions in the different crystals. They are chromian diopsides (Fig. 8) with high Mg#s  
322 (0.88-0.92; Mg/(Mg+Fe<sup>tot</sup>)) and SiO<sub>2</sub> contents (51.2-53.7 wt.%), and varying Cr<sub>2</sub>O<sub>3</sub> and Al<sub>2</sub>O<sub>3</sub>  
323 contents (0.28-1.4 wt.% and 2.8-6.1 wt.%, respectively). They are generally low in TiO<sub>2</sub> (up  
324 to 0.48 wt.%) and have low Ti/Al ratios ( $\leq 0.07$ ) and high Al<sup>VI</sup>/Al<sup>IV</sup> ratios (0.81-1.3). The  
325 compositions of these colourless xenocrystic cores are similar to those of the clinopyroxenes  
326 from the peridotite xenoliths in the Balaton Highland (Figs. 8, 9).

327

328 Green cores

329

330 Representative analyses of green cores are in Table 3 (analyses No. 6 and 8). The green  
331 cores are homogeneous and enriched in iron (Fig. 8). Their Mg#s (Mg/(Mg+Fe<sup>tot</sup>)) varies  
332 between 0.59-0.69 which is lower than those of the overgrowth rims. Their TiO<sub>2</sub> and Al<sub>2</sub>O<sub>3</sub>



333 contents are relatively low (0.49-0.76 wt.% and 4.5-6.6 wt.%, respectively) and the amount of  
334 Cr<sub>2</sub>O<sub>3</sub> is around (or below) the detection limit. The compositions of these xenocrystic cores  
335 resemble those of the clinopyroxenes of the lower crustal granulite xenoliths in the Balaton  
336 Highland (Figs. 8, 9). Their Ti/Al and Al<sup>VI</sup>/Al<sup>IV</sup> ratios are in the same range as in the  
337 colourless cores (Fig. 9e, f). One of the green cores has a different composition: it has slightly  
338 lower Mg# (0.58) and significantly lower TiO<sub>2</sub> (0.28 wt.%) and Al<sub>2</sub>O<sub>3</sub> (1.5 wt.%) contents  
339 than the other green cores of the samples.

340

#### 341 Megacrysts

342

343 The interiors of the megacrysts are homogeneous. The colourless megacrysts show a  
344 restricted range of composition (Figs. 8, 9; Table 3, analyses No. 10 and 13). Their Mg#s  
345 (Mg/(Mg+Fe<sup>tot</sup>)) are 0.81-0.83, the TiO<sub>2</sub> and Al<sub>2</sub>O<sub>3</sub> contents are in the range of 0.91-1.3 wt.%  
346 and 8.7-9.2 wt.%, respectively. They are characterized by low Ti/Al (0.07-0.09) and high  
347 Al<sup>VI</sup>/Al<sup>IV</sup> ratios (0.90-1.2) (Fig. 9e, f). They have high Na<sub>2</sub>O contents (1.2-1.3 wt.%)  
348 compared to the phenocrysts, and do not contain Cr<sub>2</sub>O<sub>3</sub> in detectable amount. The  
349 clinopyroxene composition in the spongy part is slightly different from that of the interior of  
350 the megacryst having higher TiO<sub>2</sub> (1.1-2.2 wt.%), lower Al<sub>2</sub>O<sub>3</sub> (6.2-8 wt.%) and Na<sub>2</sub>O (0.48-  
351 0.73 wt.%), while the Mg# is the same.

352 | The green megacryst ~~can be~~ characterized by lower Mg# (0.57) and Al<sub>2</sub>O<sub>3</sub> (7.5 wt.%),  
353 and higher TiO<sub>2</sub> (1.6 wt.%) and Na<sub>2</sub>O (2.1 wt.%) contents than the other megacrysts. It has  
354 similar Al<sup>VI</sup>/Al<sup>IV</sup> (0.93), but a slightly higher Ti/Al ratio (0.14) compared to the colourless  
355 megacrysts.

356

357 Phenocrysts, microphenocrysts and groundmass grains

358

359 The pale brown clinopyroxene phenocrysts (i.e., the overgrowth rims on clinopyroxene  
360 xenocrysts and megacrysts as well as on the reaction rim of orthopyroxene xenocrysts),  
361 microphenocrysts and microlites of the groundmass are titanian augites or titanaugites  
362 according to the traditional pyroxene nomenclature (Deer et al. 1978), but can be classified as  
363 diopside, aluminian diopside and titanian aluminian diopside according to the I.M.A.  
364 classification of pyroxenes (Morimoto et al. 1988). Some representative analyses of these  
365 clinopyroxenes can be seen in Table 3 (e.g., analyses No. 3, 7, 12 and 17). Their Mg#s  
366 ( $\text{Mg}/(\text{Mg}+\text{Fe}^{\text{tot}})$ ) range from 0.73 to 0.85 and their  $\text{TiO}_2$  and  $\text{Al}_2\text{O}_3$  contents vary between 1.5-  
367 3.9 wt.% and 4.9-10.1 wt.%, respectively. Ti and Al show positive correlation (Fig. 9e) and  
368 both elements increase with iron enrichment (Fig. 9a, b). Their increasing Ti with decreasing  
369 Mg# reflects the normal fractionation trend (e.g., Tracy and Robinson 1977). The  $\text{Cr}_2\text{O}_3$   
370 contents can reach 1 wt.% but it sharply decreases with decreasing Mg# (Fig. 9c). Their Ti/Al  
371 ratios (0.16-0.34) are higher, while the  $\text{Al}^{\text{VI}}/\text{Al}^{\text{IV}}$  ratios (0.12-0.48) are lower than those of any  
372 other type of the studied clinopyroxenes (Fig. 9e, f). These ratios imply that they could have  
373 crystallized under relatively low-pressure conditions (e.g., Yagi and Onuma 1967; Wass  
374 1979; Dobosi et al. 1991). Based on their slightly increasing Ti/Al ratios during crystallization  
375 (Fig. 9e), they could have precipitated under continuously decreasing pressure. They could  
376 have been characterized by a significantly higher crystallization rate compared to the olivine  
377 phenocrysts (as suggested by Fig. 4d).

378

### 379 *Oxide minerals*

380

381 Representative analyses of the studied oxide minerals are shown in Table 4. The  
382 xenocrysts are Mg- and Al-rich spinels showing variable compositions (Fig. 10). Their Mg#s

383 (Mg/(Mg+Fe<sup>tot</sup>)) vary between 0.63 and 0.74 and their Cr#s (100\*Cr/(Cr+Al)) range from  
384 12.3 to 45.8 (Cr<sub>2</sub>O<sub>3</sub>=11.4-37 wt.%, Al<sub>2</sub>O<sub>3</sub>=29.2-54.5 wt.%). Additionally, they have low  
385 TiO<sub>2</sub> contents (0.11-0.37 wt.%). The compositions of the studied xenocrysts are very similar  
386 to those of the spinels of the peridotite xenoliths in the Balaton Highland (Fig. 10).

387 The dark green megacrysts are also Mg-Al-rich spinels (Fig. 10) with 0.65-0.67 Mg#s,  
388 however they are characterized by higher Al<sub>2</sub>O<sub>3</sub> contents (61-61.8 wt.%) and very low Cr<sub>2</sub>O<sub>3</sub>  
389 contents (≤0.15 wt.%). The black megacryst has a completely different composition: it is a  
390 titanomagnetite with 10.4 wt.% TiO<sub>2</sub> and 76.6 wt.% FeO<sup>tot</sup> contents.

391 The oxides in the groundmass are mainly titanomagnetites which contain 17.3-23.5 wt.%  
392 TiO<sub>2</sub> and 66.8-72.5 wt.% FeO<sup>tot</sup>. Matrix ilmenites are also present characterized by 49.3-51.3  
393 wt.% TiO<sub>2</sub> and 38.8-43.1 wt.% FeO<sup>tot</sup>.

394

395 In summary, the compositional characteristics of the phenocryst (*s.s.*) phases (olivine,  
396 clinopyroxene, Fe-Ti-oxides) in the Bondoró-hegy basalt are similar to those of the  
397 phenocrysts found in other basalts in the Balaton Highland.

398

### 399 **Magma ascent rate estimates**

400

401 The Bondoró-hegy and Füzes-tó crystal-rich basalts provide a tool for estimating the  
402 magma ascent rate by a number of methods (Table 5). The detailed descriptions and  
403 background information of the different methods are presented in the Electronic Appendix.

404 1) We carried out calculations to estimate the ascent velocity for alkaline basaltic magmas  
405 in general based on fluid filled crack propagation velocities. These computations yield magma  
406 ascent rates in the range of 3.9-15.9 m/s, which are (at a given dyke width and density

407 contrast between melt and wall rock) lower than the ascent velocities of melilitites (e.g.,  
408 [Mattsson 2012](#)) and kimberlites (e.g., [Sparks et al. 2006](#)).

409 Based on this method, 4.4-9.2 m/s magma ascent rates would be reasonable for the  
410 observed dyke width ( $0.625\pm 0.055$  m; Fig. 2) in the case of the youngest eruptive phase of  
411 Bondoró-hegy (capping scoriaceous basalt and the 3<sup>rd</sup> lava flow). According to [Valentine and](#)  
412 [Krogh \(2006\)](#), complex sill and dyke systems can be present beneath small volume, alkaline  
413 basaltic volcanic centres with variable dyke widths of main / parent dykes (3-9 m) and dyke-  
414 parallel segments (few decimetres-1.2 m). The observed dyke width in Bondoró-hegy falls in  
415 the range of these dyke widths, and it may represent a part of a similar dyke system.

416 2) We calculated the settling rate of the largest (20 cm in diameter) peridotite xenoliths  
417 found at Bondoró-hegy and Fűzes-tó scoria cone. These computations yield xenolith settling  
418 rates in the range of 0.10-0.41 m/s, which corresponds to minimum ascent rates.

419 3) We used the Ca profiles of olivine xenocrysts (from the Fűzes-tó basalt) which can be  
420 appropriate for estimating magma ascent time because the profiles were measured in rapidly  
421 quenched basaltic bombs. The average of the calculated residence times for the xenocrysts  
422 ([Table 6](#)) is 3.6 days (86.4 hours) which means the time that olivine xenocrysts could have  
423 spent in the basaltic melt. Considering for example a 60 km long ascent route, this gives an  
424 ascent rate of 0.19 m/s.

425 4) We estimated the dissolution times of orthopyroxene xenocrysts based on the  
426 thicknesses of their reaction rims. The thickest studied reaction rim can form in 86-426  
427 minutes (1.4-7.1 hours). This gives the interaction time between orthopyroxene and basaltic  
428 melt which denotes the minimum time that the magma must have spent in the feeding system.  
429 Using for example a 60 km long ascent route again, this means an ascent rate of 11.9 m/s.

430 In summary, the different methods resulted in a large interval-range of ascent rates. The  
431 minimum ascent velocities are 0.10-0.19 m/s derived from the 2nd and 3rd methods

432 (respectively), and the maximum ascent rates are 9.2-11.9 m/s resulted from the 1st and 4th  
433 methods (respectively). These results imply that the Bondoró-hegy and Fűzes-tó crystal-rich  
434 magmas could have reached the surface [from their source](#) within hours to few days.

435

## 436 **Discussion**

437

438 Alkaline basalts of the Bakony-Balaton Highland Volcanic Field have phenocryst  
439 assemblages of olivine, and more rarely, clinopyroxene (e.g., [Embey-Isztin et al. 1993a](#)).  
440 Olivine is frequently the only phenocryst phase and clinopyroxene is restricted to the  
441 groundmass. In contrast, the basalts of the Bondoró-hegy and Fűzes-tó are more complex,  
442 having large textural and compositional heterogeneity, especially among clinopyroxenes.  
443 Most of the minerals could not be in equilibrium with each other and with the host magma,  
444 and many of them must be xenocrysts entrained from various depths. Here, we discuss the  
445 origins of the diverse crystals of the Bondoró-hegy basalt, the interpretations in the case of the  
446 Fűzes-tó basalt were reported in previous papers ([Jankovics et al. 2009, 2012](#)). We also  
447 provide the magma ascent history and estimates of ascent rate.

448

### 449 *Sources for the diverse mineral assemblage*

450

#### 451 Xenocrysts

452

453 The compositional range of olivine xenocrysts ([Fig. 5](#)) is typical for mantle olivines (e.g.,  
454 [Boudier et al. 1991; Hirano et al. 2004; Rohrbach et al. 2005](#)). The Fo value for average  
455 olivines in the lithospheric mantle is 90 mol% ([Sato 1977](#)). Most of the studied olivine

456 xenocrysts contain Fo around 90 mol%, but some of them have higher Fo contents suggesting  
457 that they are derived from depleted peridotites.

458 Orthopyroxene xenocrysts are also Mg-rich which is characteristic for orthopyroxenes of  
459 the upper mantle (e.g., [Embey-Isztin et al. 2001a](#)). Their reaction rims are common features of  
460 mantle-derived orthopyroxenes that are incorporated by silica-undersaturated alkaline melts.  
461 This mineral-melt reaction results in the incongruent dissolution of the orthopyroxene and  
462 formation of a reaction corona (olivine + Si-rich glass + clinopyroxene ± spinel) at the  
463 expense of the orthopyroxene (e.g., [Arai and Abe 1995](#); [Shaw et al. 1998](#); [Shaw 1999](#); [Shaw  
and Dingwell 2008](#)). Comparing the compositions of the studied enstatite xenocrysts with the  
465 orthopyroxenes from the Bondoró-hegy peridotite xenoliths ([Embey-Isztin et al. 2001a](#)), they  
466 could have derived from moderately depleted peridotite (e.g., 2.9-3 wt.% Al<sub>2</sub>O<sub>3</sub>, 33.4-33.9  
467 wt.% MgO).

468 The compositional variation of the colourless clinopyroxene xenocrysts ([Figs. 8, 9](#)) is  
469 typical for Cr-diopsides of peridotite xenoliths (e.g., [Wass 1979](#)). The low Ti/Al ratios of the  
470 colourless xenocrystic cores suggest a relatively high-pressure origin (e.g., [Yagi and Onuma  
1967](#); [Wass 1979](#); [Dobosi et al. 1991](#)). They are derived from the disaggregation of  
472 incorporated peridotite fragments (together with the olivine and orthopyroxene xenocrysts).  
473 Compared to the compositions of clinopyroxenes of peridotite xenoliths from the Bondoró-  
474 hegy ([Embey-Isztin et al. 2001a](#)), most of the studied Cr-diopside xenocrysts could represent  
475 moderately depleted peridotite and some of them could indicate fertile peridotite (e.g., lower  
476 Mg# and higher TiO<sub>2</sub>).

477 Light green clinopyroxene xenocrysts have more Fe and less Ti than the phenocrysts.  
478 Their low Ti/Al ratios reflect their relatively high-pressure origin (e.g., [Yagi and Onuma  
1967](#); [Wass 1979](#); [Dobosi et al. 1991](#)). Several interpretations exist for the origin of such  
479 green clinopyroxene cores, for example, they are cognate phases of high-pressure origin; or  
480



481 crystallized from evolved magmas; or represent locally metasomatized upper mantle wall rock  
482 (e.g., Brooks and Printzlau 1978; Wass 1979; Barton and Bergen 1981; Duda and Schmincke  
483 1985; Dobosi and Fodor 1992). Most of our studied green cores are compositionally very  
484 similar to the green clinopyroxenes found in lower crustal mafic granulite xenoliths in the  
485 Balaton Highland (Embey-Isztin et al. 2003) (Figs. 8, 9). Therefore, these light green  
486 clinopyroxene xenocrysts may represent crystals entrained from lower crustal mafic granulite.

487 According to their composition (Fig. 10), the spinel xenocrysts also have a lithospheric  
488 mantle origin. Compared with the compositions of spinels found in the peridotite xenoliths  
489 from the Bondoró-hegy (Embey-Isztin et al. 2001a), half of the studied spinel xenocrysts  
490 could have originated from fertile peridotite (e.g., lower Cr# and higher Al<sub>2</sub>O<sub>3</sub>) and half could  
491 represent moderately depleted peridotite.

492 In summary, the olivine, orthopyroxene, colourless clinopyroxene and spinel xenocrysts  
493 have diverse chemistry covering the compositional variations of minerals in peridotite  
494 xenoliths and representing variably depleted regions of the subcontinental lithospheric mantle.  
495 This is supported by the former study of spinel peridotite xenoliths having various textures  
496 and different calculated equilibrium temperatures (Embey-Isztin et al. 2001a). The xenocrysts  
497 acted as nucleation sites for the crystallization of the phenocryst phases which isolated them  
498 from the basaltic melt as crystal rims.

499

500 Megacrysts

501

502 Clinopyroxene megacrysts of alkaline basalts are frequently interpreted as high-pressure  
503 near-liquidus phases that crystallized from their host magmas (e.g., Binns et al. 1970; Ellis  
504 1976; Irving and Frey 1984) or as accidental fragments of pyroxenite veins that precipitated  
505 from melts at elevated pressures (e.g., Righter and Carmichael 1993; Shaw and Eyzaguirre

506 2000). The relatively high Mg-numbers, high  $Al^{VI}/Al^{IV}$  and low Ti/Al ratios (Fig. 9e, f) of  
507 most of the Bondoró-hegy megacrysts could reflect their high-pressure cognate origin.  
508 However, their rounded outlines and the presence of the spongy reaction zone suggest that  
509 megacrysts were in disequilibrium with the host magma during ascent implying their  
510 accidental origin. Isotope data for the megacrysts and the host alkaline basalts of the  
511 Transdanubian region (Embey-Isztin et al. 1993a; Dobosi et al. 2003) also suggest an  
512 accidental origin because the megacrysts have significantly less radiogenic Sr and Nd isotope  
513 ratios than their host basalts. Trace element abundances, however, are compatible with a  
514 cognate origin. In order to resolve this contradiction, clinopyroxene megacrysts are  
515 interpreted as accidental fragments of pegmatitic veins which crystallized from earlier  
516 alkaline basaltic melts resembling the host basalt. These melts had different radiogenic  
517 isotope ratios, but similar major and trace element compositions as the present host basalt of  
518 the megacrysts, and crystallized as pyroxenite veins in the upper mantle. The presence of  
519 pyroxenite/peridotite composite xenoliths in the Transdanubian region (Embey-Isztin et al.  
520 1989, 1990) supports this hypothesis. The earlier crystallized coarse-grained pyroxenite veins  
521 were disrupted and carried to the surface as individual megacrysts by the ascending magma of  
522 Bondoró-hegy. During ascent, the megacrysts were out of equilibrium with the basaltic  
523 magma and through incipient partial melting, spongy domains developed in the megacrysts.

524 Some clinopyroxene megacrysts contain inclusions of spinel with similar compositions to  
525 the spinel megacrysts. This may suggest that spinel megacrysts had an origin similar to that of  
526 the clinopyroxene megacrysts.- The iron-rich green clinopyroxene megacryst and the  
527 titanomagnetite megacryst probably crystallized from a differentiated melt.

528

529 *Ascent history*

530

531 The ascent history of the Bondoró-hegy alkaline basaltic magma and origin of the diverse  
532 crystals are summarized in [Fig. 11](#). The information for the Füzes-tó basaltic magma was  
533 presented by [Jankovics et al. \(2009, 2012\)](#). The model in [Fig. 11](#) also gives a general view  
534 about the ascent history of both the crystal-rich alkaline basaltic magmas (Bondoró-hegy and  
535 Füzes-tó) in the CPR. After the generation of magma in the asthenosphere, it ascended  
536 through the lithospheric mantle in a destructive fashion, fracturing the wall rock and  
537 incorporating a vast amount of fragments from the lithospheric mantle now represented by the  
538 xenocrysts and peridotite xenoliths. During ascent, the basaltic magma strongly resorbed  
539 these crystals and fragments resulted in various disequilibrium textures and modification of  
540 the host magma composition. In the uppermost lithospheric mantle, near the crust-mantle  
541 boundary (CMB), a number of bodies (veins, dykes, sills) of frozen basaltic liquids and  
542 cumulates (i.e., earlier crystallized basaltic magma batches) can be present ([Embey-Isztin et  
543 al. 1990](#)). When the ascending magma reached this region, it incorporated additional crystals  
544 – having compositions different from those of the mantle xenocrysts – represented by the  
545 observed clinopyroxene and spinel megacrysts. As the magma passed through the CMB, the  
546 style of its ascent did not change as numerous fragments and green clinopyroxene crystals  
547 were entrained from lower crustal granulite. These fragments and crystals were also resorbed  
548 and could have additionally modified the magma composition. Accordingly, at mantle depths  
549 and near the CMB there was an effective interaction between the basaltic magma and the  
550 lithosphere. An explanation for this effective interaction could be some cryptic processes. In  
551 the case of kimberlitic magmas a recent discovery ([Russell et al. 2012](#)) suggests that  
552 continuous assimilation of foreign minerals (especially orthopyroxene) – that can modify the  
553 composition of the host melt toward more silicic compositions – causes changes in the  
554 volatile solubility in the host melt. The result is volatile exsolution and due to this process the  
555 magma can fracture more effectively the wall rock. However, this model requires that the

556 parental melt of the host magma should have much lower silica content and high amount of  
557 dissolved volatiles (i.e., carbonatitic or near-carbonatitic composition). To be able to reveal  
558 similar cryptic processes in the case of the studied alkaline basaltic magmas, experimental  
559 studies would be necessary which could help to decide whether these processes can be also  
560 expanded for alkaline basalts or operate only in the case of kimberlites. Thus, the applicability  
561 of this model in our case is not obvious.

562 | ~~Oppositely~~ In contrast to the effective magma-wall rock interaction at lithospheric mantle  
563 and lower crustal depths, the ascending magma did not incorporate additional crustal material  
564 in the middle and upper part of the crust. This suggests a change in the style (and possibly in  
565 the rate) of the magma ascent. The main driving force of magma ascent is the process of  
566 magma-filled crack propagation (e.g., [Spera 1984](#); [Russell et al. 2012](#)). Change in the style  
567 and rate of ascent can be caused by the variations in volatile solubility in the melt, by the  
568 change in the physical state of magma and wall rocks along the ascent path, and by varying  
569 dyke widths. [Szabó and Bodnar \(1996\)](#) suggested a change during the ascent of alkaline  
570 basaltic magmas in the Nógrád-Gömör Volcanic Field (Fig. 1a): the magmas accelerated near  
571 the MOHO. The observed recent activity of El Hierro (2011-2012) may also support their  
572 model, as the seismic signals suggested that the erupted magma passed rapidly through the  
573 crust (e.g., [Carracedo et al. 2011](#)). This process may be a possible interpretation for the lack  
574 of middle and upper crustal wall rock fragments in our case.

575 Thermobarometric studies of basaltic magmas from ocean islands indicate melt  
576 accumulation near the CMB during the ascent of the magma batches (e.g., [Klügel et al. 2005](#);  
577 [Hildner et al. 2012](#)). The calculated ascent rates / times in the case of the Bondoró-hegy and  
578 Füzés-tó magmas, however, do not indicate a longer time of stagnation anywhere in the  
579 | lithosphere. In addition, there ~~are-is~~ no petrologic evidences for magma accumulation /

580 storage (e.g., common cognate crystal cumulates), and the large amount of dense materials  
581 also needs a continuous ascent.

582

583 *Magma ascent rates in the monogenetic volcanic fields of the Pannonian Basin*

584

585 In monogenetic volcanic fields where eruptions of basaltic magmas give scarce precursory  
586 signs, estimating magma ascent rates is essential ~~due~~ to hazard forecasting. As there are  
587 scarce direct observations about the activity of these eruptive centres, it is important to  
588 evaluate the ascent rate (as well as the ascent history) of basaltic magmas represented by  
589 diverse eruption products in various geodynamic settings.

590 In the case of other basalts in the Pannonian Basin, magma ascent time was determined by  
591 [Dégi et al. \(2009\)](#) for two eruptive centres in the Bakony-Balaton Highland Volcanic Field, by  
592 [Szabó and Bodnar \(1996\)](#) for several volcanic centres at the Nógrád-Gömör Volcanic Field  
593 and by [Harangi et al. \(in press\)](#) for two centres in the Perşani Volcanic Field. It is notable that  
594 these basalts contain a much smaller amount of lithospheric mantle-derived xenoliths and  
595 xenocrysts compared to the basalts of Bondoró-hegy and Füzes-tó. [Dégi et al. \(2009\)](#) studied  
596 the Fe-Ti-oxides in lower crustal mafic granulite xenoliths and modeled their diffusion-  
597 controlled chemical alteration. On the basis of diffusion profiles they estimated the duration  
598 of granulite xenolith–host basaltic melt interaction to be at least 9-20 h. This time interval  
599 gives a minimum ascent time and can be applied only in the crust, but the ascent time  
600 concerning the deeper parts of the lithosphere is not known. In the Nógrád-Gömör Volcanic  
601 Field, [Szabó and Bodnar \(1996\)](#) published ~37.5 hours for the residence time of upper mantle  
602 xenoliths in the host magmas and 18 hours for the residence time of a spinel xenocryst based  
603 on the thickness of its rim. [Harangi et al. \(in press\)](#) found that the residence time of mantle-  
604 derived olivine xenocrysts in the host alkaline basaltic magma was 3.6-4.8 days. This is very

605 similar to our results calculated by the same method, which is notable. These three mentioned  
606 estimations are close to our results but in the case of the first, the ascent time can be much  
607 longer.

608 So, although the studied basalts are extremely rich in xenoliths and xenocrysts, a  
609 significant difference in their magma ascent rates compared to the other alkaline basalts in the  
610 Pannonian Basin cannot be inferred. This is not in accordance with the common view that  
611 ultramafic xenolith-rich basaltic magmas reach the surface more rapidly than xenolith-poor  
612 ones.

613

## 614 **Conclusions**

615

616 The last eruptions of the Bakony-Balaton Highland Volcanic Field are represented by  
617 especially crystal- and xenolith-rich alkaline basaltic magmas ~~including-forming~~ two  
618 monogenetic eruptive centres: Bondoró-hegy and Füzés-tó scoria cone. Similar magmas did  
619 not erupt in the above mentioned volcanic field and even in the other volcanic fields in the  
620 whole Carpathian-Pannonian Region, nevertheless basalts of numerous eruptive centres  
621 contain diverse xenoliths.

622 Detailed textural and chemical analyses of the rock-forming minerals ~~highlighted-showed~~  
623 that almost the whole set of phenocrysts *s.l.* represents a mineral assemblage originating from  
624 different levels of the lithosphere. The foreign crystals have diverse compositions and are  
625 divided into three larger groups. The most abundant group originates from different regions of  
626 the subcontinental lithospheric mantle. Megacrysts can derive from pegmatitic veins / sills  
627 that probably represent crystallized magmas which froze near the crust-mantle boundary.  
628 Green clinopyroxenes show similar compositions compared to the clinopyroxenes in mafic  
629 granulites indicating lower crustal origin for these xenocrysts. Minerals that crystallized from

630 the basaltic melt are only represented by microphenocrysts and overgrowths on the foreign  
631 crystals. Consequently, the different whole-rock compositions of the studied basalts compared  
632 to those of the other basalts of the volcanic field are not caused by magma generation from a  
633 dissimilar mantle source or by differing degree of partial melting, but are the result of their  
634 different (more complex) evolution histories, i.e., incorporation of a vast amount of xenoliths  
635 and xenocrysts from the lithosphere at mantle and lower crustal depths.

636 A sudden change in the style of magma ascent is suggested by the fact that abundant  
637 crystals and xenoliths were entrained from the lithospheric mantle and lower crust but  
638 fragments from the middle-upper crust are absent from the studied basalts.

639 The xenocrysts show variable disequilibrium textures allowing us to calculate differing  
640 mineral-melt reaction times which can be used for magma ascent rate estimations. Based on  
641 our results calculated with different methods, we can conclude that despite the special feature  
642 of the Bondoró-hegy and Füzes-tó alkaline basalts, significant differences in their magma  
643 ascent velocities cannot be inferred compared to other alkaline basaltic magmas in the  
644 Pannonian Basin. The calculations indicate that these crystal-rich alkaline basaltic magmas  
645 could have reached the surface within hours to few days.

646 Based on our studies, these unique basalts enable ~~to document in detail the detailed~~  
647 documentation of the ascent history of basaltic magmas feeding monogenetic eruptions.  
648 Furthermore, they bear valuable implications for the rock types in the underlying lithosphere.

649

## 650 **Acknowledgements**

651

652 We are very grateful to R. V. Fodor for his valuable suggestions and comments as well as I.  
653 E. M. Smith for his useful advices which helped to improve the manuscript. This research was  
654 partly supported by the TÉT\_10-1-2011-0694 project (Hungarian-Austrian Cooperation) and

655 | by the Hungarian Scientific Research Fund OTKA no. 68587. B. Kiss was funded in the  
656 | frames of TÁMOP 4.2.4. A/2-11-1-2012-0001 „National Excellence Program – Elaborating  
657 | and operating an inland student and researcher personal support system convergence  
658 | program” and was subsidized by the European Union and co-financed by the European Social  
659 | Fund.

Formatted: Font: Times New Roman, 12 pt

Formatted: Font: Times New Roman, 12 pt

## 661 | **References**

- 662
- 663 | Ancochea E, Munoz M, Sagredo J (1987) Las rocas volcánicas neógenas de Nuévalos  
664 | (provincia de Zaragoza). Geogaceta 3:7-10
- 665 | Aoki K-i, Kushiro I (1968) Some clinopyroxenes from ultramafic inclusions in Dreiser  
666 | Weiher, Eifel. Contributions to Mineralogy and Petrology 18(4):326-337
- 667 | Arai S, Abe N (1995) Reaction of orthopyroxene in peridotite xenoliths with alkali-basalt  
668 | melt and its implication for genesis of alpine-type chromitite. American Mineralogist  
669 | 80:1041-1047
- 670 | Bada G, Horváth F (2001) On the structure and tectonic of the Pannonian Basin and  
671 | surrounding orogens. Acta Geologica Hungarica 44(2-3):301-327
- 672 | Balogh K, Árvai-Sós E, Pécskay Z, Ravasz-Baranyai L (1986) K/Ar dating of post-Sarmatian  
673 | alkali basaltic rocks in Hungary. Acta Mineralogica et Petrographica Szeged 28:75-93
- 674 | Balogh K, Pécskay Z (2001) K/Ar and Ar/Ar geochronological studies in the Pannonian-  
675 | Carpathians-Dinarides (PANCARDI) region. Acta Geologica Hungarica 44:281-299
- 676 | Barton M, Bergen vMJ (1981) Green clinopyroxenes and associated phases in a potassium-  
677 | rich lava from the Leucite Hills, Wyoming. Contributions to Mineralogy and Petrology  
678 | 77(2):101-114
- 679 | Best MG (2003) Igneous and Metamorphic Petrology. Blackwell Publishing company,



680 Blackwell

681 Binns RA, Duggan MB, Wilkinson JFG (1970) High pressure megacrysts in alkaline lavas  
682 from northeastern New South Wales. *American Journal of Science* 269(2):132-168

683 Boudier F (1991) Olivine xenocrysts in picritic magmas: An experimental and microstructural  
684 study. *Contributions to Mineralogy and Petrology* 109(1):114-123

685 Bowen NL, Anderson O (1914) The binary system MgO-SiO<sub>2</sub>. *American Journal of Science*  
686 37:487-500

687 Brearley M, Scarfe CM (1986) Dissolution Rates of Upper Mantle Minerals in an Alkali  
688 Basalt Melt at High Pressure: An Experimental Study and Implications for Ultramafic  
689 Xenolith Survival. *Journal of Petrology* 27(5):1157-1182

690 Brenna M, Cronin SJ, Németh K, Smith IEM, Sohn YK (2011) The influence of magma  
691 plumbing complexity on monogenetic eruptions, Jeju Island, Korea. *Terra Nova*:1-6

692 Brenna M, Cronin SJ, Smith IEM, Sohn YK, Németh K (2010) Mechanisms driving  
693 polymagmatic activity at a monogenetic volcano, Udo, Jeju Island, South Korea.  
694 *Contributions to Mineralogy and Petrology* 160(6):931-950

695 Brooks CK, Printzlau I (1978) Magma mixing in mafic alkaline volcanic rocks: The evidence  
696 from relict phenocryst phases and other inclusions. *Journal of Volcanology and*  
697 *Geothermal Research* 4(315-331)

698 Carracedo J-C, Perez-Torrado F-J, Rodriguez-Gonzalez A, Fernandez-Turiel J-L, Klügel A,  
699 Troll VR, Wiesmaier S (2012) The ongoing volcanic eruption of El Hierro, Canary  
700 Islands. *Eos Trans. AGU* 93(9)

701 Connor CB, Conway FM (2000) Basaltic Volcanic Fields. In: Sigurdsson H (ed)  
702 *Encyclopedia of Volcanoes*. Academic Press, San Diego, pp 331-343

703 Costa F, Cohmen R, Chakraborty S (2008) Time Scales of Magmatic Processes from  
704 Modeling the Zoning Patterns of Crystals. In: Putirka KD, Tepley III FJ (eds) *Minerals,*

705 Inclusions and Volcanic Processes. Mineralogical Society of America & Geochemical  
706 Society, pp 545-594

707 Csontos L, Nagymarosy A, Horváth F, Kovác M (1992) Tertiary evolution of the Intra-  
708 Carpathian area: A model. *Tectonophysics* 208(1-3):221-241

709 Daines MJ, Kohlstedt DL (1994) The Transition from Porous to Channelized Flow Due to  
710 Melt/Rock Reaction During Melt Migration. *Geophysical Research Letters* 21(2):145-  
711 148

712 Deer WA, Howie RA, Zussman J (1978) Rock-forming minerals. Vol. 2A. Single-chain  
713 silicates. In: Longman, London, pp 3-4

714 Dégi J, Abart R, Török K, Rhede D, Petrishcheva E (2009) Evidence for xenolith-host basalt  
715 interaction from chemical patterns in Fe-Ti-oxides from mafic granulite xenoliths of the  
716 Bakony-Balaton Volcanic field (W-Hungary). *Mineralogy and Petrology* 95(3):219-234

717 Dobosi G (1989) Clinopyroxene zoning patterns in the young alkali basalts of Hungary and  
718 their petrogenetic significance. *Contributions to Mineralogy and Petrology* 101:112-121

719 Dobosi G, Downes H, Embey-Isztin A, Jenner GA (2003) Origin of megacrysts and  
720 pyroxenite xenoliths from the Pliocene alkali basalts of the Pannonian Basin (Hungary).  
721 *Neues Jahrbuch für Mineralogie - Abhandlungen* 178(3):217-237

722 Dobosi G, Fodor RV (1992) Magma fractionation, replenishment, and mixing as inferred  
723 from green-core clinopyroxenes in Pliocene basanite, southern Slovakia. *Lithos*  
724 28(2):133-150

725 Dobosi G, Schultz-Güttler R, Kurat G, Kracher A (1991) Pyroxene chemistry and evolution  
726 of alkali basaltic rocks from Burgenland and Styria, Austria. *Mineralogy and Petrology*  
727 43(4):275-292

728 Downes H, Embey-Isztin A, Thirlwall MF (1992) Petrology and geochemistry of spinel  
729 peridotite xenoliths from the western Pannonian Basin (Hungary): evidence for an

730 association between enrichment and texture in the upper mantle. Contributions to  
731 Mineralogy and Petrology 109(3):340-354

732 Downes H, Vaselli O (1995) The lithospheric mantle beneath the Carpathian-Pannonian  
733 Region: a review of trace element and isotopic evidence from ultramafic xenoliths. In:  
734 Downes H, Vaselli O (eds) Neogene and Related Magmatism in the Carpatho-Pannonian  
735 Region. Acta Vulcanologica, pp 219-229

736 Duda A, Schmincke H-U (1985) Polybaric differentiation of alkali basaltic magmas: evidence  
737 from green-core clinopyroxenes (Eifel, FRG). Contributions to Mineralogy and Petrology  
738 91(4):340-353

739 Ellis DJ (1976) High pressure cognate inclusions in the Newer Volcanics of Victoria.  
740 Contributions to Mineralogy and Petrology 58(2):149-180

741 Embey-Isztin A (1976) Amphibolite/lherzolite composite xenolith from Szigliget, north of the  
742 lake Balaton, Hungary. Earth and Planetary Science Letters 31(2):297-304

743 Embey-Isztin A, Dobosi G (1995) Mantle source characteristics for Miocene-Pleistocene  
744 alkali basalts, Carpathian-Pannonian Region: A review of trace elements and isotopic  
745 composition. In: Downes H, Vaselli O (eds) Neogene and Related Magmatism in the  
746 Carpatho-Pannonian Region. Acta Vulcanologica, pp 155-166

747 Embey-Isztin A, Dobosi G (2007) Composition of olivines in the young alkali basalts and  
748 their peridotite xenoliths from the Pannonian Basin. Annales Historico-Naturales Musei  
749 Nationalis Hungarici 99:5-22

750 Embey-Isztin A, Dobosi G, Altherr R, Meyer H-P (2001a) Thermal evolution of the  
751 lithosphere beneath the western Pannonian Basin: evidence from deep-seated xenoliths.  
752 Tectonophysics 331(3):285-306

753 Embey-Isztin A, Dobosi G, James D, Downes H, Poultidis C, Scharbert HG (1993b) A  
754 compilation of new major, trace and isotope geochemical analyses of the young alkali

755 basalts from the Pannonian Basin. *Fragmenta Mineralogica et Palaeontologica* 16:5–26

756 Embey-Isztin A, Downes H, Dobosi G (2001b) Geochemical characterization of the  
757 Pannonian Basin mantle lithosphere and asthenosphere: an overview. *Acta Geologica*  
758 *Hungarica* 44(2-3):259-280

759 Embey-Isztin A, Downes H, James DE, Upton BGJ, Dobosi G, Ingram GA, Harmon RS,  
760 Scharbert HG (1993a) The petrogenesis of Pliocene alkaline volcanic rocks from the  
761 Pannonian Basin, Eastern Central Europe. *Journal of Petrology* 34:317-343

762 Embey-Isztin A, Downes H, Kempton PD, Dobosi G, Thirlwall M (2003) Lower crustal  
763 granulite xenoliths from the Pannonian Basin, Hungary. Part 1: mineral chemistry,  
764 thermobarometry and petrology. *Contributions to Mineralogy and Petrology* 144:652-670

765 Embey-Isztin A, Scharbert HG, Dietrich H, Poulitidis H (1989) Petrology and Geochemistry  
766 of Peridotite Xenoliths in Alkali Basalts from the Transdanubian Volcanic Region, West  
767 Hungary. *Journal of Petrology* 30(1):79-105

768 Embey-Isztin A, Scharbert HG, Dietrich H, Poulitidis H (1990) Mafic granulites and  
769 clinopyroxenite xenoliths from the Transdanubian Volcanic Region (Hungary):  
770 implications for the deep structure of the Pannonian Basin. *Mineralogical Magazine*  
771 54:463-483

772 Fodor L, Csontos L, Bada G, Benkovics L, Györfi I (1999) Tertiary tectonic evolution of the  
773 Carpatho-Pannonian region: A new synthesis of palaeostress data. In: Durand B, Jolivet  
774 L, F. H, Séranne M (eds) *The Mediterranean Basins: Tertiary Extension within the*  
775 *Alpine Orogen*. Geological Society, London, Special Publications, pp 295-334

776 Granet M, Wilson M, Achauer U (1995) Imaging a mantle plume beneath the French Massif  
777 Central. *Earth and Planetary Science Letters* 136(3-4):281-296

778 Gurenko AA, Hansteen TH, Schmincke H-U (1996) Evolution of parental magmas of  
779 Miocene shield basalts of Gran Canaria (Canary Islands): constraints from crystal, melt

780 and fluid inclusions in minerals. *Contributions to Mineralogy and Petrology* 124(3):422-  
781 435

782 Harangi S (2001) Volcanology and petrology of the Late Miocene to Pliocene alkali basaltic  
783 volcanism in the Western Pannonian Basin. In: Ádám A, Szarka L (eds) PANCARDI  
784 2001 Field Guide. Sopron, pp 51-81

785 Harangi S (2009) Volcanism of the Carpathian-Pannonian region, Europe: The role of  
786 subduction, extension and mantle plumes. In:  
787 <http://www.mantleplumes.org/CarpathianPannonian.html>.

788 Harangi S, Lenkey L (2007) Genesis of the Neogene to Quaternary volcanism in the  
789 Carpathian-Pannonian region: Role of subduction, extension, and mantle plume.  
790 *Geological Society of America Special Papers* 418:67-92

791 Harangi S, Sági T, Seghedi I, Ntaflos T A mineral-scale investigation to reveal the origin of  
792 the basaltic magmas of the Perşani monogenetic volcanic field, Romania, eastern-central  
793 Europe. *Lithos*

794 Hasenaka T, Carmichael ISE (1985) The cinder cones of Michoacán-Guanajuato, central  
795 Mexico: their age, volume and distribution, and magma discharge rate. *Journal of*  
796 *Volcanology and Geothermal Research* 25(1-2):105-124

797 Hidas K, Falus G, Szabó C, Szabó PJ, Kovács I, Földes T (2007) Geodynamic implications of  
798 flattened tabular equigranular textured peridotites from the Bakony-Balaton Highland  
799 Volcanic Field (Western Hungary). *Journal of Geodynamics* 43(4-5):484-503

800 Hildner E, Kügel A, Hansteen TH (2012) Barometry of lavas from the 1951 eruption of Fogo,  
801 Cape Verde Islands: Implications for historic and prehistoric magma plumbing systems.  
802 *Journal of Volcanology and Geothermal Research* 217-218:73-90

803 Hirano N, Yamamoto J, Kagi H, Ishii T (2004) Young, olivine xenocryst-bearing alkali-basalt  
804 from the oceanward slope of the Japan Trench. *Contributions to Mineralogy and*

805 Petrology 148(1):47-54

806 Hoernle K, Zhang YS, Graham D (1995) Seismic and geochemical evidence for large-scale  
807 mantle upwelling beneath the eastern Atlantic and western and central Europe. *Nature*  
808 374:34-39

809 Horváth F (1993) Towards a mechanical model for the formation of the Pannonian Basin.  
810 *Tectonophysics* 226(1-4):333-357

811 Horváth F (1995) Phases of compression during the evolution of the Pannonian Basin and its  
812 bearing on hydrocarbon exploration. *Marine and Petroleum Geology* 12(8):837-844

813 Horváth F, Cloetingh S (1996) Stress-induced late-stage subsidence anomalies in the  
814 Pannonian Basin. *Tectonophysics* 266(1-4):287-300

815 Irving AJ, Frey FA (1984) Trace element abundances in megacrysts and their host basalts:  
816 Constraints on partition coefficients and megacryst genesis. *Geochimica et*  
817 *Cosmochimica Acta* 48(6):1201-1221

818 Jankovics É, Harangi S, Ntaflós T (2009) A mineral-scale investigation on the origin of the  
819 2.6 Ma Füzes-tó basalt, Bakony-Balaton Highland Volcanic Field (Pannonian Basin,  
820 Hungary). *Central European Geology* 52(2):97-124

821 Jankovics MÉ, Harangi S, Kiss B, Ntaflós T (2012) Open-system evolution of the Füzes-tó  
822 alkaline basaltic magma, western Pannonian Basin: Constraints from mineral textures and  
823 compositions. *Lithos* 140-141(0):25-37

824 Jugovics L (1968) The Transdanubian basalt and basaltic tuff fields (in Hungarian). *Yearly*  
825 *Report of the Hungarian Geological Institute about the year 1967*:75-82

826 Jugovics L (1976) The chemical character of the Hungarian basalts (in Hungarian). *Yearly*  
827 *Report of the Hungarian Geological Institute about the year 1974*:431-470

828 Jurewicz AJG, Watson EB (1988) Cations in olivine, Part 2: Diffusion in olivine xenocrysts,  
829 with applications to petrology and mineral physics. *Contributions to Mineralogy and*

830 Petrology 99(2):186-201

831 Kereszturi G, Csillag G, Németh K, Sebe K, Balogh K, Jáger V (2010) Volcanic architecture,  
832 eruption mechanism and landform evolution of a Plio/Pleistocene intracontinental  
833 basaltic polycyclic monogenetic volcano from the Bakony-Balaton Highland Volcanic  
834 Field, Hungary. *Central European Journal of Geosciences* 2(3):362-384

835 Kil Y, Wendlandt RF (2004) Pressure and temperature evolution of upper mantle under the  
836 Rio Grande Rift. *Contributions to Mineralogy and Petrology* 148(3):265-280

837 Klügel A (1998) Reactions between mantle xenoliths and host magma beneath La Palma  
838 (Canary Islands): constraints on magma ascent rates and crustal reservoirs. *Contributions*  
839 *to Mineralogy and Petrology* 131(2):237-257

840 Klügel A, Hansteen TH, Galipp K (2005) Magma storage and underplating beneath Cumbre  
841 Vieja volcano, La Palma (Canary Islands). *Earth and Planetary Science Letters* 236(1-  
842 2):211-226

843 Larsen LM, Pedersen AK (2000) Processes in High-Mg, High-T Magmas: Evidence from  
844 Olivine, Chromite and Glass in Palaeogene Picrites from West Greenland. *Journal of*  
845 *Petrology* 41(7):1071-1098

846 Lasaga AC (1998) *Kinetic theory in the earth sciences*. Princeton University Press, p 728

847 Lenkey L, Dövényi P, Horváth F, Cloetingh S (2002) Geothermics of the Pannonian Basin  
848 and its bearing on the neotectonics. *European Geophysical Union Stephan Mueller*  
849 *Special Publications, Series 3*:29-40

850 Lister JR, Kerr RC (1991) Fluid-Mechanical Models of Crack Propagation and Their  
851 Application to Magma Transport in Dykes. *Journal of Geophysical Research*  
852 96(B6):10049-10077

853 Maaloe S, Hansen B (1982) Olivine phenocrysts of Hawaiian olivine tholeiite and oceanite.  
854 *Contributions to Mineralogy and Petrology* 81(3):203-211

855 Martin U, Németh K (2005) Eruptive and depositional history of a Pliocene tuff ring that  
856 developed in a fluvio-lacustrine basin: Kissomlyó volcano (western Hungary). *Journal of*  
857 *Volcanology and Geothermal Research* 147(3-4):342-356

858 Martin U, Németh K, Auer A, Breitzkreuz C (2003) Mio-Pliocene Phreatomagmatic  
859 Volcanism in a Fluvio-Lacustrine Basin in Western Hungary. *Geolines* 15:84-90

860 Mattsson HB (2012) Rapid magma ascent and short eruption durations in the Lake Natron-  
861 Engaruka monogenetic volcanic field (Tanzania): A case study of the olivine melilititic  
862 Pello Hill scoria cone. *Journal of Volcanology and Geothermal Research* 247-248:16-25

863 McGee LE, Millet M-A, Smith IEM, Németh K, Lindsay JM (2012) The inception and  
864 progression of melting in a monogenetic eruption: Motukorea Volcano, the Auckland  
865 Volcanic Field, New Zealand. *Lithos* 155(0):360-374

866 Morimoto N, Fabries J, Ferguson AK, Ginzburg IV, Ross M, Seifert FA, Zussman J, Aoki K,  
867 Gottardi G (1988) Nomenclature of pyroxenes. *Mineralogical Magazine* 52:535–550

868 Needham AJ, Lindsay JM, Smith IEM, Augustinus P, Shane PA (2011) Sequential eruption  
869 of alkaline and sub-alkaline magmas from a small monogenetic volcano in the Auckland  
870 Volcanic Field, New Zealand. *Journal of Volcanology and Geothermal Research* 201(1-  
871 4):126-142

872 Németh K, Martin U (1999a) Large hydrovolcanic field in the Pannonian Basin: general  
873 characteristics of the Bakony-Balaton Highland Volcanic Field, Hungary. *Acta*  
874 *Vulcanologica* 11(2):271-282

875 Németh K, Martin U (1999b) Late Miocene paleo-geomorphology of the Bakony-Balaton  
876 Highland Volcanic Field (Hungary) using physical volcanology data. *Zeitschrift für*  
877 *Geomorphologie N. F.* 43(4):417-438

878 Reiners PW (2002) Temporal-compositional trends in intraplate basalt eruptions: Implications  
879 for mantle heterogeneity and melting processes. *Geochemistry Geophysics Geosystems*



880 3(2)

881 Righter K, Carmichael ISE (1993) Mega-xenocrysts in alkali olivine basalts: fragments of  
882 disrupted mantle assemblages. *American Mineralogist* 78:1230-1245

883 Rock NMS (1990) The International Mineralogical Association (IMA/CNMMN) pyroxene  
884 nomenclature scheme: Computerization and its consequences. *Mineralogy and Petrology*  
885 43(2):99-119

886 Roeder P, Gofton E, Thornber C (2006) Cotectic Proportions of Olivine and Spinel in  
887 Olivine-Tholeiitic Basalt and Evaluation of Pre-Eruptive Processes. *Journal of Petrology*  
888 47(5):883-900

889 Roeder PL, Poustovetov A, Oskarsson N (2001) Growth Forms and Composition of  
890 Chromian Spinel in MORB Magma: Diffusion-Controlled Crystallization of Chromian  
891 Spinel. *Canadian Mineralogist* 39(2):397-416

892 Roeder PL, Thornber C, Poustovetov A, Grant A (2003) Morphology and composition of  
893 spinel in Pu'u 'O'o lava (1996-1998), Kilauea volcano, Hawaii. *Journal of Volcanology*  
894 and Geothermal Research 123(3-4):245-265

895 Rohrbach A, Schuth S, Ballhaus C, Münker C, Matveev S, Qopoto C (2005) Petrological  
896 constraints on the origin of arc picrites, New Georgia Group, Solomon Islands.  
897 *Contributions to Mineralogy and Petrology* 149(6):685-698

898 Ruprecht P, Bachmann O (2010) Pre-eruptive reheating during magma mixing at Quizapu  
899 volcano and the implications for the explosiveness of silicic arc volcanoes. *Geology*  
900 38(10):919-922

901 Russell JK, Porritt LA, Lavalley Y, Dingwell DB (2012) Kimberlite ascent by assimilation-  
902 fuelled buoyancy. *Nature* 481(7381):352-356

903 Sato H (1977) Nickel content of basaltic magmas: identification of primary magmas and a  
904 measure of the degree of olivine fractionation. *Lithos* 10(2):113-120

905 Seghedi I, Downes H, Vaselli O, Szakács A, Balogh K, Pécskay Z (2004) Post-collisional  
906 Tertiary-Quaternary mafic alkalic magmatism in the Carpathian-Pannonian region: a  
907 review. *Tectonophysics* 393(1-4):43-62

908 Shane P, Gehrels M, Zawalna-Geer A, Augustinus P, Lindsay J, Chaillou I (2013) Longevity  
909 of a small shield volcano revealed by crypto-tephra studies (Rangitoto volcano, New  
910 Zealand): Change in eruptive behavior of a basaltic field. *Journal of Volcanology and*  
911 *Geothermal Research* 257(0):174-183

912 Shaw C, Dingwell D (2008) Experimental peridotite-melt reaction at one atmosphere: a  
913 textural and chemical study. *Contributions to Mineralogy and Petrology* 155(2):199-214

914 Shaw CSJ (1999) Dissolution of orthopyroxene in basanitic magma between 0.4 and 2 GPa:  
915 further implications for the origin of Si-rich alkaline glass inclusions in mantle xenoliths.  
916 *Contributions to Mineralogy and Petrology* 135(2):114-132

917 Shaw CSJ, Eyzaguirre J (2000) Origin of megacrysts in the mafic alkaline lavas of the West  
918 Eifel volcanic field, Germany. *Lithos* 50(1-3):75-95

919 Shaw CSJ, Thibault Y, Edgar AD, Lloyd FE (1998) Mechanisms of orthopyroxene  
920 dissolution in silica-undersaturated melts at 1 atmosphere and implications for the origin  
921 of silica-rich glass in mantle xenoliths. *Contributions to Mineralogy and Petrology*  
922 132(4):354-370

923 Smith DR, Leeman WP (2005) Chromian spinel-olivine phase chemistry and the origin of  
924 primitive basalts of the southern Washington Cascades. *Journal of Volcanology and*  
925 *Geothermal Research* 140(1-3):49-66

926 Sparks RSJ, Baker L, Brown RJ, Field M, Schumacher J, Stripp G, Walters A (2006)  
927 Dynamical constraints on kimberlite volcanism. *Journal of Volcanology and Geothermal*  
928 *Research* 155(1-2):18-48

929 Sparks RSJ, Pinkerton H, Macdonald R (1977) The transport of xenoliths in magmas. *Earth*

930 and Planetary Science Letters 35(2):234-238

931 Spera FJ (1984) Carbon dioxide in petrogenesis III: role of volatiles in the ascent of alkaline  
932 magma with special reference to xenolith-bearing mafic lavas. Contributions to  
933 Mineralogy and Petrology 88(3):217-232

934 Stormer JC (1973) Calcium zoning in olivine and its relationship to silica activity and  
935 pressure. Geochimica et Cosmochimica Acta 37(8):1815-1821

936 Szabó C, Bodnar RJ (1996) Changing magma ascent rates in the Nógrád–Gömör volcanic  
937 field, Northern Hungary/Southern Slovakia: evidence from CO<sub>2</sub>-rich fluid inclusions in  
938 metasomatized upper mantle xenoliths. Petrology 4(3):221-230

939 Szabó C, Falus G, Zajacz Z, Kovács I, Bali E (2004) Composition and evolution of  
940 lithosphere beneath the Carpathian-Pannonian Region: a review. Tectonophysics 393(1-  
941 4):119-137

942 Takada A (1994) The influence of regional stress and magmatic input on styles of  
943 monogenetic and polygenetic volcanism. Journal of Geophysical Research  
944 99(B7):13563-13573

945 Tari G, Dövényi P, Horváth F, Dunkl I, Lenkey L, Stefanescu M, Szafián P, Tóth T (1999)  
946 Lithospheric structure of the Pannonian Basin derived from seismic, gravity and  
947 geothermal data. In: Durand B, Jolivet L, Horváth F, Séranne M (eds) The Mediterranean  
948 Basins: Tertiary extension within the Alpine orogen. Geological Society, London, Special  
949 Publication, pp 215-250

950 Tracy RJ, Robinson P (1977) Zoned titanian augite in alkali olivine basalt from Tahiti and the  
951 nature of titanium substitutions in augite. American Mineralogist 62(7-8):634-645

952 Ulrych J, Ackerman L, Balogh K, Hegner E, Jelínek E, Pécskay Z, Přichystal A, Upton BGJ,  
953 Zimák J, Foltýnová R (2013) Plio-Pleistocene basanitic and melilititic series of the  
954 Bohemian Massif: K-Ar ages, major/trace element and Sr–Nd isotopic data. Chemie der

955 Erde – Geochemistry. <http://dx.doi.org/10.1016/j.chemer.2013.02.001>

956 Valentine GA, Krogh KEC (2006) Emplacement of shallow dikes and sills beneath a small  
957 basaltic volcanic center – The role of pre-existing structure (Paiute Ridge, southern  
958 Nevada, USA). *Earth and Planetary Science Letters* 246(3–4):217-230

959 Walker GPL (1993) Basaltic-volcano systems. Geological Society, London, Special  
960 Publications 76(1):3-38

961 Wass SY (1979) Multiple origins of clinopyroxenes in alkali basaltic rocks. *Lithos* 12(2):115-  
962 132

963 Wijbrans J, Németh K, Martin U, Balogh K (2007)  $^{40}\text{Ar}/^{39}\text{Ar}$  geochronology of Neogene  
964 phreatomagmatic volcanism in the western Pannonian Basin, Hungary. *Journal of*  
965 *Volcanology and Geothermal Research* 164(4):193-204

966 Yagi K, Onuma K (1967) The Join  $\text{CaMgSi}_2\text{O}_6\text{-CaTiAl}_2\text{O}_6$  and its bearing on the  
967 Titanaugites. *Journal of the Faculty of Science, Hokkaido University. Series 4, Geology*  
968 *and Mineralogy* 13(4):463-483

969 Zhang H-F (2005) Transformation of lithospheric mantle through peridotite-melt reaction: A  
970 case of Sino-Korean craton. *Earth and Planetary Science Letters* 237(3-4):768-780

971

972 **Figure captions**

973

974 Fig. 1

975 a) Geological sketch map of the Carpathian-Pannonian Region. Alkaline basaltic volcanic  
976 fields are assigned with numbers: 1=Styrian Basin, 2=Little Hungarian Plain, 3=Bakony-  
977 Balaton Highland, 4=Stiavnica-Nógrád-Gömör, 5=Kecel, 6=Banat, 7= Perşani; b) Simplified  
978 geological map of the Bakony-Balaton Highland Volcanic Field (after [Jugovics 1968](#);

979 [Harangi 2001](#)) with the locality of the Bondoró-hegy and the Füzes-tó scoria cone (and the  
980 names of some other volcanic centres).

981

982 Fig. 2

983 Outcrop photo of the scoria cone remnant, first shown by [Kereszturi et al. \(2010\)](#). The  
984 scoriaceous breccia of the cone is cross-cut by a massive basalt dyke (the boundaries of the  
985 dyke are marked by the white dashed lines), that we interpret as a feeder dyke based on field  
986 observations. The white arrow indicates the direction of the dyke injection. The hammer  
987 (shown by the black arrow) is 30 cm in length.

988

989 Fig. 3

990 a) Typical petrographic appearance of the studied crystal-rich alkaline basalts  
991 (photomicrograph, XN, sample: Ft3). Note that almost all of the phenocrysts *s.l.* are foreign  
992 minerals; b) Amphibole-bearing spinel peridotite xenolith occasionally occur in the studied  
993 alkaline basalts (photomicrograph, 1N, sample: Fuz3). Ol – olivine, opx – orthopyroxene, cpx  
994 – clinopyroxene, am – amphibole.

995

996 Fig. 4

997 a) Anhedral, embayed olivine which has a bright rim and contains a light green spinel that has  
998 a bright overgrowth rim adjacent to the groundmass; b) Rounded spinel crystal with a bright  
999 overgrowth rim; c) Orthopyroxene and its fine-grained rim consisting of olivine,  
1000 clinopyroxene and glass; d) Crystal clot that consists of an anhedral olivine and a  
1001 clinopyroxene with a rounded colourless core; e) Clinopyroxene crystal having an anhedral  
1002 colourless core and a sector zoned rim; f) Clinopyroxene crystal with a resorbed light green  
1003 core and a sector zoned rim; g) Homogeneous, colourless clinopyroxene megacryst that has a

1004 thick spongy zone and a zoned clinopyroxene overgrowth on it; h) Enlargement of the spongy  
1005 zone of the clinopyroxene megacryst (g) containing feldspar and spinel inclusions; i) Sector  
1006 zoned clinopyroxene phenocryst. SEM backscattered electron images. Ol – olivine, sp –  
1007 spinel, opx – orthopyroxene, cpx – clinopyroxene, fp – feldspar.

1008

1009 Fig. 5

1010 a) Relationship between the Fo (mol%) and CaO (wt.%) content of the studied olivine  
1011 crystals; b) Plot of Fo (mol%) and NiO (wt.%) contents of the studied olivines. Light grey  
1012 dashed line fields indicate the compositions of olivines in upper mantle peridotite xenoliths  
1013 from the Balaton Highland ([Embey-Isztin et al. 2001a](#)).

1014

1015 Fig. 6

1016 Fo (mol%), Ni and Ca (ppm) profiles of olivine xenocrysts (a, b) and an olivine phenocryst  
1017 *s.s.* (c). The lines of measured points are indicated by the A-B lines in each picture (SEM  
1018 backscattered electron images). In the case of the xenocrysts, at the crystal margins (in a 50-  
1019 100  $\mu\text{m}$  thick band) points were measured with  $\sim 5 \mu\text{m}$  gaps between each other, while in the  
1020 central part of the olivine the gaps were increased to 20-50  $\mu\text{m}$ . In the case of olivine  
1021 phenocrysts, the whole profile was prepared with 5  $\mu\text{m}$  gaps (5  $\mu\text{m}$  distances between  
1022 measuring points were necessary because of the effect of the  $e^-$  beam on the crystal surface).

1023

1024 Fig. 7

1025 Fo (mol%) vs. NiO (wt.%) relationship of representative olivine xenocrysts (Fig. 6a, b) and  
1026 normal zoned phenocryst (Fig. 6c). The different core-to-rim trends are indicative for  
1027 diffusion- or growth-related development of the zoning (for details see text).

1028

1029 Fig. 8

1030 Compositions of the studied clinopyroxenes plotted in the atomic Mg-Fe-Ca ternary diagram  
1031 (boundaries after [Morimoto et al. 1988](#)). The light grey dashed line field indicates the  
1032 compositions of clinopyroxenes in upper mantle peridotite xenoliths from the Balaton  
1033 Highland ([Embey-Isztin et al. 2001a](#)), the dark grey dashed line field indicates the  
1034 compositions of clinopyroxenes in lower crustal mafic granulite xenoliths from the Balaton  
1035 Highland ([Embey-Isztin et al. 2003](#)).

1036

1037 Fig. 9

1038 Variation of Mg# ( $\text{Mg}/(\text{Mg}+\text{Fe}^{\text{tot}})$ ) vs. Ti (a), Al (b), Cr (c) and Na (d) (cations per formula  
1039 unit based on 6 O); e) Plot of Ti vs. Al (cations per formula unit based on 6 O); f)  $^{\text{IV}}\text{Al}$  vs.  
1040  $^{\text{VI}}\text{Al}$  diagram ([Aoki and Kushiro 1968](#)). Symbols as in Fig. 8. Light and dark grey dashed line  
1041 fields indicate the same clinopyroxene compositions as in Fig. 8 (the Cr content of granulitic  
1042 clinopyroxenes were not analysed in [Embey-Isztin et al. 2003](#)).

1043

1044 Fig. 10

1045 a) Cr-Al-Fe<sup>3+</sup> ternary plot of the studied spinels; b) Variation of MgO (wt.%) vs. Al<sub>2</sub>O<sub>3</sub>  
1046 (wt.%) contents in the studied spinel grains. Light grey dashed line fields indicate the  
1047 compositions of spinels in upper mantle peridotite xenoliths from the Balaton Highland  
1048 ([Embey-Isztin et al. 2001a](#)).

1049

1050 Fig. 11

1051 Schematic cartoon of the proposed model for the ascent history of the Bondoró-hegy and  
1052 Füzes-tó alkaline basaltic magmas. Enlargements of the ascent path show the dominant  
1053 processes (see the text for details). The figure is to scale. LAB – lithosphere–asthenosphere

1054 boundary, gt – garnet, sp – spinel. The source for the crustal and lithospheric thicknesses is:

1055 [http://geophysics.elte.hu/atlas/geodin\\_atlas.htm](http://geophysics.elte.hu/atlas/geodin_atlas.htm).

1056

1057 **Table captions**

1058

1059 Table 1

1060 Major and trace element analyses of the BON683 sample from Bondoró-hegy ([Embey-Isztin](#)

1061 [et al. 1993a](#))

1062

1063 Table 2

1064 Representative compositions of the studied olivines

1065

1066 Table 3

1067 Representative analyses of the studied orthopyroxenes and clinopyroxenes

1068

1069 Table 4

1070 Representative compositions of the studied spinels

1071

1072 Table 5

1073 Details of the different methods and results of the estimated magma ascent rates and times

1074

1075 Table 6

1076 Calculated residence times of the studied olivine xenocrysts



1 M. Éva Jankovics<sup>1,\*</sup>, Gábor Dobosi<sup>2,3</sup>, Antal Embey-Isztin<sup>4</sup>, Balázs Kiss<sup>1,2</sup>, Tamás Sági<sup>1</sup>,  
2 Szabolcs Harangi<sup>1,2</sup>, Theodoros Ntaflou<sup>5</sup>

3

4 Origin and ascent history of unusually crystal-rich alkaline basaltic magmas from the western  
5 Pannonian Basin

6

7 <sup>1</sup>Department of Petrology and Geochemistry, Eötvös Loránd University, Pázmány Péter  
8 sétány 1/C, H-1117 Budapest, Hungary

9 <sup>2</sup>MTA-ELTE Volcanology Research Group, Pázmány Péter sétány 1/C, H-1117 Budapest,  
10 Hungary

11 <sup>3</sup>Institute for Geological and Geochemical Research, Research Centre for Astronomy and  
12 Earth Sciences, Hungarian Academy of Sciences, Budaörsi út 45., H-1112 Budapest, Hungary

13 <sup>4</sup>Department of Mineralogy and Petrology, Hungarian Natural History Museum, Ludovika tér  
14 2., H-1083 Budapest, Hungary

15 <sup>5</sup>Department of Lithospheric Research, University of Vienna, Althanstrasse 14, A-1090  
16 Vienna, Austria

17

18 \*Corresponding author. E-mail address: jeva182@gmail.com

19 Telephone number: +36-1/372 25 00/8359; +36-30/547 33 71

20 Fax number: +36-1/381 21 08

21

## 22 **Abstract**

23

24 The last eruptions of the monogenetic Bakony-Balaton Highland Volcanic Field (western  
25 Pannonian Basin, Hungary) produced unusually crystal- and xenolith-rich alkaline basalts

26 which are unique among the alkaline basalts of the Carpathian-Pannonian Region. Similar  
27 alkaline basalts are only rarely known in other volcanic fields of the world. These special  
28 basaltic magmas fed the eruptions of two closely located volcanic centres: the Bondoró-hegy  
29 and the Fűzes-tó scoria cone. Their uncommon enrichment in diverse crystals produced  
30 unique rock textures and modified original magma compositions (13.1-14.2 wt.% MgO, 459-  
31 657 ppm Cr, 455-564 ppm Ni contents).

32 Detailed mineral-scale textural and chemical analyses revealed that the Bondoró-hegy and  
33 Fűzes-tó alkaline basaltic magmas have a complex ascent history, and that most of their  
34 minerals (~30 vol.% of the rocks) represent foreign crystals derived from different levels of  
35 the underlying lithosphere. The most abundant xenocrysts, olivine, orthopyroxene,  
36 clinopyroxene and spinel, were incorporated from different regions and rock types of the  
37 subcontinental lithospheric mantle. Megacrysts of clinopyroxene and spinel could have  
38 originated from pegmatitic veins / sills which probably represent magmas crystallized near the  
39 crust-mantle boundary. Green clinopyroxene xenocrysts could have been derived from lower  
40 crustal mafic granulites. Minerals that crystallized in situ from the alkaline basaltic melts  
41 (olivine with Cr-spinel inclusions, clinopyroxene, plagioclase, Fe-Ti oxides) are only  
42 represented by microphenocrysts and overgrowths on the foreign crystals. The vast amount of  
43 peridotitic (most common) and mafic granulitic materials indicates a highly effective  
44 interaction between the ascending magmas and wall rocks at lithospheric mantle and lower  
45 crustal levels. However, fragments from the middle and upper crust are absent from the  
46 studied basalts, suggesting a change in the style (and possibly rate) of magma ascent in the  
47 crust. These xenocryst- and xenolith-rich basalts yield diverse tools for estimating magma  
48 ascent rate that is important for hazard forecasting in monogenetic volcanic fields. According  
49 to the estimated ascent rates, the Bondoró-hegy and Fűzes-tó alkaline basaltic magmas could  
50 have reached the surface within hours to few days, similarly to the estimates for other eruptive

51 centres in the Pannonian Basin which were fed by "normal" (crystal- and xenolith-poor)

52 alkaline basalts.

53

54 **Keywords**

55 alkaline basalt, ascent history, crystal-rich, magma ascent rate, monogenetic volcanism,

56 xenocryst, xenolith

57

## 58 **Introduction**

59

60 Monogenetic basaltic volcanic fields consist of small individual eruptive centres  
61 characterized by a single brief eruption (Walker, 1993) and low magma supply (e.g.,  
62 Hasenaka and Carmichael, 1985; Takada, 1994). These monogenetic eruptions of basalt are  
63 generally assumed to be simple in terms of volcanology and petrology. That is, they produce  
64 small volcanic edifices during continuous activity within a relatively short time span, and are  
65 fed by a single, compositionally discrete batch of magma (e.g., Connor and Conway 2000).  
66 However, several authors suggested that individual eruptive centres can be characterized by  
67 multiple eruptions involving different magma batches with hiatuses during their activity (e.g.,  
68 Reiners 2002; Martin and Németh 2005; Brenna et al. 2010, 2011; Needham et al. 2011,  
69 Shane et al. 2013) implying a complex evolution history of the magmatic system. These  
70 studies focused mainly on the compositional variations of the feeding magma batches and  
71 suggest differences in their source regions and / or degrees of partial melting. However,  
72 processes acting during the ascent of the magma batches are also important (Brenna et al.  
73 2010). This is essential information because the evolution of the magma in the feeding system  
74 can have a significant effect on the rate and style of magma ascent, and therefore on the  
75 nature of eruptions (e.g., Ruprecht and Bachmann 2010; McGee et al. 2012; Russell et al.  
76 2012). Detailed textural and chemical analyses of phenocrysts in basalts can provide insights  
77 into the details of their magma evolution (e.g., Dobosi 1989; Dobosi et al. 1991; Roeder et al.  
78 2001, 2003, 2006; Smith and Leeman 2005; Jankovics et al. 2009, 2012).

79 The monogenetic Bakony-Balaton Highland Volcanic Field, located in the western part of  
80 the Carpathian-Pannonian Region, was active for approximately 6 My. Its last active phase  
81 was closed by two eruptive centres: the Bondoró-hegy (2.3 Ma; Balogh and Pécskay 2001)  
82 and the Füzés-tó scoria cone (2.6 Ma; Wijbrans et al. 2007) each fed by alkaline basaltic

83 magmas with special compositions and petrological appearance (Jankovics et al. 2009, 2012).  
84 These alkaline basalts are characterized by extremely high Mg, Ni and Cr contents and are  
85 unusually rich in diverse crystals and xenoliths (peridotite, mafic granulite). Similar magmas  
86 did not erupt in the above mentioned volcanic field and even in the other six volcanic fields in  
87 the whole Carpathian-Pannonian Region (CPR). Nevertheless, basalts of numerous eruptive  
88 centres in the region contain diverse xenoliths. In other volcanic fields of the world, magmas  
89 with characteristics similar to those of the Bondoró-hegy and Füzés-tó scoria cone are known  
90 (e.g., Ancochea et al. 1987; Mattsson 2012; Kozákov Hill in Ulrych et al. in press) but they  
91 are rare. Due to their crystal-rich feature these rocks provide unique insights into the ascent  
92 history of basaltic magmas. Following the detailed investigations and descriptions of the  
93 Füzés-tó basalt (Jankovics et al. 2009, 2012), in this study we analyse the similar (both in age  
94 and petrology) basalt of Bondoró-hegy and reveal its ascent history. It is generally assumed  
95 that such xenolith-rich magmas can reach the surface very rapidly. We estimate the ascent  
96 rates of these xenocryst- and xenolith-rich alkaline basalts, and compare the results with  
97 xenolith-poor basalts. Understanding the ascent history and estimating the magma ascent  
98 velocity is important in monogenetic volcanic fields for their volcanic hazard assessments.  
99 This study demonstrates the importance of the especially crystal-rich basaltic magmas of  
100 monogenetic volcanic fields for enabling estimating the magma ascent rate by several  
101 different methods.

102

### 103 **Geological setting**

104

105 The Pannonian Basin is a Miocene extensional back-arc basin surrounded by the Alpine,  
106 Carpathian and Dinarides orogenic belts (Fig.1a). It is characterized by thin lithosphere (50-  
107 80 km) and crust (22-30 km) coupled with high heat flow ( $>80$  mW/m<sup>2</sup>; Csontos et al. 1992;

108 [Fodor et al. 1999](#); [Tari et al. 1999](#); [Bada and Horváth 2001](#); [Lenkey et al. 2002](#)). These  
109 features are due to the initial syn-rift phase (17–12 Ma; [Horváth 1995](#)) of the Pannonian Basin  
110 that was characterized by subduction roll-back, related back-arc extension and lithospheric  
111 thinning ([Csontos et al. 1992](#); [Horváth 1993](#); [Tari et al. 1999](#)). This was followed by the Late  
112 Miocene–Pliocene post-rift phase (e.g., [Horváth 1995](#)) which was accompanied by thermal  
113 subsidence, thickening of the lithosphere and sedimentation in the basin areas. Tectonic  
114 inversion has characterized the Pannonian Basin since the late Pliocene due to the push of the  
115 Adriatic plate from the southwest and blocking by the East European platform in the east  
116 ([Horváth and Cloetingh 1996](#)).

117 Post-extensional alkaline basaltic volcanism occurred from 11 to 0.13 Ma in the region,  
118 mainly on its marginal parts, which formed monogenetic volcanic fields. The tectonic  
119 background of the alkaline basaltic magmatism is still under debate. Several researchers  
120 suggested that localised mantle plume fingers (deriving from a common mantle reservoir  
121 named "European Asthenospheric Reservoir"; [Hoernle et al. 1995](#)) could be responsible for  
122 the alkaline basaltic volcanism in Western and Central Europe, accordingly in the Pannonian  
123 Basin as well ([Granet et al. 1995](#); [Seghedi et al. 2004](#)). However, [Harangi and Lenkey \(2007\)](#)  
124 and [Harangi \(2009\)](#) argued against the plume-related magmatism. They suggested that the  
125 significantly stretched Pannonian Basin provided suction in the sublithospheric mantle and  
126 generated an asthenospheric mantle flow from below the thick Alpine regime which could  
127 lead to the partial melting of the heterogeneous upper mantle.

128 The Bakony-Balaton Highland Volcanic Field ([Fig. 1b](#)) comprises approximately 150-200  
129 eruptive centres ([Németh and Martin 1999a, 1999b](#)) that are erosional remnants of maars, tuff  
130 rings, scoria cones and shield volcanoes (e.g., [Jugovics 1968](#); [Németh and Martin 1999a,](#)  
131 [1999b](#); [Martin et al. 2003](#)). Several of these alkaline basalt occurrences contain ultramafic and  
132 mafic xenoliths, as well as discrete megacrysts which were extensively studied in the past

133 decades (e.g., Embey-Isztin 1976; Embey-Isztin et al. 1989, 1990, 2001a, 2001b, 2003;  
134 Downes et al. 1992; Downes and Vaselli 1995; Dobosi et al. 2003; Dégi et al. 2009). These  
135 studies together with those for whole-rock geochemistry of the basalts (e.g., Embey-Isztin et  
136 al. 1993a, 1993b; Embey-Isztin and Dobosi 1995; Seghedi et al. 2004) have yielded important  
137 information on the nature of the upper mantle beneath the area and the partial melting  
138 processes. Based on several studies (e.g., Embey-Isztin et al. 1989, 1990, 2001a; Szabó et al.  
139 2004; Hidas et al. 2007; Dégi et al. 2009) we have an extensive knowledge about the structure  
140 of the whole lithosphere as well.

141

## 142 **Volcanological background**

143

144 In this paper, we describe the volcanological background for the Bondoró-hegy eruptive  
145 centre. The features of the Fűzes-tó scoria cone were reported in a previous paper (Jankovics  
146 et al. 2009). Bondoró-hegy volcano is one of the most complex eruption centres of this  
147 volcanic field and consists of several discrete eruptive units: basal tuff ring pyroclastics with a  
148 lava lake, reworked basaltic debris beds, lava flow units (1<sup>st</sup> and 2<sup>nd</sup> lava flow) and capping  
149 scoria cone associated with the 3<sup>rd</sup> lava flow (Kereszturi et al. 2010). The capping scoriaceous  
150 basalt (e.g., spindle and scoriaceous bombs) and the 3<sup>rd</sup> lava flow unit (representing the  
151 youngest eruptive phase) are rich in xenoliths of upper mantle and lower crustal origins  
152 (peridotite, wehrlite, clinopyroxenite, mafic granulite) and in clinopyroxene and spinel  
153 megacrysts.

154 In an outcrop of the capping scoria unit (in the breached side of the scoria cone remnant),  
155 Kereszturi et al (2010) described a dyke that crosscuts the scoriaceous breccia. Based on our  
156 field observations (Fig. 2), this massive dyke has an average width of  $0.625 \pm 0.055$  m and can  
157 be interpreted as a feeder dyke of the scoria cone.

158 Several K-Ar ages are available: the basalt of the lava lake is estimated at about  
159  $\leq 3.86 \pm 0.20$  Ma and the 2<sup>nd</sup> lava unit at about  $2.90 \pm 0.62$  Ma (Balogh et al. 1986). A sample  
160 from the 3<sup>rd</sup> lava flow unit gave an age of  $2.29 \pm 0.22$  Ma (Balogh and Pécskay 2001).  
161 According to Kereszturi et al. (2010), these ages represent the best fit with the geological and  
162 stratigraphical observations. Unfortunately, Bondoró-hegy was not included in the  $^{40}\text{Ar}/^{39}\text{Ar}$   
163 dating of the Balaton Highland basaltic rocks (Wijbrans et al. 2007). Based on the preferred  
164 K-Ar ages (that indicate prolonged volcanic activity) and the discordance between the  
165 phreatomagmatic unit and the subsequent lava flows (implying a significant time gap),  
166 Bondoró-hegy can be regarded as a polycyclic monogenetic volcano (Kereszturi et al. 2010).

167

## 168 **Petrography and whole-rock compositions**

169

170 Samples of the Bondoró-hegy were collected from the 3<sup>rd</sup> lava flow unit. Samples of the  
171 Füzes-tó scoria cone were collected in the inner slope around the central depression (various  
172 basaltic bombs). In this paper, we describe only the features of the Bondoró-hegy basalt, the  
173 descriptions of the Füzes-tó basalt are in Jankovics et al. (2009, 2012). Figure 3a shows the  
174 typical petrographic appearance of the studied crystal-rich alkaline basalts.

175 The term ‘phenocryst’ is here used in a general sense, i.e., for larger, up to 5 mm, crystals  
176 in fine-grained groundmasses, regardless of their origins (i.e., phenocryst *sensu lato*). In the  
177 following, the term ‘phenocryst’ has been used in a genetic sense, i.e., for crystals that have  
178 grown in situ in the magma in which they are found now (i.e., phenocryst *sensu stricto*).

179 The studied lava samples have porphyritic texture characterized by non- to low-  
180 vesicularity and ~30 vol.% anhedral to euhedral phenocrysts (on a vesicle-free basis). The  
181 phenocryst assemblage consists of olivine, clinopyroxene, orthopyroxene and spinel  
182 characterized by variable forms and sizes, and crystals often occur together as crystal clots



183 (Fig. 4d). Microphenocrysts (<150  $\mu\text{m}$ ) are clinopyroxene, olivine, plagioclase and Fe-Ti-  
184 oxides. The fine-grained groundmass is composed of microlitic feldspars (plagioclase and  
185 alkali feldspar), clinopyroxene, olivine, Fe-Ti-oxides, apatite and some glass.

186 Most of the olivine phenocrysts (up to 5 mm) are characterized by rounded and embayed  
187 margins. These crystals commonly show undulose extinction, and have bright rims (with  
188 diffuse boundaries toward the crystal interiors) in the backscattered electron (BSE) images  
189 (e.g., Fig. 4a). They frequently contain subhedral-anhedral (often rounded), light green to  
190 brown spinel inclusions which range in size from ~50 to 300  $\mu\text{m}$ . The smaller (150-900  $\mu\text{m}$ )  
191 olivine grains are euhedral to subhedral and often skeletal and their outermost margin is  
192 frequently iddingsitised. They often contain black, euhedral-subhedral chromian spinel  
193 inclusions (~3-10  $\mu\text{m}$ ).

194 Orthopyroxene crystals (up to 2.4 mm) are always surrounded by fine-grained rims of  
195 various thicknesses (Fig. 4c) consisting of olivine, clinopyroxene, glass and rarely spinel. The  
196 outermost part of this corona often contains numerous Fe-Ti-oxides as well. This fine-grained  
197 rim is frequently overgrown by a pale brown, twinned and sector zoned clinopyroxene.

198 Clinopyroxene phenocrysts (up to 3 mm) are euhedral to subhedral in shape and usually  
199 have an anhedral, rounded core (with a sharp boundary) and a pale brown, twinned, sector  
200 zoned rim characterized by various thicknesses (rarely some sector zoned clinopyroxenes  
201 without a rounded crystal core are also found; Fig. 4i). Two types of the anhedral, variously  
202 resorbed cores can be distinguished. The first and more frequent type is colourless under the  
203 optical microscope, and darker grey than the rim in the BSE images (Fig. 4d, e). The other  
204 type is light green under the optical microscope, and lighter grey than the surrounding rim in  
205 the BSE images (Fig. 4f) which indicates reverse zoning. The green cores often have spongy  
206 or sieved texture.

207 Spinel crystals (up to 0.5 mm) occur as individual crystals in the matrix (Fig. 4b) and as  
208 inclusions in olivine phenocrysts (Fig. 4a). They usually have ragged, anhedral margins, are  
209 characterized by variable colours (light green to brown), and often have a bright (Ti-  
210 magnetite) overgrowth rim (with a relatively sharp boundary toward the crystal interior) in the  
211 BSE images where it is in contact with the groundmass (Fig. 4a, b).

212 All these disequilibrium textures (ragged, rounded, resorbed, embayed, spongy features)  
213 suggest a xenocrystic origin for the anhedral olivines, colourless and green cores of  
214 clinopyroxene phenocrysts, orthopyroxenes and spinels.

215 In addition to the abundant xenocrysts, the studied samples include numerous peridotite  
216 xenoliths. These are spinel peridotites which occasionally contain amphiboles (Fig. 3b).  
217 Along the contact between the peridotite and basalt the peridotitic orthopyroxene grains have  
218 the same fine-grained rims as the orthopyroxene xenocrysts in the basaltic groundmass.  
219 Therefore, these rims are interpreted as mineral-melt reaction products. Similar to most of the  
220 olivine xenocrysts, the olivine grains in the peridotite xenoliths often have undulose  
221 extinction which implies deformation.

222 Additionally, clinopyroxene and spinel megacrysts are also common. Most of the  
223 clinopyroxene megacrysts (up to 6 cm, elongated) are colourless, they have homogeneous  
224 interiors crosscutting with cracks filled with secondary fluid inclusions, and are overgrown by  
225 a pale brown, zoned clinopyroxene rim similar to that of the clinopyroxene xenocrysts.  
226 Spongy zones are present between this rim and the homogeneous part of the megacrysts (Fig.  
227 4g). In the spongy zones, small inclusions of feldspars (plagioclase and alkali feldspar) and  
228 skeletal spinels are present (Fig. 4h). Besides the colourless megacrysts, one piece of a green  
229 clinopyroxene megacryst has also been found. The spinel megacrysts are ~1-2 cm in size,  
230 mostly dark green, but one was black, under the optical microscope.

231 The whole rock composition of the Bondoró-hegy basalt has been described by [Jugovics](#)  
232 [\(1976\)](#) and [Embey-Isztin et al. \(1993a, 1993b\)](#). The compositional data identify the lavas of  
233 Bondoró-hegy as undersaturated basanite ([Table 1](#)), similar to the compositions of the other  
234 basalts in the region, however, the basaltic rocks from Bondoró-hegy are extremely rich in  
235 MgO (13.1-13.9 wt.%). Similar MgO enrichment has been reported only at the Fűzes-tó  
236 scoria cone from the Pannonian Basin (see [Fig. 1b](#)), which has 13.4-14.2 wt.% MgO content  
237 ([Jankovics et al. 2009](#)). This is correlated with the abundance of xenocrystic olivine and  
238 orthopyroxene. The high MgO content is accompanied by extreme enrichment in Ni and Cr  
239 contents (455-474 and 459-489 ppm, respectively; [Embey-Isztin et al. 1993a, 1993b](#)), also  
240 caused by the presence of abundant peridotitic xenocrysts. The incompatible trace element  
241 content of the Bondoró-hegy basalt is approximately the same as that of the other basalts of  
242 the region, though some incompatible trace element and radiogenic isotope ratios are  
243 different. While the lavas of the Bakony-Balaton Highland Volcanic Field tend to show  
244 higher K/Nb, Rb/Nb and lower Ce/Pb, as well as higher  $^{207}\text{Pb}/^{204}\text{Pb}$  and  $^{87}\text{Sr}/^{86}\text{Sr}$ , the opposite  
245 is true for the Bondoró-hegy basalt. This is explained by the involvement of an enriched  
246 lithospheric component in the lavas, which is missing from the Bondoró-hegy basaltic magma  
247 ([Embey-Isztin et al. 1993b](#)).

248

## 249 **Mineral chemistry**

250

251 Analyses of minerals in the Bondoró-hegy basalt were obtained on a JEOL Superprobe  
252 733 using wavelength-dispersive spectrometers at the Institute for Geological and  
253 Geochemical Research in Budapest, Hungary. Analytical conditions were 20 kV accelerating  
254 voltage, 35 nA beam current, and all analyses were made against mineral standards. Raw data  
255 were corrected by the ZAF correction program of JEOL. Olivine profiles of the Fűzes-tó

256 basalt were determined using a CAMECA SX100 electron microprobe equipped with four  
257 WDS and one EDS at the University of Vienna, Department of Lithospheric Research  
258 (Austria). The operating conditions were as follows: 15 kV accelerating voltage, 20 nA beam  
259 current, 20 s counting time on peak position, focused beam diameter and PAP correction  
260 procedure for data reduction. The following standards were applied: albite (for Si, Al);  
261 almandine (for Fe); olivine (for Mg); wollastonite (for Ca); spessartine (for Mn) and Ni-oxide  
262 (for Ni). The mineral compositions of the Füzes-tó basalt are discussed in [Jankovics et al.](#)  
263 [\(2009, 2012\)](#).

264

### 265 *Olivine*

266

267 Olivine crystals display a wide range of Fo ([Table 2](#)). The xenocrysts are chemically  
268 homogeneous and typically have Fo from 89.5 to 92 mol% ( $Fo=100*Mg/(Mg+Fe)$ , all Fe is  
269 assumed to be divalent). They have thin rims with lower Fo (72.1-81.4 mol%), which overlap  
270 that of the groundmass olivines (76.1-76.7 mol%).

271 Olivine xenocrysts have low CaO and high NiO contents (0.05-0.12 wt.% and 0.33-0.39  
272 wt.%, respectively), while their rims are enriched in CaO (0.16-0.40 wt.%) and depleted in  
273 NiO (0.16-0.34 wt.%) ([Fig. 5](#)). CaO shows a weak negative, whereas NiO shows a weak  
274 positive correlation with Fo content ([Fig. 5](#)). The highest Ca and lowest Ni contents are in  
275 groundmass olivines (0.38-0.57 wt.% CaO and 0.14-0.18 wt.% NiO). The compositions of  
276 the studied xenocrysts resemble those of the olivines of the peridotite xenoliths in the Balaton  
277 Highland ([Fig. 5](#)).

278 All olivine Fo profiles are symmetric to the centre of the grain, but their shapes differ  
279 ([Fig. 6](#)). Olivine xenocrysts have well-defined inner plateaus bounded by large compositional  
280 gradients toward the rims ([Fig. 6a, b](#)). Their inner part contains less than 500 ppm Ca, ~3000

281 ppm Ni and ~90 mol% Fo. In the rims, Ca sharply increases to >3000 ppm, while Ni and Fo  
282 sharply decrease to <1000 ppm and to 75 mol%, respectively. In several xenocrysts, the inner  
283 plateaus show some compositional variations (maybe related to healed cracks or tiny  
284 inclusions) (Fig. 6b). The profiles of olivine phenocrysts have a shield-like shape indicating a  
285 gradual compositional variation toward the rims (Fig. 6c). The Ca and Ni profiles are less  
286 smooth than those in xenocrysts, which may be the result of skeletal growth of the  
287 phenocrysts. Compared to the xenocrysts, the Ca content of their inner part is significantly  
288 higher (~1250 ppm), while the Ni and Fo contents are lower (between ~2000-2500 ppm and  
289 ~87 mol%, respectively). Phenocrysts and xenocrysts can be distinguished in the Fo-NiO  
290 diagram (Fig. 7), which shows that olivine xenocrysts show linear trends towards the rims  
291 indicating that the formation of core-to-rim zoning was mainly driven by diffusion. However,  
292 phenocrystic olivine has a curved trend towards the rims that can be interpreted as mainly  
293 growth-related core-to-rim zoning considering the implications of Costa et al. (2008).

294 The compositions of the xenocryst rims (Fig. 5, 6a) are similar to those of the olivine  
295 xenocryst rims and olivine phenocryst rims in the Füzés-tó basalt (Jankovics et al. 2009,  
296 2012). The formation of these Fe-rich rims can be explained by diffusion during re-  
297 equilibration of the xenocryst with the host basaltic magma (note the diffuse boundary toward  
298 the crystal interior; Fig. 4a, d) as well as some subsequent crystallization of phenocrystic  
299 olivine on the xenocrysts.

300

### 301 *Orthopyroxene*

302

303 Orthopyroxenes occur only as xenocrysts in the studied basalt. They are enstatites  
304 (Morimoto et al., 1988) with high Mg#s (0.91-0.92;  $Mg/(Mg+Fe^{tot})$ ) and contain 2.9-3 wt.%

305 Al<sub>2</sub>O<sub>3</sub> (Table 3). These compositions are characteristic for mantle orthopyroxenes similar to  
306 those of the peridotite xenoliths in the Balaton Highland (Embey-Isztin et al. 2001a).

307

308 *Clinopyroxene*

309

310 The clinopyroxene compositions are highly variable (Table 3, Figs. 8, 9) but basically four  
311 different types can be distinguished. They are: 1) colourless xenocrystic cores, 2) light green  
312 xenocrystic cores, 3) megacrysts, 4) phenocrysts, microphenocrysts and groundmass  
313 clinopyroxenes.

314

315 Colourless cores

316

317 Colourless cores (Table 3, analyses No. 2 and 4) are homogeneous but have variable  
318 compositions in the different crystals. They are chromian diopsides (Fig. 8) with high Mg#s  
319 (0.88-0.92; Mg/(Mg+Fe<sup>tot</sup>)) and SiO<sub>2</sub> contents (51.2-53.7 wt.%), and varying Cr<sub>2</sub>O<sub>3</sub> and Al<sub>2</sub>O<sub>3</sub>  
320 contents (0.28-1.4 wt.% and 2.8-6.1 wt.%, respectively). They are generally low in TiO<sub>2</sub> (up  
321 to 0.48 wt.%) and have low Ti/Al ratios ( $\leq 0.07$ ) and high Al<sup>VI</sup>/Al<sup>IV</sup> ratios (0.81-1.3). The  
322 compositions of these colourless xenocrystic cores are similar to those of the clinopyroxenes  
323 from the peridotite xenoliths in the Balaton Highland (Figs. 8, 9).

324

325 Green cores

326

327 Representative analyses of green cores are in Table 3 (analyses No. 6 and 8). The green  
328 cores are homogeneous and enriched in iron (Fig. 8). Their Mg#s (Mg/(Mg+Fe<sup>tot</sup>)) varies  
329 between 0.59-0.69 which is lower than those of the overgrowth rims. Their TiO<sub>2</sub> and Al<sub>2</sub>O<sub>3</sub>

330 contents are relatively low (0.49-0.76 wt.% and 4.5-6.6 wt.%, respectively) and the amount of  
331 Cr<sub>2</sub>O<sub>3</sub> is around (or below) the detection limit. The compositions of these xenocrystic cores  
332 resemble those of the clinopyroxenes of the lower crustal granulite xenoliths in the Balaton  
333 Highland (Figs. 8, 9). Their Ti/Al and Al<sup>VI</sup>/Al<sup>IV</sup> ratios are in the same range as in the  
334 colourless cores (Fig. 9e, f). One of the green cores has a different composition: it has slightly  
335 lower Mg# (0.58) and significantly lower TiO<sub>2</sub> (0.28 wt.%) and Al<sub>2</sub>O<sub>3</sub> (1.5 wt.%) contents  
336 than the other green cores of the samples.

337

338 Megacrysts

339

340 The interiors of the megacrysts are homogeneous. The colourless megacrysts show a  
341 restricted range of composition (Figs. 8, 9; Table 3, analyses No. 10 and 13). Their Mg#s  
342 (Mg/(Mg+Fe<sup>tot</sup>)) are 0.81-0.83, the TiO<sub>2</sub> and Al<sub>2</sub>O<sub>3</sub> contents are in the range of 0.91-1.3 wt.%  
343 and 8.7-9.2 wt.%, respectively. They are characterized by low Ti/Al (0.07-0.09) and high  
344 Al<sup>VI</sup>/Al<sup>IV</sup> ratios (0.90-1.2) (Fig. 9e, f). They have high Na<sub>2</sub>O contents (1.2-1.3 wt.%)  
345 compared to the phenocrysts, and do not contain Cr<sub>2</sub>O<sub>3</sub> in detectable amount. The  
346 clinopyroxene composition in the spongy part is slightly different from that of the interior of  
347 the megacryst having higher TiO<sub>2</sub> (1.1-2.2 wt.%), lower Al<sub>2</sub>O<sub>3</sub> (6.2-8 wt.%) and Na<sub>2</sub>O (0.48-  
348 0.73 wt.%), while the Mg# is the same.

349 The green megacryst are characterized by lower Mg# (0.57) and Al<sub>2</sub>O<sub>3</sub> (7.5 wt.%), and  
350 higher TiO<sub>2</sub> (1.6 wt.%) and Na<sub>2</sub>O (2.1 wt.%) contents than the other megacrysts. It has similar  
351 Al<sup>VI</sup>/Al<sup>IV</sup> (0.93), but a slightly higher Ti/Al ratio (0.14) compared to the colourless  
352 megacrysts.

353

354 Phenocrysts, microphenocrysts and groundmass grains

355

356 The pale brown clinopyroxene phenocrysts (i.e., the overgrowth rims on clinopyroxene  
357 xenocrysts and megacrysts as well as on the reaction rim of orthopyroxene xenocrysts),  
358 microphenocrysts and microlites of the groundmass are titanian augites or titanaugites  
359 according to the traditional pyroxene nomenclature (Deer et al. 1978), but can be classified as  
360 diopside, aluminian diopside and titanian aluminian diopside according to the I.M.A.  
361 classification of pyroxenes (Morimoto et al. 1988). Some representative analyses of these  
362 clinopyroxenes can be seen in Table 3 (e.g., analyses No. 3, 7, 12 and 17). Their Mg#s  
363 ( $\text{Mg}/(\text{Mg}+\text{Fe}^{\text{tot}})$ ) range from 0.73 to 0.85 and their  $\text{TiO}_2$  and  $\text{Al}_2\text{O}_3$  contents vary between 1.5-  
364 3.9 wt.% and 4.9-10.1 wt.%, respectively. Ti and Al show positive correlation (Fig. 9e) and  
365 both elements increase with iron enrichment (Fig. 9a, b). Their increasing Ti with decreasing  
366 Mg# reflects the normal fractionation trend (e.g., Tracy and Robinson 1977). The  $\text{Cr}_2\text{O}_3$   
367 contents can reach 1 wt.% but it sharply decreases with decreasing Mg# (Fig. 9c). Their Ti/Al  
368 ratios (0.16-0.34) are higher, while the  $\text{Al}^{\text{VI}}/\text{Al}^{\text{IV}}$  ratios (0.12-0.48) are lower than those of any  
369 other type of the studied clinopyroxenes (Fig. 9e, f). These ratios imply that they could have  
370 crystallized under relatively low-pressure conditions (e.g., Yagi and Onuma 1967; Wass  
371 1979; Dobosi et al. 1991). Based on their slightly increasing Ti/Al ratios during crystallization  
372 (Fig. 9e), they could have precipitated under continuously decreasing pressure. They could  
373 have been characterized by a significantly higher crystallization rate compared to the olivine  
374 phenocrysts (as suggested by Fig. 4d).

375

### 376 *Oxide minerals*

377

378 Representative analyses of the studied oxide minerals are shown in Table 4. The  
379 xenocrysts are Mg- and Al-rich spinels showing variable compositions (Fig. 10). Their Mg#s



380 (Mg/(Mg+Fe<sup>tot</sup>)) vary between 0.63 and 0.74 and their Cr#s ( $100 \cdot \text{Cr}/(\text{Cr}+\text{Al})$ ) range from  
381 12.3 to 45.8 (Cr<sub>2</sub>O<sub>3</sub>=11.4-37 wt.%, Al<sub>2</sub>O<sub>3</sub>=29.2-54.5 wt.%). Additionally, they have low  
382 TiO<sub>2</sub> contents (0.11-0.37 wt.%). The compositions of the studied xenocrysts are very similar  
383 to those of the spinels of the peridotite xenoliths in the Balaton Highland (Fig. 10).

384 The dark green megacrysts are also Mg-Al-rich spinels (Fig. 10) with 0.65-0.67 Mg#s,  
385 however they are characterized by higher Al<sub>2</sub>O<sub>3</sub> contents (61-61.8 wt.%) and very low Cr<sub>2</sub>O<sub>3</sub>  
386 contents ( $\leq 0.15$  wt.%). The black megacryst has a completely different composition: it is a  
387 titanomagnetite with 10.4 wt.% TiO<sub>2</sub> and 76.6 wt.% FeO<sup>tot</sup> contents.

388 The oxides in the groundmass are mainly titanomagnetites which contain 17.3-23.5 wt.%  
389 TiO<sub>2</sub> and 66.8-72.5 wt.% FeO<sup>tot</sup>. Matrix ilmenites are also present characterized by 49.3-51.3  
390 wt.% TiO<sub>2</sub> and 38.8-43.1 wt.% FeO<sup>tot</sup>.

391

392 In summary, the compositional characteristics of the phenocryst (*s.s.*) phases (olivine,  
393 clinopyroxene, Fe-Ti-oxides) in the Bondoró-hegy basalt are similar to those of the  
394 phenocrysts found in other basalts in the Balaton Highland.

395

### 396 **Magma ascent rate estimates**

397

398 The Bondoró-hegy and Füzes-tó crystal-rich basalts provide a tool for estimating the  
399 magma ascent rate by a number of methods (Table 5). The detailed descriptions and  
400 background information of the different methods are presented in the Electronic Appendix.

401 1) We carried out calculations to estimate the ascent velocity for alkaline basaltic magmas  
402 in general based on fluid filled crack propagation velocities. These computations yield magma  
403 ascent rates in the range of 3.9-15.9 m/s, which are (at a given dyke width and density

404 contrast between melt and wall rock) lower than the ascent velocities of melilitites (e.g.,  
405 [Mattsson 2012](#)) and kimberlites (e.g., [Sparks et al. 2006](#)).

406 Based on this method, 4.4-9.2 m/s magma ascent rates would be reasonable for the  
407 observed dyke width ( $0.625\pm 0.055$  m; Fig. 2) in the case of the youngest eruptive phase of  
408 Bondoró-hegy (capping scoriaceous basalt and the 3<sup>rd</sup> lava flow). According to [Valentine and](#)  
409 [Krogh \(2006\)](#), complex sill and dyke systems can be present beneath small volume, alkaline  
410 basaltic volcanic centres with variable dyke widths of main / parent dykes (3-9 m) and dyke-  
411 parallel segments (few decimetres-1.2 m). The observed dyke width in Bondoró-hegy falls in  
412 the range of these dyke widths, and it may represent a part of a similar dyke system.

413 2) We calculated the settling rate of the largest (20 cm in diameter) peridotite xenoliths  
414 found at Bondoró-hegy and Füzés-tó scoria cone. These computations yield xenolith settling  
415 rates in the range of 0.10-0.41 m/s, which corresponds to minimum ascent rates.

416 3) We used the Ca profiles of olivine xenocrysts (from the Füzés-tó basalt) which can be  
417 appropriate for estimating magma ascent time because the profiles were measured in rapidly  
418 quenched basaltic bombs. The average of the calculated residence times for the xenocrysts  
419 ([Table 6](#)) is 3.6 days (86.4 hours) which means the time that olivine xenocrysts could have  
420 spent in the basaltic melt. Considering for example a 60 km long ascent route, this gives an  
421 ascent rate of 0.19 m/s.

422 4) We estimated the dissolution times of orthopyroxene xenocrysts based on the  
423 thicknesses of their reaction rims. The thickest studied reaction rim can form in 86-426  
424 minutes (1.4-7.1 hours). This gives the interaction time between orthopyroxene and basaltic  
425 melt which denotes the minimum time that the magma must have spent in the feeding system.  
426 Using for example a 60 km long ascent route again, this means an ascent rate of 11.9 m/s.

427 In summary, the different methods resulted in a large range of ascent rates. The minimum  
428 ascent velocities are 0.10-0.19 m/s derived from the 2nd and 3rd methods (respectively), and

429 the maximum ascent rates are 9.2-11.9 m/s resulted from the 1st and 4th methods  
430 (respectively). These results imply that the Bondoró-hegy and Füzes-tó crystal-rich magmas  
431 could have reached the surface from their source within hours to few days.

432

## 433 **Discussion**

434

435 Alkaline basalts of the Bakony-Balaton Highland Volcanic Field have phenocryst  
436 assemblages of olivine, and more rarely, clinopyroxene (e.g., [Embey-Isztin et al. 1993a](#)).  
437 Olivine is frequently the only phenocryst phase and clinopyroxene is restricted to the  
438 groundmass. In contrast, the basalts of the Bondoró-hegy and Füzes-tó are more complex,  
439 having large textural and compositional heterogeneity, especially among clinopyroxenes.  
440 Most of the minerals could not be in equilibrium with each other and with the host magma,  
441 and many of them must be xenocrysts entrained from various depths. Here, we discuss the  
442 origins of the diverse crystals of the Bondoró-hegy basalt, the interpretations in the case of the  
443 Füzes-tó basalt were reported in previous papers ([Jankovics et al. 2009, 2012](#)). We also  
444 provide the magma ascent history and estimates of ascent rate.

445

### 446 *Sources for the diverse mineral assemblage*

447

#### 448 Xenocrysts

449

450 The compositional range of olivine xenocrysts ([Fig. 5](#)) is typical for mantle olivines (e.g.,  
451 [Boudier et al. 1991; Hirano et al. 2004; Rohrbach et al. 2005](#)). The Fo value for average  
452 olivines in the lithospheric mantle is 90 mol% ([Sato 1977](#)). Most of the studied olivine

453 xenocrysts contain Fo around 90 mol%, but some of them have higher Fo contents suggesting  
454 that they are derived from depleted peridotites.

455 Orthopyroxene xenocrysts are also Mg-rich which is characteristic for orthopyroxenes of  
456 the upper mantle (e.g., [Embey-Isztin et al. 2001a](#)). Their reaction rims are common features of  
457 mantle-derived orthopyroxenes that are incorporated by silica-undersaturated alkaline melts.  
458 This mineral-melt reaction results in the incongruent dissolution of the orthopyroxene and  
459 formation of a reaction corona (olivine + Si-rich glass + clinopyroxene ± spinel) at the  
460 expense of the orthopyroxene (e.g., [Arai and Abe 1995](#); [Shaw et al. 1998](#); [Shaw 1999](#); [Shaw  
461 and Dingwell 2008](#)). Comparing the compositions of the studied enstatite xenocrysts with the  
462 orthopyroxenes from the Bondoró-hegy peridotite xenoliths ([Embey-Isztin et al. 2001a](#)), they  
463 could have derived from moderately depleted peridotite (e.g., 2.9-3 wt.% Al<sub>2</sub>O<sub>3</sub>, 33.4-33.9  
464 wt.% MgO).

465 The compositional variation of the colourless clinopyroxene xenocrysts ([Figs. 8, 9](#)) is  
466 typical for Cr-diopsides of peridotite xenoliths (e.g., [Wass 1979](#)). The low Ti/Al ratios of the  
467 colourless xenocrystic cores suggest a relatively high-pressure origin (e.g., [Yagi and Onuma  
468 1967](#); [Wass 1979](#); [Dobosi et al. 1991](#)). They are derived from the disaggregation of  
469 incorporated peridotite fragments (together with the olivine and orthopyroxene xenocrysts).  
470 Compared to the compositions of clinopyroxenes of peridotite xenoliths from the Bondoró-  
471 hegy ([Embey-Isztin et al. 2001a](#)), most of the studied Cr-diopside xenocrysts could represent  
472 moderately depleted peridotite and some of them could indicate fertile peridotite (e.g., lower  
473 Mg# and higher TiO<sub>2</sub>).

474 Light green clinopyroxene xenocrysts have more Fe and less Ti than the phenocrysts.  
475 Their low Ti/Al ratios reflect their relatively high-pressure origin (e.g., [Yagi and Onuma  
476 1967](#); [Wass 1979](#); [Dobosi et al. 1991](#)). Several interpretations exist for the origin of such  
477 green clinopyroxene cores, for example, they are cognate phases of high-pressure origin; or

478 crystallized from evolved magmas; or represent locally metasomatized upper mantle wall rock  
479 (e.g., [Brooks and Printzlau 1978](#); [Wass 1979](#); [Barton and Bergen 1981](#); [Duda and Schmincke](#)  
480 [1985](#); [Dobosi and Fodor 1992](#)). Most of our studied green cores are compositionally very  
481 similar to the green clinopyroxenes found in lower crustal mafic granulite xenoliths in the  
482 Balaton Highland ([Embey-Isztin et al. 2003](#)) ([Figs. 8, 9](#)). Therefore, these light green  
483 clinopyroxene xenocrysts may represent crystals entrained from lower crustal mafic granulite.

484 According to their composition ([Fig. 10](#)), the spinel xenocrysts also have a lithospheric  
485 mantle origin. Compared with the compositions of spinels found in the peridotite xenoliths  
486 from the Bondoró-hegy ([Embey-Isztin et al. 2001a](#)), half of the studied spinel xenocrysts  
487 could have originated from fertile peridotite (e.g., lower Cr# and higher Al<sub>2</sub>O<sub>3</sub>) and half could  
488 represent moderately depleted peridotite.

489 In summary, the olivine, orthopyroxene, colourless clinopyroxene and spinel xenocrysts  
490 have diverse chemistry covering the compositional variations of minerals in peridotite  
491 xenoliths and representing variably depleted regions of the subcontinental lithospheric mantle.  
492 This is supported by the former study of spinel peridotite xenoliths having various textures  
493 and different calculated equilibrium temperatures ([Embey-Isztin et al. 2001a](#)). The xenocrysts  
494 acted as nucleation sites for the crystallization of the phenocryst phases which isolated them  
495 from the basaltic melt as crystal rims.

496

497 Megacrysts

498

499 Clinopyroxene megacrysts of alkaline basalts are frequently interpreted as high-pressure  
500 near-liquidus phases that crystallized from their host magmas (e.g., [Binns et al. 1970](#); [Ellis](#)  
501 [1976](#); [Irving and Frey 1984](#)) or as accidental fragments of pyroxenite veins that precipitated  
502 from melts at elevated pressures (e.g., [Righter and Carmichael 1993](#); [Shaw and Eyzaguirre](#)

503 2000). The relatively high Mg-numbers, high  $Al^{VI}/Al^{IV}$  and low Ti/Al ratios (Fig. 9e, f) of  
504 most of the Bondoró-hegy megacrysts could reflect their high-pressure cognate origin.  
505 However, their rounded outlines and the presence of the spongy reaction zone suggest that  
506 megacrysts were in disequilibrium with the host magma during ascent implying their  
507 accidental origin. Isotope data for the megacrysts and the host alkaline basalts of the  
508 Transdanubian region (Embey-Isztin et al. 1993a; Dobosi et al. 2003) also suggest an  
509 accidental origin because the megacrysts have significantly less radiogenic Sr and Nd isotope  
510 ratios than their host basalts. Trace element abundances, however, are compatible with a  
511 cognate origin. In order to resolve this contradiction, clinopyroxene megacrysts are  
512 interpreted as accidental fragments of pegmatitic veins which crystallized from earlier  
513 alkaline basaltic melts resembling the host basalt. These melts had different radiogenic  
514 isotope ratios, but similar major and trace element compositions as the present host basalt of  
515 the megacrysts, and crystallized as pyroxenite veins in the upper mantle. The presence of  
516 pyroxenite/peridotite composite xenoliths in the Transdanubian region (Embey-Isztin et al.  
517 1989, 1990) supports this hypothesis. The earlier crystallized coarse-grained pyroxenite veins  
518 were disrupted and carried to the surface as individual megacrysts by the ascending magma of  
519 Bondoró-hegy. During ascent, the megacrysts were out of equilibrium with the basaltic  
520 magma and through incipient partial melting, spongy domains developed in the megacrysts.

521 Some clinopyroxene megacrysts contain inclusions of spinel with similar compositions to  
522 the spinel megacrysts. This may suggest that spinel megacrysts had an origin similar to that of  
523 the clinopyroxene megacrysts.- The iron-rich green clinopyroxene megacryst and the  
524 titanomagnetite megacryst probably crystallized from a differentiated melt.

525

526 *Ascent history*

527

528 The ascent history of the Bondoró-hegy alkaline basaltic magma and origin of the diverse  
529 crystals are summarized in [Fig. 11](#). The information for the Füzes-tó basaltic magma was  
530 presented by [Jankovics et al. \(2009, 2012\)](#). The model in [Fig. 11](#) also gives a general view  
531 about the ascent history of both the crystal-rich alkaline basaltic magmas (Bondoró-hegy and  
532 Füzes-tó) in the CPR. After the generation of magma in the asthenosphere, it ascended  
533 through the lithospheric mantle in a destructive fashion, fracturing the wall rock and  
534 incorporating a vast amount of fragments from the lithospheric mantle now represented by the  
535 xenocrysts and peridotite xenoliths. During ascent, the basaltic magma strongly resorbed  
536 these crystals and fragments resulted in various disequilibrium textures and modification of  
537 the host magma composition. In the uppermost lithospheric mantle, near the crust-mantle  
538 boundary (CMB), a number of bodies (veins, dykes, sills) of frozen basaltic liquids and  
539 cumulates (i.e., earlier crystallized basaltic magma batches) can be present ([Embey-Isztin et](#)  
540 [al. 1990](#)). When the ascending magma reached this region, it incorporated additional crystals  
541 – having compositions different from those of the mantle xenocrysts – represented by the  
542 observed clinopyroxene and spinel megacrysts. As the magma passed through the CMB, the  
543 style of its ascent did not change as numerous fragments and green clinopyroxene crystals  
544 were entrained from lower crustal granulite. These fragments and crystals were also resorbed  
545 and could have additionally modified the magma composition. Accordingly, at mantle depths  
546 and near the CMB there was an effective interaction between the basaltic magma and the  
547 lithosphere. An explanation for this effective interaction could be some cryptic processes. In  
548 the case of kimberlitic magmas a recent discovery ([Russell et al. 2012](#)) suggests that  
549 continuous assimilation of foreign minerals (especially orthopyroxene) – that can modify the  
550 composition of the host melt toward more silicic compositions – causes changes in the  
551 volatile solubility in the host melt. The result is volatile exsolution and due to this process the  
552 magma can fracture more effectively the wall rock. However, this model requires that the

553 parental melt of the host magma should have much lower silica content and high amount of  
554 dissolved volatiles (i.e., carbonatitic or near-carbonatitic composition). To be able to reveal  
555 similar cryptic processes in the case of the studied alkaline basaltic magmas, experimental  
556 studies would be necessary which could help to decide whether these processes can be also  
557 expanded for alkaline basalts or operate only in the case of kimberlites. Thus, the applicability  
558 of this model in our case is not obvious.

559 In contrast to the effective magma-wall rock interaction at lithospheric mantle and lower  
560 crustal depths, the ascending magma did not incorporate additional crustal material in the  
561 middle and upper part of the crust. This suggests a change in the style (and possibly in the  
562 rate) of the magma ascent. The main driving force of magma ascent is the process of magma-  
563 filled crack propagation (e.g., [Spera 1984](#); [Russell et al. 2012](#)). Change in the style and rate of  
564 ascent can be caused by the variations in volatile solubility in the melt, by the change in the  
565 physical state of magma and wall rocks along the ascent path, and by varying dyke widths.  
566 [Szabó and Bodnar \(1996\)](#) suggested a change during the ascent of alkaline basaltic magmas in  
567 the Nógrád-Gömör Volcanic Field (Fig. 1a): the magmas accelerated near the MOHO. The  
568 observed recent activity of El Hierro (2011-2012) may also support their model, as the  
569 seismic signals suggested that the erupted magma passed rapidly through the crust (e.g.,  
570 [Carracedo et al. 2011](#)). This process may be a possible interpretation for the lack of middle  
571 and upper crustal wall rock fragments in our case.

572 Thermobarometric studies of basaltic magmas from ocean islands indicate melt  
573 accumulation near the CMB during the ascent of the magma batches (e.g., [Klügel et al. 2005](#);  
574 [Hildner et al. 2012](#)). The calculated ascent rates / times in the case of the Bondoró-hegy and  
575 Füzes-tó magmas, however, do not indicate a longer time of stagnation anywhere in the  
576 lithosphere. In addition, there is no petrologic evidence for magma accumulation / storage



577 (e.g., common cognate crystal cumulates), and the large amount of dense materials also needs  
578 a continuous ascent.

579

580 *Magma ascent rates in the monogenetic volcanic fields of the Pannonian Basin*

581

582 In monogenetic volcanic fields where eruptions of basaltic magmas give scarce precursory  
583 signs, estimating magma ascent rates is essential to hazard forecasting. As there are scarce  
584 direct observations about the activity of these eruptive centres, it is important to evaluate the  
585 ascent rate (as well as the ascent history) of basaltic magmas represented by diverse eruption  
586 products in various geodynamic settings.

587 In the case of other basalts in the Pannonian Basin, magma ascent time was determined by  
588 [Dégi et al. \(2009\)](#) for two eruptive centres in the Bakony-Balaton Highland Volcanic Field, by  
589 [Szabó and Bodnar \(1996\)](#) for several volcanic centres at the Nógrád-Gömör Volcanic Field  
590 and by [Harangi et al. \(in press\)](#) for two centres in the Perşani Volcanic Field. It is notable that  
591 these basalts contain a much smaller amount of lithospheric mantle-derived xenoliths and  
592 xenocrysts compared to the basalts of Bondoró-hegy and Füzes-tó. [Dégi et al. \(2009\)](#) studied  
593 the Fe-Ti-oxides in lower crustal mafic granulite xenoliths and modeled their diffusion-  
594 controlled chemical alteration. On the basis of diffusion profiles they estimated the duration  
595 of granulite xenolith–host basaltic melt interaction to be at least 9-20 h. This time interval  
596 gives a minimum ascent time and can be applied only in the crust, but the ascent time  
597 concerning the deeper parts of the lithosphere is not known. In the Nógrád-Gömör Volcanic  
598 Field, [Szabó and Bodnar \(1996\)](#) published ~37.5 hours for the residence time of upper mantle  
599 xenoliths in the host magmas and 18 hours for the residence time of a spinel xenocryst based  
600 on the thickness of its rim. [Harangi et al. \(in press\)](#) found that the residence time of mantle-  
601 derived olivine xenocrysts in the host alkaline basaltic magma was 3.6-4.8 days. This is very

602 similar to our results calculated by the same method, which is notable. These three mentioned  
603 estimations are close to our results but in the case of the first, the ascent time can be much  
604 longer.

605 So, although the studied basalts are extremely rich in xenoliths and xenocrysts, a  
606 significant difference in their magma ascent rates compared to the other alkaline basalts in the  
607 Pannonian Basin cannot be inferred. This is not in accordance with the common view that  
608 ultramafic xenolith-rich basaltic magmas reach the surface more rapidly than xenolith-poor  
609 ones.

610

## 611 **Conclusions**

612

613 The last eruptions of the Bakony-Balaton Highland Volcanic Field are represented by  
614 especially crystal- and xenolith-rich alkaline basaltic magmas forming two monogenetic  
615 eruptive centres: Bondoró-hegy and Füzes-tó scoria cone. Similar magmas did not erupt in the  
616 above mentioned volcanic field and even in the other volcanic fields in the whole Carpathian-  
617 Pannonian Region, nevertheless basalts of numerous eruptive centres contain diverse  
618 xenoliths.

619 Detailed textural and chemical analyses of the rock-forming minerals showed that almost  
620 the whole set of phenocrysts *s.l.* represents a mineral assemblage originating from different  
621 levels of the lithosphere. The foreign crystals have diverse compositions and are divided into  
622 three larger groups. The most abundant group originates from different regions of the  
623 subcontinental lithospheric mantle. Megacrysts can derive from pegmatitic veins / sills that  
624 probably represent crystallized magmas which froze near the crust-mantle boundary. Green  
625 clinopyroxenes show similar compositions compared to the clinopyroxenes in mafic  
626 granulites indicating lower crustal origin for these xenocrysts. Minerals that crystallized from

627 the basaltic melt are only represented by microphenocrysts and overgrowths on the foreign  
628 crystals. Consequently, the different whole-rock compositions of the studied basalts compared  
629 to those of the other basalts of the volcanic field are not caused by magma generation from a  
630 dissimilar mantle source or by differing degree of partial melting, but are the result of their  
631 different (more complex) evolution histories, i.e., incorporation of a vast amount of xenoliths  
632 and xenocrysts from the lithosphere at mantle and lower crustal depths.

633 A sudden change in the style of magma ascent is suggested by the fact that abundant  
634 crystals and xenoliths were entrained from the lithospheric mantle and lower crust but  
635 fragments from the middle-upper crust are absent from the studied basalts.

636 The xenocrysts show variable disequilibrium textures allowing us to calculate differing  
637 mineral-melt reaction times which can be used for magma ascent rate estimations. Based on  
638 our results calculated with different methods, we can conclude that despite the special feature  
639 of the Bondoró-hegy and Füzes-tó alkaline basalts, significant differences in their magma  
640 ascent velocities cannot be inferred compared to other alkaline basaltic magmas in the  
641 Pannonian Basin. The calculations indicate that these crystal-rich alkaline basaltic magmas  
642 could have reached the surface within hours to few days.

643 Based on our studies, these unique basalts enable the detailed documentation of the ascent  
644 history of basaltic magmas feeding monogenetic eruptions. Furthermore, they bear valuable  
645 implications for the rock types in the underlying lithosphere.

646

#### 647 **Acknowledgements**

648

649 We are very grateful to R. V. Fodor for his valuable suggestions and comments as well as I.  
650 E. M. Smith for his useful advices which helped to improve the manuscript. This research was  
651 partly supported by the TÉT\_10-1-2011-0694 project (Hungarian-Austrian Cooperation) and

652 by the Hungarian Scientific Research Fund OTKA no. 68587. B. Kiss was funded in the  
653 frames of TÁMOP 4.2.4. A/2-11-1-2012-0001 „National Excellence Program – Elaborating  
654 and operating an inland student and researcher personal support system convergence  
655 program” and was subsidized by the European Union and co-financed by the European Social  
656 Fund.

657

## 658 **References**

659

660 Ancochea E, Munoz M, Sagredo J (1987) Las rocas volcánicas neógenas de Nuévalos  
661 (provincia de Zaragoza). *Geogaceta* 3:7-10

662 Aoki K-i, Kushiro I (1968) Some clinopyroxenes from ultramafic inclusions in Dreiser  
663 Weiher, Eifel. *Contributions to Mineralogy and Petrology* 18(4):326-337

664 Arai S, Abe N (1995) Reaction of orthopyroxene in peridotite xenoliths with alkali-basalt  
665 melt and its implication for genesis of alpine-type chromitite. *American Mineralogist*  
666 80:1041-1047

667 Bada G, Horváth F (2001) On the structure and tectonic of the Pannonian Basin and  
668 surrounding orogens. *Acta Geologica Hungarica* 44(2-3):301-327

669 Balogh K, Árva-Sós E, Pécskay Z, Ravasz-Baranyai L (1986) K/Ar dating of post-Sarmatian  
670 alkali basaltic rocks in Hungary. *Acta Mineralogica et Petrographica Szeged* 28:75-93

671 Balogh K, Pécskay Z (2001) K/Ar and Ar/Ar geochronological studies in the Pannonian-  
672 Carpathians-Dinarides (PANCARDI) region. *Acta Geologica Hungarica* 44:281-299

673 Barton M, Bergen vMJ (1981) Green clinopyroxenes and associated phases in a potassium-  
674 rich lava from the Leucite Hills, Wyoming. *Contributions to Mineralogy and Petrology*  
675 77(2):101-114

676 Best MG (2003) *Igneous and Metamorphic Petrology*. Blackwell Publishing company,

677 Blackwell

678 Binns RA, Duggan MB, Wilkinson JFG (1970) High pressure megacrysts in alkaline lavas  
679 from northeastern New South Wales. *American Journal of Science* 269(2):132-168

680 Boudier F (1991) Olivine xenocrysts in picritic magmas: An experimental and microstructural  
681 study. *Contributions to Mineralogy and Petrology* 109(1):114-123

682 Bowen NL, Anderson O (1914) The binary system MgO-SiO<sub>2</sub>. *American Journal of Science*  
683 37:487-500

684 Brearley M, Scarfe CM (1986) Dissolution Rates of Upper Mantle Minerals in an Alkali  
685 Basalt Melt at High Pressure: An Experimental Study and Implications for Ultramafic  
686 Xenolith Survival. *Journal of Petrology* 27(5):1157-1182

687 Brenna M, Cronin SJ, Németh K, Smith IEM, Sohn YK (2011) The influence of magma  
688 plumbing complexity on monogenetic eruptions, Jeju Island, Korea. *Terra Nova*:1-6

689 Brenna M, Cronin SJ, Smith IEM, Sohn YK, Németh K (2010) Mechanisms driving  
690 polymagmatic activity at a monogenetic volcano, Udo, Jeju Island, South Korea.  
691 *Contributions to Mineralogy and Petrology* 160(6):931-950

692 Brooks CK, Printzlau I (1978) Magma mixing in mafic alkaline volcanic rocks: The evidence  
693 from relict phenocryst phases and other inclusions. *Journal of Volcanology and*  
694 *Geothermal Research* 4(315-331)

695 Carracedo J-C, Perez-Torrado F-J, Rodriguez-Gonzalez A, Fernandez-Turiel J-L, Klügel A,  
696 Troll VR, Wiesmaier S (2012) The ongoing volcanic eruption of El Hierro, Canary  
697 Islands. *Eos Trans. AGU* 93(9)

698 Connor CB, Conway FM (2000) Basaltic Volcanic Fields. In: Sigurdsson H (ed)  
699 *Encyclopedia of Volcanoes*. Academic Press, San Diego, pp 331-343

700 Costa F, Cohmen R, Chakraborty S (2008) Time Scales of Magmatic Processes from  
701 Modeling the Zoning Patterns of Crystals. In: Putirka KD, Tepley III FJ (eds) *Minerals,*

702 Inclusions and Volcanic Processes. Mineralogical Society of America & Geochemical  
703 Society, pp 545-594

704 Csontos L, Nagymarosy A, Horváth F, Kovác M (1992) Tertiary evolution of the Intra-  
705 Carpathian area: A model. *Tectonophysics* 208(1-3):221-241

706 Daines MJ, Kohlstedt DL (1994) The Transition from Porous to Channelized Flow Due to  
707 Melt/Rock Reaction During Melt Migration. *Geophysical Research Letters* 21(2):145-  
708 148

709 Deer WA, Howie RA, Zussman J (1978) Rock-forming minerals. Vol. 2A. Single-chain  
710 silicates. In: Longman, London, pp 3-4

711 Dégi J, Abart R, Török K, Rhede D, Petrishcheva E (2009) Evidence for xenolith-host basalt  
712 interaction from chemical patterns in Fe-Ti-oxides from mafic granulite xenoliths of the  
713 Bakony-Balaton Volcanic field (W-Hungary). *Mineralogy and Petrology* 95(3):219-234

714 Dobosi G (1989) Clinopyroxene zoning patterns in the young alkali basalts of Hungary and  
715 their petrogenetic significance. *Contributions to Mineralogy and Petrology* 101:112-121

716 Dobosi G, Downes H, Embey-Isztin A, Jenner GA (2003) Origin of megacrysts and  
717 pyroxenite xenoliths from the Pliocene alkali basalts of the Pannonian Basin (Hungary).  
718 *Neues Jahrbuch für Mineralogie - Abhandlungen* 178(3):217-237

719 Dobosi G, Fodor RV (1992) Magma fractionation, replenishment, and mixing as inferred  
720 from green-core clinopyroxenes in Pliocene basanite, southern Slovakia. *Lithos*  
721 28(2):133-150

722 Dobosi G, Schultz-Güttler R, Kurat G, Kracher A (1991) Pyroxene chemistry and evolution  
723 of alkali basaltic rocks from Burgenland and Styria, Austria. *Mineralogy and Petrology*  
724 43(4):275-292

725 Downes H, Embey-Isztin A, Thirlwall MF (1992) Petrology and geochemistry of spinel  
726 peridotite xenoliths from the western Pannonian Basin (Hungary): evidence for an

727 association between enrichment and texture in the upper mantle. Contributions to  
728 Mineralogy and Petrology 109(3):340-354

729 Downes H, Vaselli O (1995) The lithospheric mantle beneath the Carpathian-Pannonian  
730 Region: a review of trace element and isotopic evidence from ultramafic xenoliths. In:  
731 Downes H, Vaselli O (eds) Neogene and Related Magmatism in the Carpatho-Pannonian  
732 Region. Acta Vulcanologica, pp 219-229

733 Duda A, Schmincke H-U (1985) Polybaric differentiation of alkali basaltic magmas: evidence  
734 from green-core clinopyroxenes (Eifel, FRG). Contributions to Mineralogy and Petrology  
735 91(4):340-353

736 Ellis DJ (1976) High pressure cognate inclusions in the Newer Volcanics of Victoria.  
737 Contributions to Mineralogy and Petrology 58(2):149-180

738 Embey-Isztin A (1976) Amphibolite/lherzolite composite xenolith from Szigliget, north of the  
739 lake Balaton, Hungary. Earth and Planetary Science Letters 31(2):297-304

740 Embey-Isztin A, Dobosi G (1995) Mantle source characteristics for Miocene-Pleistocene  
741 alkali basalts, Carpathian-Pannonian Region: A review of trace elements and isotopic  
742 composition. In: Downes H, Vaselli O (eds) Neogene and Related Magmatism in the  
743 Carpatho-Pannonian Region. Acta Vulcanologica, pp 155-166

744 Embey-Isztin A, Dobosi G (2007) Composition of olivines in the young alkali basalts and  
745 their peridotite xenoliths from the Pannonian Basin. Annales Historico-Naturales Musei  
746 Nationalis Hungarici 99:5-22

747 Embey-Isztin A, Dobosi G, Altherr R, Meyer H-P (2001a) Thermal evolution of the  
748 lithosphere beneath the western Pannonian Basin: evidence from deep-seated xenoliths.  
749 Tectonophysics 331(3):285-306

750 Embey-Isztin A, Dobosi G, James D, Downes H, Poultidis C, Scharbert HG (1993b) A  
751 compilation of new major, trace and isotope geochemical analyses of the young alkali

752 basalts from the Pannonian Basin. *Fragmenta Mineralogica et Palaeontologica* 16:5–26

753 Embey-Isztin A, Downes H, Dobosi G (2001b) Geochemical characterization of the  
754 Pannonian Basin mantle lithosphere and asthenosphere: an overview. *Acta Geologica*  
755 *Hungarica* 44(2-3):259-280

756 Embey-Isztin A, Downes H, James DE, Upton BGJ, Dobosi G, Ingram GA, Harmon RS,  
757 Scharbert HG (1993a) The petrogenesis of Pliocene alkaline volcanic rocks from the  
758 Pannonian Basin, Eastern Central Europe. *Journal of Petrology* 34:317-343

759 Embey-Isztin A, Downes H, Kempton PD, Dobosi G, Thirlwall M (2003) Lower crustal  
760 granulite xenoliths from the Pannonian Basin, Hungary. Part 1: mineral chemistry,  
761 thermobarometry and petrology. *Contributions to Mineralogy and Petrology* 144:652-670

762 Embey-Isztin A, Scharbert HG, Dietrich H, Poultidis H (1989) Petrology and Geochemistry  
763 of Peridotite Xenoliths in Alkali Basalts from the Transdanubian Volcanic Region, West  
764 Hungary. *Journal of Petrology* 30(1):79-105

765 Embey-Isztin A, Scharbert HG, Dietrich H, Poultidis H (1990) Mafic granulites and  
766 clinopyroxenite xenoliths from the Transdanubian Volcanic Region (Hungary):  
767 implications for the deep structure of the Pannonian Basin. *Mineralogical Magazine*  
768 54:463-483

769 Fodor L, Csontos L, Bada G, Benkovics L, Györfi I (1999) Tertiary tectonic evolution of the  
770 Carpatho-Pannonian region: A new synthesis of palaeostress data. In: Durand B, Jolivet  
771 L, F. H, Séranne M (eds) *The Mediterranean Basins: Tertiary Extension within the*  
772 *Alpine Orogen*. Geological Society, London, Special Publications, pp 295-334

773 Granet M, Wilson M, Achauer U (1995) Imaging a mantle plume beneath the French Massif  
774 Central. *Earth and Planetary Science Letters* 136(3-4):281-296

775 Gurenko AA, Hansteen TH, Schmincke H-U (1996) Evolution of parental magmas of  
776 Miocene shield basalts of Gran Canaria (Canary Islands): constraints from crystal, melt



777 and fluid inclusions in minerals. *Contributions to Mineralogy and Petrology* 124(3):422-  
778 435

779 Harangi S (2001) Volcanology and petrology of the Late Miocene to Pliocene alkali basaltic  
780 volcanism in the Western Pannonian Basin. In: Ádám A, Szarka L (eds) PANCARDI  
781 2001 Field Guide. Sopron, pp 51-81

782 Harangi S (2009) Volcanism of the Carpathian-Pannonian region, Europe: The role of  
783 subduction, extension and mantle plumes. In:  
784 <http://www.mantleplumes.org/CarpathianPannonian.html>.

785 Harangi S, Lenkey L (2007) Genesis of the Neogene to Quaternary volcanism in the  
786 Carpathian-Pannonian region: Role of subduction, extension, and mantle plume.  
787 *Geological Society of America Special Papers* 418:67-92

788 Harangi S, Sági T, Seghedi I, Ntaflós T A mineral-scale investigation to reveal the origin of  
789 the basaltic magmas of the Perşani monogenetic volcanic field, Romania, eastern-central  
790 Europe. *Lithos*

791 Hasenaka T, Carmichael ISE (1985) The cinder cones of Michoacán-Guanajuato, central  
792 Mexico: their age, volume and distribution, and magma discharge rate. *Journal of*  
793 *Volcanology and Geothermal Research* 25(1-2):105-124

794 Hidas K, Falus G, Szabó C, Szabó PJ, Kovács I, Földes T (2007) Geodynamic implications of  
795 flattened tabular equigranular textured peridotites from the Bakony-Balaton Highland  
796 Volcanic Field (Western Hungary). *Journal of Geodynamics* 43(4-5):484-503

797 Hildner E, Kügel A, Hansteen TH (2012) Barometry of lavas from the 1951 eruption of Fogo,  
798 Cape Verde Islands: Implications for historic and prehistoric magma plumbing systems.  
799 *Journal of Volcanology and Geothermal Research* 217-218:73-90

800 Hirano N, Yamamoto J, Kagi H, Ishii T (2004) Young, olivine xenocryst-bearing alkali-basalt  
801 from the oceanward slope of the Japan Trench. *Contributions to Mineralogy and*

802 Petrology 148(1):47-54

803 Hoernle K, Zhang YS, Graham D (1995) Seismic and geochemical evidence for large-scale  
804 mantle upwelling beneath the eastern Atlantic and western and central Europe. *Nature*  
805 374:34-39

806 Horváth F (1993) Towards a mechanical model for the formation of the Pannonian Basin.  
807 *Tectonophysics* 226(1-4):333-357

808 Horváth F (1995) Phases of compression during the evolution of the Pannonian Basin and its  
809 bearing on hydrocarbon exploration. *Marine and Petroleum Geology* 12(8):837-844

810 Horváth F, Cloetingh S (1996) Stress-induced late-stage subsidence anomalies in the  
811 Pannonian Basin. *Tectonophysics* 266(1-4):287-300

812 Irving AJ, Frey FA (1984) Trace element abundances in megacrysts and their host basalts:  
813 Constraints on partition coefficients and megacryst genesis. *Geochimica et*  
814 *Cosmochimica Acta* 48(6):1201-1221

815 Jankovics É, Harangi S, Ntaflos T (2009) A mineral-scale investigation on the origin of the  
816 2.6 Ma Füzes-tó basalt, Bakony-Balaton Highland Volcanic Field (Pannonian Basin,  
817 Hungary). *Central European Geology* 52(2):97-124

818 Jankovics MÉ, Harangi S, Kiss B, Ntaflos T (2012) Open-system evolution of the Füzes-tó  
819 alkaline basaltic magma, western Pannonian Basin: Constraints from mineral textures and  
820 compositions. *Lithos* 140-141(0):25-37

821 Jugovics L (1968) The Transdanubian basalt and basaltic tuff fields (in Hungarian). Yearly  
822 Report of the Hungarian Geological Institute about the year 1967:75-82

823 Jugovics L (1976) The chemical character of the Hungarian basalts (in Hungarian). Yearly  
824 Report of the Hungarian Geological Institute about the year 1974:431-470

825 Jurewicz AJG, Watson EB (1988) Cations in olivine, Part 2: Diffusion in olivine xenocrysts,  
826 with applications to petrology and mineral physics. *Contributions to Mineralogy and*

827        Petrology 99(2):186-201

828    Kereszturi G, Csillag G, Németh K, Sebe K, Balogh K, Jáger V (2010) Volcanic architecture,  
829        eruption mechanism and landform evolution of a Plio/Pleistocene intracontinental  
830        basaltic polycyclic monogenetic volcano from the Bakony-Balaton Highland Volcanic  
831        Field, Hungary. Central European Journal of Geosciences 2(3):362-384

832    Kil Y, Wendlandt RF (2004) Pressure and temperature evolution of upper mantle under the  
833        Rio Grande Rift. Contributions to Mineralogy and Petrology 148(3):265-280

834    Klügel A (1998) Reactions between mantle xenoliths and host magma beneath La Palma  
835        (Canary Islands): constraints on magma ascent rates and crustal reservoirs. Contributions  
836        to Mineralogy and Petrology 131(2):237-257

837    Klügel A, Hansteen TH, Galipp K (2005) Magma storage and underplating beneath Cumbre  
838        Vieja volcano, La Palma (Canary Islands). Earth and Planetary Science Letters 236(1-  
839        2):211-226

840    Larsen LM, Pedersen AK (2000) Processes in High-Mg, High-T Magmas: Evidence from  
841        Olivine, Chromite and Glass in Palaeogene Picrites from West Greenland. Journal of  
842        Petrology 41(7):1071-1098

843    Lasaga AC (1998) Kinetic theory in the earth sciences. Princeton University Press, p 728

844    Lenkey L, Dövényi P, Horváth F, Cloetingh S (2002) Geothermics of the Pannonian Basin  
845        and its bearing on the neotectonics. European Geophysical Union Stephan Mueller  
846        Special Publications, Series 3:29-40

847    Lister JR, Kerr RC (1991) Fluid-Mechanical Models of Crack Propagation and Their  
848        Application to Magma Transport in Dykes. Journal of Geophysical Research  
849        96(B6):10049-10077

850    Maaloe S, Hansen B (1982) Olivine phenocrysts of Hawaiian olivine tholeiite and oceanite.  
851        Contributions to Mineralogy and Petrology 81(3):203-211

852 Martin U, Németh K (2005) Eruptive and depositional history of a Pliocene tuff ring that  
853 developed in a fluvio-lacustrine basin: Kissomlyó volcano (western Hungary). *Journal of*  
854 *Volcanology and Geothermal Research* 147(3-4):342-356

855 Martin U, Németh K, Auer A, Breitzkreuz C (2003) Mio-Pliocene Phreatomagmatic  
856 Volcanism in a Fluvio-Lacustrine Basin in Western Hungary. *Geolines* 15:84-90

857 Mattsson HB (2012) Rapid magma ascent and short eruption durations in the Lake Natron-  
858 Engaruka monogenetic volcanic field (Tanzania): A case study of the olivine melilititic  
859 Pello Hill scoria cone. *Journal of Volcanology and Geothermal Research* 247-248:16-25

860 McGee LE, Millet M-A, Smith IEM, Németh K, Lindsay JM (2012) The inception and  
861 progression of melting in a monogenetic eruption: Motukorea Volcano, the Auckland  
862 Volcanic Field, New Zealand. *Lithos* 155(0):360-374

863 Morimoto N, Fabries J, Ferguson AK, Ginzburg IV, Ross M, Seifert FA, Zussman J, Aoki K,  
864 Gottardi G (1988) Nomenclature of pyroxenes. *Mineralogical Magazine* 52:535–550

865 Needham AJ, Lindsay JM, Smith IEM, Augustinus P, Shane PA (2011) Sequential eruption  
866 of alkaline and sub-alkaline magmas from a small monogenetic volcano in the Auckland  
867 Volcanic Field, New Zealand. *Journal of Volcanology and Geothermal Research* 201(1-  
868 4):126-142

869 Németh K, Martin U (1999a) Large hydrovolcanic field in the Pannonian Basin: general  
870 characteristics of the Bakony-Balaton Highland Volcanic Field, Hungary. *Acta*  
871 *Vulcanologica* 11(2):271-282

872 Németh K, Martin U (1999b) Late Miocene paleo-geomorphology of the Bakony-Balaton  
873 Highland Volcanic Field (Hungary) using physical volcanology data. *Zeitschrift für*  
874 *Geomorphologie N. F.* 43(4):417-438

875 Reiners PW (2002) Temporal-compositional trends in intraplate basalt eruptions: Implications  
876 for mantle heterogeneity and melting processes. *Geochemistry Geophysics Geosystems*

877 3(2)

878 Righter K, Carmichael ISE (1993) Mega-xenocrysts in alkali olivine basalts: fragments of  
879 disrupted mantle assemblages. *American Mineralogist* 78:1230-1245

880 Rock NMS (1990) The International Mineralogical Association (IMA/CNMMN) pyroxene  
881 nomenclature scheme: Computerization and its consequences. *Mineralogy and Petrology*  
882 43(2):99-119

883 Roeder P, Gofton E, Thornber C (2006) Cotectic Proportions of Olivine and Spinel in  
884 Olivine-Tholeiitic Basalt and Evaluation of Pre-Eruptive Processes. *Journal of Petrology*  
885 47(5):883-900

886 Roeder PL, Poustovetov A, Oskarsson N (2001) Growth Forms and Composition of  
887 Chromian Spinel in MORB Magma: Diffusion-Controlled Crystallization of Chromian  
888 Spinel. *Canadian Mineralogist* 39(2):397-416

889 Roeder PL, Thornber C, Poustovetov A, Grant A (2003) Morphology and composition of  
890 spinel in Pu'u 'O'o lava (1996-1998), Kilauea volcano, Hawaii. *Journal of Volcanology*  
891 and Geothermal Research 123(3-4):245-265

892 Rohrbach A, Schuth S, Ballhaus C, Münker C, Matveev S, Qopoto C (2005) Petrological  
893 constraints on the origin of arc picrites, New Georgia Group, Solomon Islands.  
894 *Contributions to Mineralogy and Petrology* 149(6):685-698

895 Ruprecht P, Bachmann O (2010) Pre-eruptive reheating during magma mixing at Quizapu  
896 volcano and the implications for the explosiveness of silicic arc volcanoes. *Geology*  
897 38(10):919-922

898 Russell JK, Porritt LA, Lavalley Y, Dingwell DB (2012) Kimberlite ascent by assimilation-  
899 fuelled buoyancy. *Nature* 481(7381):352-356

900 Sato H (1977) Nickel content of basaltic magmas: identification of primary magmas and a  
901 measure of the degree of olivine fractionation. *Lithos* 10(2):113-120

902 Seghedi I, Downes H, Vaselli O, Szakács A, Balogh K, Pécskay Z (2004) Post-collisional  
903 Tertiary-Quaternary mafic alkalic magmatism in the Carpathian-Pannonian region: a  
904 review. *Tectonophysics* 393(1-4):43-62

905 Shane P, Gehrels M, Zawalna-Geer A, Augustinus P, Lindsay J, Chaillou I (2013) Longevity  
906 of a small shield volcano revealed by crypto-tephra studies (Rangitoto volcano, New  
907 Zealand): Change in eruptive behavior of a basaltic field. *Journal of Volcanology and*  
908 *Geothermal Research* 257(0):174-183

909 Shaw C, Dingwell D (2008) Experimental peridotite-melt reaction at one atmosphere: a  
910 textural and chemical study. *Contributions to Mineralogy and Petrology* 155(2):199-214

911 Shaw CSJ (1999) Dissolution of orthopyroxene in basanitic magma between 0.4 and 2 GPa:  
912 further implications for the origin of Si-rich alkaline glass inclusions in mantle xenoliths.  
913 *Contributions to Mineralogy and Petrology* 135(2):114-132

914 Shaw CSJ, Eyzaguirre J (2000) Origin of megacrysts in the mafic alkaline lavas of the West  
915 Eifel volcanic field, Germany. *Lithos* 50(1-3):75-95

916 Shaw CSJ, Thibault Y, Edgar AD, Lloyd FE (1998) Mechanisms of orthopyroxene  
917 dissolution in silica-undersaturated melts at 1 atmosphere and implications for the origin  
918 of silica-rich glass in mantle xenoliths. *Contributions to Mineralogy and Petrology*  
919 132(4):354-370

920 Smith DR, Leeman WP (2005) Chromian spinel-olivine phase chemistry and the origin of  
921 primitive basalts of the southern Washington Cascades. *Journal of Volcanology and*  
922 *Geothermal Research* 140(1-3):49-66

923 Sparks RSJ, Baker L, Brown RJ, Field M, Schumacher J, Stripp G, Walters A (2006)  
924 Dynamical constraints on kimberlite volcanism. *Journal of Volcanology and Geothermal*  
925 *Research* 155(1-2):18-48

926 Sparks RSJ, Pinkerton H, Macdonald R (1977) The transport of xenoliths in magmas. *Earth*

927 and Planetary Science Letters 35(2):234-238

928 Spera FJ (1984) Carbon dioxide in petrogenesis III: role of volatiles in the ascent of alkaline  
929 magma with special reference to xenolith-bearing mafic lavas. Contributions to  
930 Mineralogy and Petrology 88(3):217-232

931 Stormer JC (1973) Calcium zoning in olivine and its relationship to silica activity and  
932 pressure. Geochimica et Cosmochimica Acta 37(8):1815-1821

933 Szabó C, Bodnar RJ (1996) Changing magma ascent rates in the Nógrád–Gömör volcanic  
934 field, Northern Hungary/Southern Slovakia: evidence from CO<sub>2</sub>-rich fluid inclusions in  
935 metasomatized upper mantle xenoliths. Petrology 4(3):221-230

936 Szabó C, Falus G, Zajacz Z, Kovács I, Bali E (2004) Composition and evolution of  
937 lithosphere beneath the Carpathian-Pannonian Region: a review. Tectonophysics 393(1-  
938 4):119-137

939 Takada A (1994) The influence of regional stress and magmatic input on styles of  
940 monogenetic and polygenetic volcanism. Journal of Geophysical Research  
941 99(B7):13563-13573

942 Tari G, Dövényi P, Horváth F, Dunkl I, Lenkey L, Stefanescu M, Szafián P, Tóth T (1999)  
943 Lithospheric structure of the Pannonian Basin derived from seismic, gravity and  
944 geothermal data. In: Durand B, Jolivet L, Horváth F, Séranne M (eds) The Mediterranean  
945 Basins: Tertiary extension within the Alpine orogen. Geological Society, London, Special  
946 Publication, pp 215-250

947 Tracy RJ, Robinson P (1977) Zoned titanian augite in alkali olivine basalt from Tahiti and the  
948 nature of titanium substitutions in augite. American Mineralogist 62(7-8):634-645

949 Ulrych J, Ackerman L, Balogh K, Hegner E, Jelínek E, Pécskay Z, Přichystal A, Upton BGJ,  
950 Zimák J, Foltýnová R (2013) Plio-Pleistocene basanitic and melilititic series of the  
951 Bohemian Massif: K-Ar ages, major/trace element and Sr–Nd isotopic data. Chemie der

- 952 Erde – Geochemistry. <http://dx.doi.org/10.1016/j.chemer.2013.02.001>
- 953 Valentine GA, Krogh KEC (2006) Emplacement of shallow dikes and sills beneath a small  
954 basaltic volcanic center – The role of pre-existing structure (Paiute Ridge, southern  
955 Nevada, USA). *Earth and Planetary Science Letters* 246(3–4):217-230
- 956 Walker GPL (1993) Basaltic-volcano systems. Geological Society, London, Special  
957 Publications 76(1):3-38
- 958 Wass SY (1979) Multiple origins of clinopyroxenes in alkali basaltic rocks. *Lithos* 12(2):115-  
959 132
- 960 Wijbrans J, Németh K, Martin U, Balogh K (2007)  $^{40}\text{Ar}/^{39}\text{Ar}$  geochronology of Neogene  
961 phreatomagmatic volcanism in the western Pannonian Basin, Hungary. *Journal of*  
962 *Volcanology and Geothermal Research* 164(4):193-204
- 963 Yagi K, Onuma K (1967) The Join  $\text{CaMgSi}_2\text{O}_6$ - $\text{CaTiAl}_2\text{O}_6$  and its bearing on the  
964 Titanaugites. *Journal of the Faculty of Science, Hokkaido University. Series 4, Geology*  
965 *and Mineralogy* 13(4):463-483
- 966 Zhang H-F (2005) Transformation of lithospheric mantle through peridotite-melt reaction: A  
967 case of Sino-Korean craton. *Earth and Planetary Science Letters* 237(3-4):768-780

968

969 **Figure captions**

970

971 Fig. 1

972 a) Geological sketch map of the Carpathian-Pannonian Region. Alkaline basaltic volcanic  
973 fields are assigned with numbers: 1=Styrian Basin, 2=Little Hungarian Plain, 3=Bakony-  
974 Balaton Highland, 4=Stiavnica-Nógrád-Gömör, 5=Kecel, 6=Banat, 7= Perşani; b) Simplified  
975 geological map of the Bakony-Balaton Highland Volcanic Field (after [Jugovics 1968](#);



976 [Harangi 2001](#)) with the locality of the Bondoró-hegy and the Fűzes-tó scoria cone (and the  
977 names of some other volcanic centres).

978

979 Fig. 2

980 Outcrop photo of the scoria cone remnant, first shown by [Kereszturi et al. \(2010\)](#). The  
981 scoriaceous breccia of the cone is cross-cut by a massive basalt dyke (the boundaries of the  
982 dyke are marked by the white dashed lines), that we interpret as a feeder dyke based on field  
983 observations. The white arrow indicates the direction of the dyke injection. The hammer  
984 (shown by the black arrow) is 30 cm in length.

985

986 Fig. 3

987 a) Typical petrographic appearance of the studied crystal-rich alkaline basalts  
988 (photomicrograph, XN, sample: Ft3). Note that almost all of the phenocrysts *s.l.* are foreign  
989 minerals; b) Amphibole-bearing spinel peridotite xenolith occasionally occur in the studied  
990 alkaline basalts (photomicrograph, 1N, sample: Fuz3). Ol – olivine, opx – orthopyroxene, cpx  
991 – clinopyroxene, am – amphibole.

992

993 Fig. 4

994 a) Anhedral, embayed olivine which has a bright rim and contains a light green spinel that has  
995 a bright overgrowth rim adjacent to the groundmass; b) Rounded spinel crystal with a bright  
996 overgrowth rim; c) Orthopyroxene and its fine-grained rim consisting of olivine,  
997 clinopyroxene and glass; d) Crystal clot that consists of an anhedral olivine and a  
998 clinopyroxene with a rounded colourless core; e) Clinopyroxene crystal having an anhedral  
999 colourless core and a sector zoned rim; f) Clinopyroxene crystal with a resorbed light green  
1000 core and a sector zoned rim; g) Homogeneous, colourless clinopyroxene megacryst that has a

1001 thick spongy zone and a zoned clinopyroxene overgrowth on it; h) Enlargement of the spongy  
1002 zone of the clinopyroxene megacryst (g) containing feldspar and spinel inclusions; i) Sector  
1003 zoned clinopyroxene phenocryst. SEM backscattered electron images. Ol – olivine, sp –  
1004 spinel, opx – orthopyroxene, cpx – clinopyroxene, fp – feldspar.

1005

1006 Fig. 5

1007 a) Relationship between the Fo (mol%) and CaO (wt.%) content of the studied olivine  
1008 crystals; b) Plot of Fo (mol%) and NiO (wt.%) contents of the studied olivines. Light grey  
1009 dashed line fields indicate the compositions of olivines in upper mantle peridotite xenoliths  
1010 from the Balaton Highland ([Embey-Isztin et al. 2001a](#)).

1011

1012 Fig. 6

1013 Fo (mol%), Ni and Ca (ppm) profiles of olivine xenocrysts (a, b) and an olivine phenocryst  
1014 *s.s.* (c). The lines of measured points are indicated by the A-B lines in each picture (SEM  
1015 backscattered electron images). In the case of the xenocrysts, at the crystal margins (in a 50-  
1016 100  $\mu\text{m}$  thick band) points were measured with  $\sim 5 \mu\text{m}$  gaps between each other, while in the  
1017 central part of the olivine the gaps were increased to 20-50  $\mu\text{m}$ . In the case of olivine  
1018 phenocrysts, the whole profile was prepared with 5  $\mu\text{m}$  gaps (5  $\mu\text{m}$  distances between  
1019 measuring points were necessary because of the effect of the  $e^-$  beam on the crystal surface).

1020

1021 Fig. 7

1022 Fo (mol%) vs. NiO (wt.%) relationship of representative olivine xenocrysts (Fig. 6a, b) and  
1023 normal zoned phenocryst (Fig. 6c). The different core-to-rim trends are indicative for  
1024 diffusion- or growth-related development of the zoning (for details see text).

1025

1026 Fig. 8

1027 Compositions of the studied clinopyroxenes plotted in the atomic Mg-Fe-Ca ternary diagram  
1028 (boundaries after [Morimoto et al. 1988](#)). The light grey dashed line field indicates the  
1029 compositions of clinopyroxenes in upper mantle peridotite xenoliths from the Balaton  
1030 Highland ([Embey-Isztin et al. 2001a](#)), the dark grey dashed line field indicates the  
1031 compositions of clinopyroxenes in lower crustal mafic granulite xenoliths from the Balaton  
1032 Highland ([Embey-Isztin et al. 2003](#)).

1033

1034 Fig. 9

1035 Variation of Mg# ( $\text{Mg}/(\text{Mg}+\text{Fe}^{\text{tot}})$ ) vs. Ti (a), Al (b), Cr (c) and Na (d) (cations per formula  
1036 unit based on 6 O); e) Plot of Ti vs. Al (cations per formula unit based on 6 O); f)  $^{\text{IV}}\text{Al}$  vs.  
1037  $^{\text{VI}}\text{Al}$  diagram ([Aoki and Kushiro 1968](#)). Symbols as in Fig. 8. Light and dark grey dashed line  
1038 fields indicate the same clinopyroxene compositions as in Fig. 8 (the Cr content of granulitic  
1039 clinopyroxenes were not analysed in [Embey-Isztin et al. 2003](#)).

1040

1041 Fig. 10

1042 a) Cr-Al-Fe<sup>3+</sup> ternary plot of the studied spinels; b) Variation of MgO (wt.%) vs. Al<sub>2</sub>O<sub>3</sub>  
1043 (wt.%) contents in the studied spinel grains. Light grey dashed line fields indicate the  
1044 compositions of spinels in upper mantle peridotite xenoliths from the Balaton Highland  
1045 ([Embey-Isztin et al. 2001a](#)).

1046

1047 Fig. 11

1048 Schematic cartoon of the proposed model for the ascent history of the Bondoró-hegy and  
1049 Füzes-tó alkaline basaltic magmas. Enlargements of the ascent path show the dominant  
1050 processes (see the text for details). The figure is to scale. LAB – lithosphere–asthenosphere

1051 boundary, gt – garnet, sp – spinel. The source for the crustal and lithospheric thicknesses is:  
1052 [http://geophysics.elte.hu/atlas/geodin\\_atlas.htm](http://geophysics.elte.hu/atlas/geodin_atlas.htm).

1053

1054 **Table captions**

1055

1056 Table 1

1057 Major and trace element analyses of the BON683 sample from Bondoró-hegy ([Embey-Isztin](#)  
1058 [et al. 1993a](#))

1059

1060 Table 2

1061 Representative compositions of the studied olivines

1062

1063 Table 3

1064 Representative analyses of the studied orthopyroxenes and clinopyroxenes

1065

1066 Table 4

1067 Representative compositions of the studied spinels

1068

1069 Table 5

1070 Details of the different methods and results of the estimated magma ascent rates and times

1071

1072 Table 6

1073 Calculated residence times of the studied olivine xenocrysts